University of Alberta

Heterogeneity Consideration and Upscaling of Elastic Properties in Coupled Geomechanical Flow Simulation of SAGD

by

Mohammad Mehdi Khajeh

A thesis submitted to the Faculty of Graduate Studies and Research
in partial fulfillment of the requirements for the degree of

Doctor of Philosophy

in

Geotechnical Engineering

Civil and Environmental Engineering Department

Fall 2013
Edmonton, Alberta

To
My Lovely Parents; **Saeed** & **Zohreh**

ABSTRACT

Geomechanical processes occurring during steam assisted gravity drainage (SAGD) thermal recovery influence petrophysical and rock mechanical properties of both reservoir and caprock formations. While geostatistical techniques provide multiple equiprobable geological realizations for petrophysical properties, rock mechanical properties are traditionally considered as homogenously in reservoir geomechanical simulations of the SAGD process. This research has shown that consideration of heterogeneous facies and rock mechanical properties will result in a larger range of possible outcomes, such as vertical displacement within the reservoir, than simulation models that adopt homogeneous facies and property distributions.

Typically, only a select number of geological realizations are selected for simulation. Randomly selecting geological realizations will not accurately represent uncertainty and they should be selected based on appropriate ranking criteria. A ranking criterion, which is in good correlation with expected elastic deformation of reservoir, has been developed in this research. The developed ranking technique is based on expected elastic deformation of each cell considered in numerical simulation of SAGD. Geometrical calibration parameters are adopted within the developed ranking technique.

Upscaling of geological models and moving from high resolution geological models to coarse scale simulation models results in reduction of number of cells and accordingly reduction of computational cost. A new numerical technique for

upscaling of elastic properties has been proposed. Two major advantages of the new geomechanical upscaling technique include the ability to consider transversely isotropic deformation and independence from coarse scale properties with respect to facies configuration.

The ranking and upscaling approaches were applied to a McMurray Formation field case study dataset. In comparison to upscaling techniques based on averaging, the numerical upscaling technique provided a reduction in simulation error. In addition, application of the upscaling technique to real field data confirmed the reduction in computational time for reservoir geomechanical simulations.

ACKNOWLEDGEMENTS

Completion of this dissertation would not have been possible without help of several individuals who considered their valuable support and assistance in their different ways.

I would like to express my deepest gratitude to my supervisor, Dr. Rick Chalaturnyk. I greatly appreciate his support, guidance and advice during completion of this work. In addition, Dr. Chalaturnyk strongly supported this work by ensuring funding and many other resources required for completion of this work.

I am also grateful to my co-supervisor, Dr. Jeff Boisvert. Geostatistics is one of the main keywords of current research and Dr. Boisvert's valuable knowledge and experience in this field helped me a lot. His keen interest, guidance, detailed discussion and encouragement is gratefully thanked.

I would like to express my appreciation to Dr. Clayton Deutsch, co-director of Centre for Computational Geostatistics (CCG) at University of Alberta. His help and support to link me to industry is highly appreciated.

I would like to thank all of my friends and colleagues, particularly Nathan Deisman, Dr. Ali Azad, Dr. Mohsen Nicksiar, Hadi Derakhshan and Dr. Rahman (Mehran) Mohammad Hassanpour. Special thanks to Nathan who considered his time to review some of my chapters.

Last but not least, I would like to thank my parents and sisters for their unconditional emotional support throughout my degree. Patience and understanding shown by them is greatly appreciated.

TABLE OF CONTENTS

LIST OF TABLES

CHAPTER 1

CHAPTER 2

CHAPTER 3

CHAPTER 4

LIST OF FIGURES

CHAPTER 1

CHAPTER 2

CHAPTER 3

CHAPTER 4

CHAPTER 5

LIST OF SYMBOLS, NOMENCLATURE OR ABBREVIATIONS

ε_v	Volumetric strain
$\overline{a_{v_r}}$	average volumetric/shear strain of the fine scale cells in the r^{th} upscaled block
a_{v_i}	volumetric/shear strain in the i^{th} fine scale cell within the upscaled block
a_{v_r}	volumetric/shear strain in the r^{th} upscaled block
Δt_c	Compression wave travel time
Δt_s	Shear wave travel time
A_{ijmn}	General form of 4^{th} order elastic tensor
COP	Cumulative oil production
CSS	Cyclic steam stimulation
E	Young modulus
EEM	Equivalent elastic media
e_{mn}	2^{nd} order strain tensor
E_x	Young modulus in X direction
E_z	Young modulus in Z direction
$F_{ai,j}$	Angle discounting factor
$F_{di,j}$	Distance discounting factor
$F_{si,j}$	Number of steps discounting factor
G	Shear modulus
G^*	Shear modulus of composite material
GR	Geomechanical ranking

G_{xy}	Shear modulus between the plane of isotropy and the perpendicular plane
H_O	Over burden height
H_R	Reservoir height
H_U	Under burden height
ISC	In situ combustion
K	Permeability
K	Bulk modulus
K^*_x	Upscaled permeability in X direction
K^*_y	Upscaled permeability in Y direction
K_0	Initial permeability
L_1	Initial length of coarse scale cell in X direction
L_2	Initial length of coarse scale cell in Y direction
Log	Logarithmic function
L_R	Reservoir length
L_S	Side burden length
MD	Measured depth
MEM	Mechanical earth model
n_r	Number of blocks in the upscaled model
OOIP	Original oil in place
SAGD	Steam assisted gravity drainage
SOR	Steam oil ratio
S_w	Water saturation

U	Displacement vector
VAPEX	Vapor extraction
V_b	Volume of upscaled (coarse scale) cell
VD_{GR}	Vertical displacement, obtained from geomechanical ranking technique
VDP	Vertical displacement profile
ν	Poisson ratio
ν^*	Poisson ratio of composite material
ν_{xz}	Poisson ratio in XZ plane
ρ_b	Bulk density
σ_{ij}	2^{nd} order stress tensor
Φ	Porosity
$\Phi(y)$	Fine scale porosity
Φ^*	Upscaled porosity
Φ_0	Initial porosity
ω	Averaging power between -1 and 1

CHAPTER 1: INTRODUCTION

INTRODUCTION

Canada has large heavy oil (oilsand) resources which are distributed in three major areas in Alberta; Athabasca, Cold Lake and Peace River. Oil sand is deposited mainly in Lower Cretaceous McMurray Formation. Surface mining technology and in situ recovery techniques are two main recovery technologies. About 18% of oilsand deposits which are close to the surface (<45m) can be recovered using surface mining technology and the remaining must be extracted using in situ techniques such as; hot water injection, in situ combustion (ISC), vapor extraction (VAPEX), steam flooding, cyclic steam stimulation (CSS) and steam assisted gravity drainage (SAGD). SAGD, the most promising technology among different in situ recovery techniques for development of oil sand reserves was introduced in early 1980's (Butler et al., 1980; Butler et al., 1981; Butler and Stephens, 1981).

The fundamental concept of SAGD is the heating of oil sand by the injection of steam into the reservoir. In this process, two parallel horizontal wells are drilled in the formation, the first about 5 meter above the base of the reservoir and the second about 4 to 6 meters above the first well. The upper well, named as injector, injects steam. Due to lower density of injected steam, it moves upward and sideward and gradually forms a steam saturated zone known as steam chamber. Thermal energy reduces the viscosity of the oil within the bitumen, facilitating the oil's flow by gravitational gradient and the lower well, named as producer, collects the heated crude oil or bitumen that flows out of the formation, along with any water from the condensation of injected steam. Figure 1-1 shows a schematic of the SAGD process.

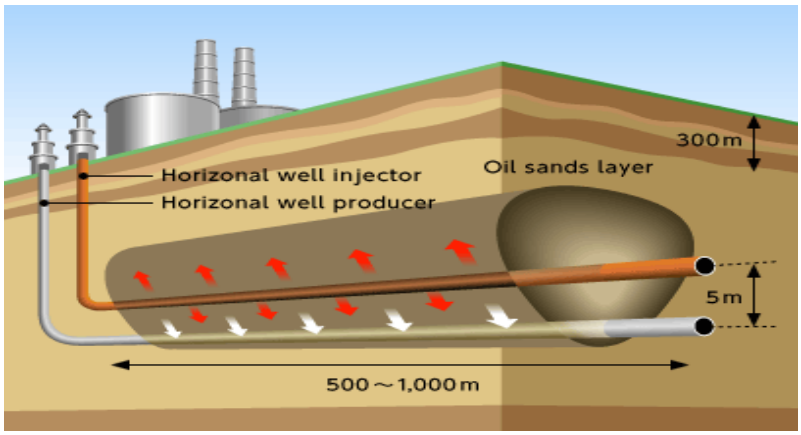

Figure 1-1 Schematic of SAGD process
(Courtesy of http://www.japex.co.jp/english/business/oversea/sagd.html).

Numerical flow simulation is used widely by reservoir engineers to predict performance of SAGD process as a reservoir characterization tool. The processes considered widely in numerical simulators for simulation of SAGD process are basically fluid flow, heat transfer and mass transfer. Numerous works illustrate the application and improvement of numerical simulation of SAGD (Chow and Butler, 1996; Ito and Suzuki, 1996; Law et al., 2003).

Oil sands in the McMurray Formation have in situ interlocked fabric configurations (Dusseault and Morgenstern, 1978). As a result of temperature and pressure variation during the SAGD process, in situ stresses inside the reservoir will be affected and accordingly deformation will occur. Temperature increase, results in thermal expansion of sand grains, reservoir matrix and pore fluids which accordingly results in increase in total stresses and pore pressure increase results in decreasing of effective stresses. These geomechanical responses as a result of temperature and pressure variations affect reservoir parameters, i.e. porosity and permeability. Isotropic unloading, due to effective stress decreasing, shear dilation when failure criteria of reservoir material is satisfied, due to anisotropic stress variation, and compaction are three main geomechanical responses which occur during SAGD (Li, 2006).

Experimental studies by Dusseault and Morgenstern (1978), Agar et al. (1986), Kosar et al. (1987), Oldakowski (1994), Scott et al. (1994), Chalaturnyk (1996), Samieh and Wong (1996) and Touhidi-Baghini (1998) have shown that

geomechanics can play significant role due to temperature and pressure variation in the SAGD process.

Conventional reservoir simulators don't take in to account interaction between fluid and solid and accordingly changes in reservoir parameters as a result of geomechanical response. However SAGD performance is highly affected by reservoir parameters such as porosity and permeability. So, it is necessary to consider coupled geomechanical flow simulation rather than conventional flow simulation to predict SAGD performance in a more precise manner. In coupled geomechanical flow simulation, stress-strain variations, i.e. geomechanical responses, as a result of temperature and pressure variations are taken in to account. Previous numerical studies (Chalaturnyk, 1996; Settari et al., 2001; Tran et al., 2005a and b; Li, 2006; Du and Wong, 2007; and Azad, 2012, to name a few) have shown that geomechanics has a significant role in the SAGD process.

Geological models are one of the most important input data required for each kind of numerical simulation, including coupled geomechanical flow simulation of SAGD. In the modern oil industry, geostatistical property models are built for different purposes such as resource estimation and flow simulation. Processing of multiple realizations, obtained from geostatistical simulation techniques, helps assess uncertainty analysis which is important for development planning and decision making processes.

STATEMENT OF PROBLEM

Each geostatistically built geological realization is a combination of structural, facies, and attributes models. In the case of conventional simulation process, i.e. without considering geomechanical simulation, petrophysical properties, i.e. porosity, permeability and saturation, are the only attributes required to be modeled. These parameters are included in the fluid flow governing equations. Rock mechanical properties play a similar role in geomechanical simulation as petrophysical properties play in fluid flow. In the case of coupled geomechanical flow simulation processes, geostatistical modeling for geomechanical attributes

has yet to be incorporated. Therefore, uncertainty assessment could be underestimated according to the spatial distribution of these parameters.

To capture extreme upper and lower bound of range of uncertainties in both flow and geomechanical responses of SAGD, large number of realizations should be passed through coupled geomechanical flow simulation. However due to computational time, it is impractical to use all realizations for simulation. Random selection of a few realizations results in inaccurate representation of ranges of uncertainty and they should be ranked based on a criterion which is in high correlation with expected response of geological realization during SAGD process. Existing ranking criteria for SAGD just focus on flow response of media and no ranking measures found in literature based on expected geomechanical response. Proposing ranking criteria which is in robust correlation with expected geomechanical response of media is required.

To capture heterogeneity of small scale features, geological models are usually built at fine scales which are not suitable for simulation process due to computational cost. So, appropriate upscaling techniques must be used to move from fine scale geological models to coarser scale simulation models. Existing analytical upscaling techniques are usually developed for simplified facies configuration which may not work very well for complex facies configuration such as sand/shale facies configuration of McMurray Formation. So, development of appropriate upscaling technique for rock mechanical properties, elastic properties in this research, which could be applied for complex facies configuration, seems to be required.

OBJECTIVE, METHODOLOGY AND SCOPE OF RESEARCH

The main objectives of this research are categorized in three main parts as follow;

1. Investigate the effect of heterogeneity in rock mechanical properties on SAGD performance.
2. Proposing ranking criteria which is in good correlation with elastic deformation of reservoir in numerical simulation of SAGD process.

3. Proposing new numerical upscaling approach for upscaling of elastic properties which could be applied for complex facies configurations such as sand/shale sequences of McMurray Formation.

To accomplish objectives of this research;

- Consequences of geological realizations, representative of shale/sand sequences of McMurray Formation are built using geostatistical techniques.
- To reach to the first objective of this research, multiple realizations are passed through coupled geomechanical flow simulation of SAGD process. Uncertainty analysis is performed on two output variables of flow, i.e. cumulative oil production (COP) and steam oil ratio (SOR), and one output variable of geomechanical response, i.e. vertical displacement profile (VDP) on top of reservoir.
- Equivalent elastic media (EEM) is defined as homogenized value which is representative of heterogeneous map of elastic property. Numerical approach to obtain EEM for complex sand/shale facies configuration, representative of McMurray Formation is proposed.
- To achieve the second objective of this research, the applicability of traditional techniques for determination of EEM is compared with a proposed numerical technique. EEM values obtained from traditional techniques have considerable difference with numerically determined EEM. It is shown that, for specific sand/shale percentile and by considering multiple equi probable geological realizations, assessing singular EEM value to these realizations is impractical and range of EEM values are determined.
- To resolve this issue, a ranking technique is proposed. In developing and formulating ranking criteria, main geometrical characteristics of geological realizations which have effect on expected elastic deformation of reservoir during SAGD process are considered. VDP is considered as

the geomechanical response of reservoir. To check applicability of proposed ranking technique, VDP's obtained from ranking technique should be checked with numerically determined VDP's. This step is done on 100 synthetic sand/shale facies which are built using geostatistical techniques and VDP's, obtained from ranking technique, are in acceptable ranking correlation with VDP's, obtained from numerical simulation. Considering proposed ranking technique in further coupled geomechanical flow simulation of SAGD helps to select few realizations out of many. In that manner analyzing uncertainty accompanied by heterogeneous elastic propagation and saving computational time, required for passing all geological realization through coupled geomechanical flow simulation of SAGD could be assessed simultaneously.

- To reach to the third objective of this research, a numerical local upscaling technique, developed for upscaling of permeability/transmissibility, is considered to develop numerical local upscaling technique applicable for upscaling of elastic properties. Considering complex facies configuration and anisotropic elastic deformation are two main advantages of this approach.
- Based on an available field data set, the applicability of proposed ranking measurement and upscaling technique are assessed.

No experimental research was conducted in this research as a sufficient body of geomechanical lab test results obtained by previous researchers was available for use in building geological models which were subsequently used for numerical simulation and up-scaling purposes of this research. Commercial simulators, STARS (©CMG) and FLAC (© ITASCA) are used for flow and geomechanical simulation process respectively.

BACKGROUND

Mechanical Earth Model (MEM)

A Mechanical Earth Model (MEM) is an integration process characterizing the area under study in terms of geomechanical parameters. A MEM could be defined for a well (1^D), for a field and/or for a reservoir (3^D). Standard outputs from a MEM are elastic properties, rock strength, pore pressure and in situ stress magnitudes and directions which are the main input for failure analysis. Comprehensive MEM realizations, including both petrophysical and rock mechanical properties, are geological models which should be used for coupled geomechanical flow simulation of SAGD process. Seismic section, logging data, core measurements and field tests are the main sources of data which might be used to build a MEM.

Elastic moduli properties are related to the sonic wave travel time and density logs with the following equations:

$$\upsilon = \frac{\frac{1}{2}\left(\frac{\Delta t_s}{\Delta t_c}\right)^2 - 1}{\left(\frac{\Delta t_s}{\Delta t_c}\right)^2 - 1}; \tag{1-1}$$

$$G = \frac{\rho_b}{\Delta t_s{}^2}; \tag{1-2}$$

$$E = 2G\,(1 + \upsilon); \text{ and} \tag{1-3}$$

$$K = \rho_b \left(\frac{1}{\Delta t_c{}^2} - \frac{4}{3\Delta t_s{}^2}\right). \tag{1-4}$$

in which;

ν: Poisson ratio

E: Young modulus

G: Shear modulus

K: Bulk modulus

ρ_b: Bulk density

Δt_s: Shear wave travel time

Δt_p: Compression wave travel time

Elastic properties which were obtained from wire line log analysis are termed as dynamic. Static datasets from laboratory core tests are used as geomechanical references and to calibrate a dynamic MEM.

Uniaxial compressive strength (UCS), tensile strength, friction and dilation angles are rock strength parameters considered in MEM. Various empirical correlations exist in literature from which rock strength parameters could be determined as a function of static elastic moduli, bulk density and compression/shear wave velocities.

In situ stresses are usually described by the overburden stress (σ_v), minimum horizontal stress (σ_h) and maximum horizontal stress (σ_H). These principle stresses are completely described by their magnitudes and directions.

A MEM is the core of any geomechanical work. In many complex drilling, completion and exploitation operations today, failure to understand a field's geomechanical behavior represents an expensive risk. Developing a consistent MEM can mitigate that risk and provide benefit throughout the life of the field.

Goodman and Connolly (2007) applied MEM to show that it provides a mean of recognizing the impact of subsurface uncertainty in well design in deepwater subsalt.

One of the main applications of MEM is to predict and therefore prevent sanding problem and casing collapse which is the result of compressive well bore failure in many oil and gas fields. Mechanical earth models should be constructed and used to evaluate potential for rock failure during production. Ohen (2003) applied a MEM to analyze these kinds of problems.

Hydraulic fracturing and acidizing are two types of well stimulation technology which are applied in sandstone formation and carbonate formation respectively to improve hydrocarbon recovery. In hydraulic fracturing mechanism, modeling geomechanical rock properties as accurate as possible is essential for ensuring a successful fracturing job design and execution. Al-Qahtani and Rahim (2001)

applied the concept of MEM and parameters included in MEM for Khuff and Pre-Khuff formations of Ghawar field which are deep gas condensate reservoirs to improve the efficiency of hydraulic fracturing mechanism applied on these formations.

Sayers et al. (2006) used MEM to quantify reservoir compaction, casing failure and surface subsidence for a deepwater Gulf of Mexico turbidite.

Qui et al. (2008) used calibrated and validated MEM to resolve problems related to production reduction, sand production and well bore stability of one of the oil fields in Libya.

Coupled Geomechanical Flow Simulation

Generally time coupling geomechanical fluid flow simulation process could be divided in to four main types; fully coupling (Du et al., 2005; Yin et al., 2009, to name a few), iterative coupling (Settari and Mourits, 1998; Tran et al., 2005a, to name a few), explicit coupling (Minkoff et al., 1999; Tran et al., 2005b, to name a few) and pseudo coupling (Tran et al., 2005b; Espinoza, 1983, to name a few). Each type of coupling has advantages and disadvantages, and each one is used depending on the kind of problem and engineers' point of view. A brief description of each method is mentioned here.

Fully coupled approach: This is the tightest coupling since reservoir pressure and temperature and deformation are solved simultaneously. The solution is reliable and can be used as a benchmark for other coupling approaches. However, this coupling is not widely used for large scale simulation since the solution is very time consuming, as it requires the simultaneous solution of the flow variables (pressure, saturations, composition, temperature) and the geomechanics variables (displacements, stresses and strains).

Iterative coupled approach: This coupling method is less tight than the fully coupling method since the geomechanics calculations are not performed at the same time as the reservoir flow calculations but one step behind. In this coupling, the information computed in the reservoir simulator and in the geomechanics module is exchanged back and forth. Therefore, the reservoir flow is affected by

the geomechanical responses. The main advantage of this coupling is its flexibility, i.e., the coupling between a reservoir simulator and a geomechanics module could be implemented without much modification to both codes.

Explicit coupled approach: This approach is considered as a special case of the iterative coupled approach. The information from a reservoir simulator is sent to a geomechanics module but the calculations in the geomechanics module are not fed back to the reservoir simulator. In this case the reservoir flow is not affected by the geomechanical responses calculated by the geomechanics module. However, the change in reservoir flow variables will affect the geomechanics variables. This coupling is also called a one-way coupling method.

Pseudo coupled approach: this approach is a simplified approach which modifies permeability and porosity by using permeability and porosity multipliers inside a reservoir simulator. These multipliers are user defined curves. This approach uses only a reservoir simulator.

Tran et al. (2009) compared these approaches according to accuracy, adaptability and running time speed aspects (Figure 1-2). By accuracy they meant that numerical coupling simulation results should be approximately the same as numerical results if one is available and by adaptability they meant that coupling between flow simulator and geomechanical simulator should be performed easily without large code changes and by running speed is significantly important in the case which millions of grid cells should be simulated. Fully coupling approach is strong in accuracy but weak in two other aspects. So it could be said that this coupling techniques seat in the corner of accuracy in this triangle. The iterative coupling works well in all three aspects and this methodology of coupling seats in the centre of this triangle and explicit (one way) coupling seats in the left side of this triangle in which adaptability and running speed are acceptable but accuracy is not good.

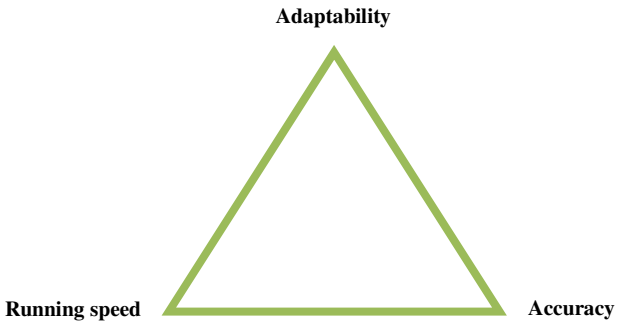

Figure 1-2 Balancing of coupling aspect (after Tran et al., 2009).

Ranking of Geostatistical Realizations

Geostatistical techniques are used to generate heterogeneous geological models. Exact determination of the true geological model is impossible. Constructing multiple equi probable geological models results in investigating geological uncertainty. By passing multiple equi probable MEM realizations through coupled geomechanical flow simulation process, influence of geological heterogeneity on production and geomechanical performance is investigated. In that way, geological uncertainties are transferred to dynamic, i.e. flow and geomechanical responses, uncertainties. Coupled geomechanical flow simulation, however, requires significant computational time and only few realizations can be passed through simulation process. Measuring specific characteristics of geological realizations which are in robust correlation with expected dynamic response of media and rank geological realizations based on that criteria, i.e. ranking technique, are not new idea in the field of petroleum engineering (Ballin et al., 1992).

The main objective of ranking in petroleum engineering is to find a simple statistical measurement in geological realization which is in good correlation with expected production performance. Generally ranking techniques are divided in two main groups (McLennan and Deutsch, 2005); static and dynamic techniques.

In static ranking techniques, statistical calculation of connectivity, conductivity, tortuosity and etc. are used to assign statistical measure to geological realizations.

Volumetric, statistical, global connectivity and local connectivity are some of the main static ranking techniques.

Volumetric ranking is the simplest class of ranking. Original oil in place (OOIP) is calculated in each realization via:

$$OOIP^{l} = \sum_{z=1}^{Z}\sum_{y=1}^{Y}\sum_{x=1}^{X} V_{(x,y,z)}.\left(1 - S^{l}_{w(x,y,z)}\right).\Phi^{l}_{(x,y,z)} \quad (1\text{-}5)$$

Where:

l: number of realization

$OOIP^{l}$: original oil in place for l^{th} realization

X, Y, Z: number of cells in east, north and elevation directions

x, y, z: 3D cell location

Φ: porosity

S_w: water saturation

V: volume of cell

In statistical ranking, average porosity (Equation 1-6.a), average permeability (Equation 1-6.b) and average water saturation (Equation 1-6.c), are used as ranking criteria:

$$\Phi^{l}_{\_avg} = \frac{\sum_{z=1}^{Z}\sum_{y=1}^{Y}\sum_{x=1}^{X}\Phi^{l}_{(x,y,z)}}{XYZ} \quad (1\text{-}6\ a)$$

$$K^{l}_{\_avg} = \frac{\sum_{z=1}^{Z}\sum_{y=1}^{Y}\sum_{x=1}^{X}K^{l}_{(x,y,z)}}{XYZ} \quad (1\text{-}6\ b)$$

$$S^{l}_{w\_avg} = \frac{\sum_{z=1}^{Z}\sum_{y=1}^{Y}\sum_{x=1}^{X} S^{l}_{w(x,y,z)}}{XYZ} \quad (1\text{-}6\ c)$$

Where:

$\Phi^{l}_{(x,y,z)}$: porosity of cell (x,y,z) in l^{th} realization

$K^{l}_{(x,y,z)}$: permeability of cell (x,y,z) in l^{th} realization

$S^{l}_{w(x,y,z):}$ water saturation of cell (x,y,z) in l^{th} realization

$\Phi^{l}_{\_avg}$: porosity average for l^{th} realization

$K^{l}_{\_avg}$: Permeability average for l^{th} realization

$S^{l}_{w\_avg}$: water saturation average for l^{th} realization

Although permeability doesn't average arithmetically, however, simplified arithmetic averaging are implemented in Equations 1-6 a, to 1-6 c.

Volumetric and statistical ranking may not be acceptable ranking for SAGD process. Efficiency of SAGD process is highly dependent on connection of the steam chamber to the surrounding reservoir. Therefore, the ranking measures must somehow account for connectivity. These have been applied both globally (Deutsch and Srinivasan, 1996) and locally (McLennan and Deutsch, 2005; Fenik et al., 2009; Wilde and Deutsch, 2012). In global connectivity the proportion of net reservoir that is connected within the drainage volume is calculated and consider as ranking criteria. This ranking technique works well only in relatively homogeneous reservoirs. McLennan and Deutsch (2005) extended global connectivity measurement by limiting calculation of connectivity to local window and named ranking measure as connected hydrocarbon volume (CHV) measurement. Fenik et al. (2009) extended the work of McLennan and Deutsch (2005) to consider those net locations outside of the local window which are visible from the producer by line of sight. Wilde and Deutsch (2012) modified work by Fenik et al. (2009) by considering; expected time and likelihood of production.

In dynamic ranking techniques, such as random walk, time of flight, tracer and streamline simulation techniques, numerical flow simulation is approximated by simplification of flow-physics. Although dynamic ranking received significant attention in the past few years, these techniques have some disadvantages in comparison to static ranking. Most importantly, dynamic ranking measures tend to depend heavily on the simplifying flow-physics approximations rather than the underlying geological heterogeneity and uncertainty (Gilman, 2005). In addition to that computational time required for dynamic ranking techniques approaches full numerical flow simulation (Saad et al., 1996).

In general, the focus of all previously developed ranking techniques are to find geological characteristics, which are in good correlation with expected flow response. For the current research, a ranking criteria is proposed which is in good correlation with expected elastic deformation of media during SAGD process.

Upscaling

Upscaling has become an increasingly important tool in recent years for converting a highly detailed geological model (fine scale models) to a simulation model (coarse scale models). A principle motivation for development of upscaling techniques has been the development of geostatistical reservoir description algorithms. These algorithms now routinely result in fine scale descriptions of reservoir properties on grids of tens of millions of cells. These reservoir description grids are far too fine to be used as grids in reservoir simulators.

Despite advances in computer hardware, most full field reservoir models still use fewer than 100000 cells, a factor of 100 down from the geological grid. Upscaling is needed to bridge the gap between these two scales (Durlofsky, 1991).

Dealing with coupled geomechanical flow simulation processes, in which heterogeneous models for both petrophysical and rock mechanical properties are considered, raises the importance of upscaling even more. In this scenario, both the flow responses and geomechanical responses obtained from simulation of the coarse model should honor responses obtained from the fine scale model with an acceptable range or error.

In the next following two subsections different techniques mentioned in the literature for up scaling of permeability (the most challenging petrophysical property for upscaling) and up scaling of elastic properties will be reviewed.

Permeability upscaling

Permeability upscaling techniques are generally divided in two groups; analytical (static) and numerical (pressure solver, dynamic) upscaling approaches.

Arithmetic, harmonic and geometric averaging are three types of analytical upscaling. A generalization of these averaging techniques is Power law averaging, developed by Deutsch (1989):

$$K_\omega = \left(\frac{1}{n}\sum_{i=1}^{n} k_i{}^{\omega}\right)^{1/\omega} \qquad (1\text{-}7)$$

In which:

ω: averaging power between -1 and 1

K_ω: averaged permeability

n: number of cells

k_i: permeability of each cell

In numerical techniques, effective permeability is calculated for a coarse block in such a manner that the flow response obtained for each block is the same as that obtained from the finer blocks.

Purely local, global, extended local and quasi-global (or local-global) are four main categories of numerical permeability upscaling techniques. In purely local (Durlofsky, 1991; Pickup et al., 1994) coarse scale parameters are computed by considering only the fine scale region corresponding to the target coarse block. In global (Tveito and Nielsen, 1998; Holden and Nielsen, 2000), the entire fine scale model is solved and the solution is used to extract coarse scale quantities. In extended Local (Gomez-Hernandez and Journel, 1994; Wen et al., 2003) coarse scale parameters are calculated by considering the fine scale region corresponding

to the target coarse block plus a fine scale border region around the target coarse block and in quasi-global (Christie and Blunt, 2001; Chen et al., 2003) instead of solving the fine scale model as in the global method, approximate solution of the global flow is obtained to provide appropriate boundary conditions which can then be used to calculate effective permeability using a procedure similar to that used in local or extended local methods, the difference being that instead of the standard constant pressure or periodic boundary conditions the boundary conditions are now informed by the approximate global flow solution.

Elastic property upscaling

The field of elastic properties upscaling is not studied very well in comparison to absolute/relative permeability upscaling. In the category of analytically upscaling (homogenizing) of elastic properties Mackenzie (1950) is one of the first authors who used a self-consistent model to determine homogenized elastic moduli of media composed of three phases. Hashin (1955), Backus (1962), Hill (1965), Budiansky (1965) and Salamon (1968) developed other analytical formulations. Although different assumptions are considered in these approaches, a common element is their consideration of a simplified configuration of phases (facies) which is typically a stratified configuration and may not be appropriate for complex facies configurations such as sand/shale facies configuration of McMurray Formation.

Numerical techniques for upscaling of elastic properties are not common. Elkateb (2003) proposed a mathematical expression for the determination of equivalent elastic moduli for a simplified layer cake model with isotropic elastic deformation.

In current research, new numerical upscaling approach is proposed. Considering transversely isotropic deformation and applicability of proposed numerical technique for complex facies configurations are two predominant advantages of the proposed technique.

SUMMARY OF EACH CHAPTER

Chapter 1: Introduction

This chapter contains the research objective and structure of thesis. In this chapter a review of relevant literature is provided. SAGD and geomechanical effect of SAGD, Mechanical Earth Model (MEM) concept, ranking techniques and upscaling techniques are main topics which are reviewed.

Chapter 2: Impact of Heterogeneous Geomechanical Properties on Coupled Geomechanical Flow Simulation of SAGD

In this chapter, ranges of uncertainties for cumulative oil production (COP), steam oil ratio (SOR) and vertical displacement profile (VDP) on top of reservoir for geological models in which rock mechanical properties are considered as heterogeneous models are compared with the cases in which this group of inherent properties is considered as homogeneous properties.

Chapter 3: Equivalent Elastic Media and Ranking of Geological Models Based on Geomechanical Response

This chapter includes two main sections. In the first part, new numerical approach for homogenization of elastic properties is proposed and accuracy of this approach is checked with traditional techniques. In the second part, a new ranking criterion is proposed.

Chapter 4: Numerical Local Upscaling of Elastic Properties

In this chapter and based on previously developed numerical upscaling of permeability/transmissibility, which has application in petroleum engineering and for fluid flow simulations, new numerical approach, named as local upscaling approach is developed for upscaling of elastic properties.

Chapter 5: Case Study

Development parts in last chapters are applied on one of Alberta oilsand reserves. For that purpose, first multiple high resolution geological realizations including both petrophysical and rock mechanical properties are built geostatistically. Then

by considering ranking criteria developed in chapter 3, one realization (P_{50}) is selected and passed through coupled geomechanical flow response by assuming elastic deformation in geomechanical simulation. Results obtained from this part are considered as truth models and compared with the results obtained from upscaled models, using numerical upscaling technique developed in chapter 4 and harmonic averaging technique.

Chapter 6: Conclusion and Recommendations for Future Studies

Outcomes of analysis performed in the previous chapters with general conclusions obtained from each of them are summarized in this chapter. Recommendations and suggestions for future works and continuation of this research are included at the end of this chapter.

REFERENCES

Agar, J.G., Morgenstern, N.R. and Scott, J.D. 1986. Shear strength and stress-strain behavior of Athabasca oil sand at elevated temperatures and pressures. Canadian Geotechnical Journal. 24: 1-10.

Al-Qahtani, M. Y. and Rahim, Z. 2001. A Mathematical Algorithm for Modelling Geomechanical Rock Properties of the Khuff and Pre-Khuff Reservoirs in Ghawar Field. Proceeding of SPE Middle East Oil Show, Bahrain, SPE No. 68194.

Azad, A. 2012. Rapid SAGD Simulation Considering Geomechanics for Closed Loop Reservoir Optimization. PhD dissertation, University of Alberta, Edmonton, Canada.

Backus, G. E. 1962. Long-wave elastic anisotropy produced by horizontal layering. Journal of Geophysical Research. 67(11): 4427-4440.

Ballin, P., Journel, A. and Aziz, K. 1992. Prediction of Uncertainty in Reservoir Performance Forecasting. Journal of Canadian Petroleum Technology. 31(4): 52-62.

Budiansky, B. 1965. On the elastic moduli of some heterogeneous materials. Journal of the Mechanics and Physics of Solids 13:223–227.

Butler, R.M. and Stephens, D.J. 1981. The gravity drainage of steam-heated heavy oil to parallel horizontal wells. Journal of Canadian Petroleum Technology. 20(2): 90-96.

Butler, R.M., McNab, G. S., and Lo, H.Y. 1981. Theoretical studies on the gravity drainage of heavy oil during Steam Heating. Canadian Journal of Chemical Engineering. 59: 455-460.

Butler, R.M., Stephens, D.J., and Weiss, M. 1980. The vertical growth of steam chambers in the in-situ thermal recovery of heavy oils. Proceeding of 30th Canadian Chemical Engineering Conference. 4: 1152-1160.

Chalaturnyk, R. 1996. Geomechanics of the Steam-Assisted Gravity Drainage Process in Heavy Oil Reservoirs. PhD dissertation, University of Alberta, Edmonton, Canada.

Chen, Y., Durlofsky, L., Gerritsen, J. M. and Wen, X. H. 2003. A coupled local-global upscaling approach for simulating flow in highly heterogeneous formations. Advances in Water Resources. 26:1041-1060.

Chow, L., and Butler, R. M. 1996. Numerical Simulation of the Steam-Assisted Gravity Drainage Process (SAGD). Journal of Canadian Petroleum Technology. 35(6): 55-62.

Deutsch, C. 1989. Calculating Effective Absolute Permeability in Sandstone/Shale Sequences. SPE Formation Evaluation. 4(3): 343-348.

Deutsch, C. and Srinivasan, S. 1996. Improved Reservoir Management through Ranking Reservoir Models. Proceeding of SPE/DOE Improved Oil Recovery Symposium, Tulsa, SPE No. 35411.

Du, J. and Wong, R.C.K. 2007. Coupled geomechanics-reservoir simulation of UTF phase A project using a full permeability tensor. Proceeding of the Petroleum Society's 8th Canadian International Petroleum Conference, 1-16.

Durlofsky, L. J. 1991. Numerical Calculation of Equivalent Grid Block Permeability Tensors for Heterogeneous Porous Media. Water Resources Research. 27(5): 699-708.

Dusseault, M. and Morgenstern, N.R. 1978. Shear strength of Athabasca oil sand. Canadian Geotechnical Journal 15: 216-238.

Elkateb, T. M. 2003. Quantification of Soil Heterogeneity. PhD dissertation, University of Alberta, Edmonton, Canada.

Espinoza, E.E. 1983. A New Formulation for Numerical Simulation of Compaction, Sensitivity Studies for Steam Injection. Proceeding of SPE Reservoir Simulation Symposium, San Francisco, California, SPE No. 12246.

Fenik, D.R., Nouri, A. and Deutsch, C. 2009. Criteria for ranking realizations in the investigation of SAGD reservoir performance. Proceedings of the Canadian International Petroleum Conference, Calgary, Canada, No.191.

Gilman, J., Meng, H., Uland, M., Dzurman, P. and Cosic, S. 2005. Statistical Ranking of Stochastic Geomodels Using Streamline Simulation: A Field Application. Proceeding of SPE Annual Technical Conference and Exhibition, San Antonio, Texas, SPE No. 77374.

Gomez-Hernandez, J. J. and Journel, A. G. 1994. Stochastic characterization of grid block permeability. SPE Formation Evaluation. 9:93-99.

Goodman, H.E. and Connolly, P. 2007. Reconciling Subsurface Uncertainty with the Appropriate Well Design using the Mechanical Earth Model (MEM) Approach. Proceeding of Nigeria Annual International Conference and Exhibition, Abuja, Nigeria, SPE No. 111913.

Hashin, Z. 1955. The moduli of an elastic solid reinforced by rigid particles. Bulletin of the Research Council of Israel. 5C:46–59.

Hill, R. 1965. A self-consistent mechanics of composite materials. Journal of the Mechanics and Physics of Solids. 13:213–222.

Holden, L. and Nielsen, B. F. 2000. Global upscaling of permeability in heterogeneous reservoirs: the Output Least Squares (OLS) method. Transport in Porous Media. 40: 115–143.

Ito, Y., and Suzuki, S. 1996. Numerical Simulation of the SAGD Process in the Hangingstone Oil Sands Reservoir. Proceeding of Annual Technical Meeting, Calgary, Canada.

Kosar, K.M., Scott, J.D. and Morgenstern, N.R. 1987. Testing to determine the geotechnical properties of oil sands. Proceeding of the 38th Annual Technical Meeting of the Petroleum Society of CIM, Calgary, Canada, 995-1010.

Law, D. H. S., Nasr, T. N., and Good, W. K. 2003. Field-Scale Numerical Simulation of SAGD Process With Top-Water Thief Zone. Journal of Canadian Petroleum Technology. 42(8): 32-38.

Li, P. 2006. Numerical simulation of the SAGD process coupled with geomechanical behavior. PhD dissertation, University of Alberta, Edmonton, Canada.

Mackenzie, J. 1950. The elastic constants of a solid containing spherical holes. Proceedings of the Royal Society London. 63(1): 2–11.

McLennan, J. and Deutsch, C. 2005. Ranking geostatistical realizations by measures of connectivity. Proceeding of SPE international thermal operations and heavy oil symposium, Calgary, Canada, SPE No. 98168.

Minkoff, S.E., Stone, C.M. Arguello, G., Bryant, S., Eaton, J., Peszynska, M. and, Wheeler, M. 1999. Staggered in Time Coupling of Reservoir Flow Simulation and Geomechanical Deformation: Step 1 – One Way Coupling. Proceeding of SPE Reservoir Simulation Symposium, Houston, Texas, SPE No. 51920.

Nielsen, B. F. and Tveito, A. 1998. An upscaling method for one-phase flow in heterogeneous reservoirs. A Weighted Output Least Squares (WOLS) approach. Computational Geosciences. 2: 93–123.

Ohen, H. A. 2003. Calibrated Wireline Mechanical Rock Properties Model for Predicting and Preventing Wellbore Collapse and Sanding. Proceeding of European Formation Damage Conference, The Hague, Netherlands, SPE No. 82236.

Oldakowski, K. 1994. Absolute Permeability of Oil Sands. PhD dissertation, University of Alberta, Edmonton, Canada.

Pickup, G.E., Ringrose, P.S. Jensen, J.L. and Sorbie, K.S. 1994. Permeability tensors for sedimentary structures. Mathematical Geology. 26(2): 227-250.

Qiu, K., Gherryo, Y. S., Shatwan, M. and Fuller, J. A. 2008. The Application of a Mechanical Earth Model on Rejuvenation of a Mature Field in Libya. Proceeding of IADC/SPE Asia Pacific Drilling Technology Conference and Exhibition, Jakarta, Indonesia, SPE No. 114633.

Saad, N., Maroongroge, V. and Kalkomery, C. 1996. Ranking Geostatistical Models Using Tracer Production Data. Proceeding of European 3-D Reservoir Modelling Conference, Stavanger, Norway, SPE No. 35494.

Salamon, M. 1968. Elastic moduli of a stratified rock mass. Journal of Rock Mechanics and Mining Sciences. 5:519–527.

Samieh, A.M. and Wong, R.C.K. 1997. Deformation of Athabasca oil sand at low effective stresses under varying boundary conditions. Canadian Geotechnical Journal. 34: 985–990.

Sayers, C. M., Boer, L. D., Lee, D. W., Hooyman, P. J. and Lawrence, R. P. 2006. Predicting Reservoir Compaction and Casing Deformation in Deepwater Turbidites using a 3D Mechanical Earth Model. Proceeding of First International Oil Conference and Exhibition, Cancun, Mexico, SPE No. 103926.

Scott, J.D., Proskin, S.A. and D.P. Adhikary. 1994. Volume and permeability changes associated with steam stimulation in an oil sands reservoir. Journal of Canadian Petroleum Technology. 33(7): 44-52.

Settari, A. and Mourits, F.M. 1998. A Coupled Reservoir and Geomechanical Simulation System. SPE Journal. 3(3): 219-226.

Settari, A., Walters, D.A. and Behie, G.A. 2001. Use of coupled reservoir and geomechanical modelling for integrated reservoir analysis and management. Journal of Canadian Petroleum Technology. 40(12): 55-61.

Touhidi-Baghini, A. 1998. Absolute Permeability of McMurray Formation Oil Sands at Low Confining Stresses. PhD dissertation, University of Alberta, Edmonton, Canada.

Tran, D., Nghiem, L. and Buchanan, L. 2005. An Overview of Iterative Coupling between Geomechanical Deformation and Reservoir Flow. Proceeding of SPE/PS-CIM/CHOA International Thermal Operations and Heavy Oil Symposium, Calgary, Canada, SPE No. 97879.

Tran, D., Nghiem, L. and Buchanan, L. 2005. Improved Iterative Coupling of Geomechanics With Reservoir Simulation. Proceeding of the SPE Reservoir Simulation Symposium, The Woodlands, USA, SPE No. 93244-MS.

Tran, D., Nghiem, L. and Buchanan, L. 2009. Aspects of Coupling between Petroleum Reservoir Flow and Geomechanics. Proceeding of 43rd U.S. Rock

Mechanics Symposium & 4th U.S. - Canada Rock Mechanics Symposium, Asheville, North Carolina, ARMA No. 09-89.

Wen, X. H., Durlofsky, L. J. and Chen, Y. 2005. Efficient three-dimensional implementation of local-global upscaling for reservoir simulation. Proceeding of the SPE Reservoir Simulation Symposium, Houston, USA, SPE No. 92965.

Wilde, B. and Deutsch, C. 2012. Calculating an Improved Connected Hydrocarbon Volume with Line-of-Sight for Ranking Realizations by SAGD Performance. Centre for Computational Geostatistics, Report 14, 205-1 – 205-7.

Yin, S., Dusseault, M.B. and Rothenburg, L. 2009. Thermal Reservoir Modeling in Petroleum Geomechanics. International Journal for Numerical and Analytical Methods in Geomechanics. 33: 449-485.

CHAPTER 2: IMPACT OF HETEROGENEOUS GEOMECHANICAL PROPERTIES ON COUPLED GEOMECHANICAL FLOW SIMULATION OF SAGD[1]

ABSTRACT

Geostatistical property models are commonly used for resource estimation and flow simulation but are rarely used to generate models of geomechanical properties for coupled geomechanical flow simulation. In a steam assisted gravity drainage (SAGD) process, geomechanical effects are known to have significant impact on reservoir performance due to changes in properties such as porosity, permeability and compressibility. Each geological realization is a combination of structural, facies, and property models. In the case of conventional flow simulation without consideration of geomechanical effects, petrophysical properties such as porosity, permeability and saturation are modeled. When coupling geomechanical and flow simulation, rock mechanical properties should be modeled stochastically to account for the uncertainty in geomechanical response.

In typical coupled geomechanical flow simulation, geomechanical property models are assumed to be a homogenous layer-cake model. However, processing multiple realizations of geomechanical properties allows for a more realistic assessment of reservoir uncertainty and ultimately improves decision making in cases where flow response is impacted by geomechanical effects.

In this chapter the consequences of assuming a layer-cake model for geomechanical properties on cumulative oil production (COP), steam oil ratios (SOR) and vertical displacement profiles (VDP) at the top of reservoir are quantified with numerical experiments. Consideration of heterogeneous models for both flow and geomechanical properties in coupled geomechanical flow simulation of SAGD results in a larger range of uncertainty for these three critical reservoir responses.

The importance of considering heterogeneous geomechanical properties is illustrated with synthetic data representative of the McMurray Formation in Alberta-Canada.

[1] A version of this chapter has been sent for publishing in Journal of Canadian Petroleum Technology.

INTRODUCTION

Canada has large heavy oil resources, which are mostly deposited in northern Alberta and Saskatchewan. Surface mining is used to extract and produce oil reserves close to the surface (<65m), however approximately 80% of the oil sands are below economical open pit mining depths (Butler, 1998). Deeper oil must be recovered with in situ recovery techniques including Steam Assisted Gravity Drainage (SAGD), Cyclic Steam Stimulation (CSS) and Vapor Extraction (VAPEX).With the exception of Imperial Oil's Cold Lake CCS operations, SAGD has been shown to be the most effective technique. In the SAGD process, two parallel horizontal wells are drilled in the formation, the first approximately 5m above the base of the reservoir and the second 4 to 6 meters above the first well. The upper well injects steam and the lower well collects the heated crude oil or bitumen that flows out of the formation along with any water from the condensation of injected steam.

Geomechanical effects on reservoirs have been shown to significantly impact SAGD performance (Chalaturnyk, 1996; Li, 2006; Azad, 2012, to name a few).Temperature and pore pressure changes in reservoirs alter effective stresses and cause deformation. This has a large effect on the sand facies and the thin shale barriers that are typically encountered in the McMurray Formation and can increase permeability by orders of magnitude (Oldakowski, 1994; Scott et al., 1994; Touhidi-Baghini, 1998). Modeling geomechanical processes is important for accurate prediction of reservoir performance and cap rock integrity; however, the scope of this work is limited to the effect of geomechanical dynamics on SAGD production performance.

Four main coupling approaches for integrating flow simulation and geomechanical simulation include: fully coupling (Du and Wong, 2005; Yin et al., 2009, to name a few); iterative coupling (Settari and Mourits, 1998; Tran et al., 2005a; Azad, 2012, to name a few); explicit coupling (Minkoff et al., 1999; Tran et al., 2005b, to name a few) and; pseudo coupling (Tran et al., 2005b; Espinoza, 1983, to name a few). Full coupling is the most realistic because reservoir

pressure, temperature and deformation are solved simultaneously. The solution is reliable and can be used as a benchmark for other coupling approaches. However, this coupling is not widely implemented for large scale simulation because the solution is computationally demanding and requires the simultaneous solution of flow variables (pressure, saturations, composition, temperature) and geomechanical variables (displacements, stresses and strains). Iterative coupling is less demanding as the geomechanical and flow calculations are not solved simultaneously. The information computed in the reservoir flow simulator and the geomechanics simulator is exchanged at user specified time intervals. Reservoir flow is affected by geomechanical responses but there is no requirement to simultaneously solve for all variables. A second advantage of this coupling is its flexibility; the coupling between a reservoir flow simulator and the geomechanics module can be implemented without modification as outputs from each simulator are used as inputs for the next time step. Explicit coupling is considered a special case of iterative coupling. Information from the reservoir flow simulator is sent to a geomechanics module but the calculations in the geomechanics module are not fed back to the flow simulator. Reservoir flow is not affected by the geomechanical responses calculated in the geomechanical simulation. However, the change in reservoir flow variables affects the geomechanical response. This coupling is also called one way coupling. Pseudo coupling is a simplified approach which modifies permeability and porosity by using permeability and porosity multipliers inside a reservoir simulator. These multipliers are user defined functions. Tran et al. (2009) compares these approaches according to accuracy, adaptability and CPU time. Accuracy is measured by comparing the results to analytical solutions. Adaptability is measured by a subjective degree of difficulty when implementing the techniques; methods that require little additional source code are preferred. Full coupling is accurate but not adaptable and requires significant CPU resources. Iterative coupling is a reasonable compromise and scores well by all measures. Explicit (one way) coupling has high adaptability and low CPU requirements but has low accuracy.

The geological structure of the McMurray Formation is fairly well understood; (Flach, 1984; Hein et al., 2000; Hein and Dolby, 2001, to name a few). This formation is not homogeneous and the major source of heterogeneity is due to differences in the rock properties of shale and sand facies (Figure 2-1).

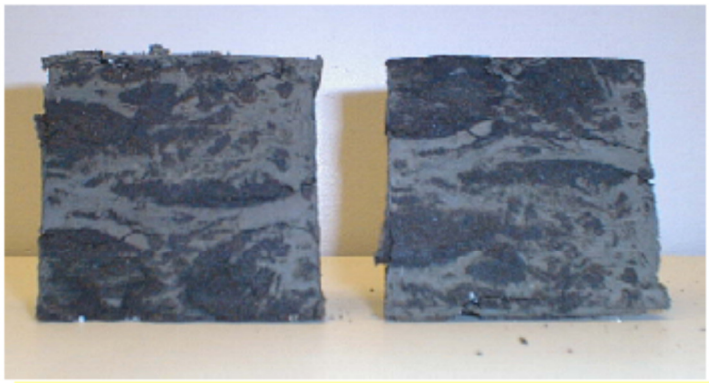

Figure 2-1 An example of complex sand/shale configuration in the McMurray Formation.

To improve the accuracy of SAGD performance prediction, detailed high-resolution stochastic facies models are built and used in numerical simulation. This probabilistic analysis allows for a quantification of the potential range of output variables (cumulative oil production (COP), steam oil ratio (SOR), and vertical displacement profile (VDP)) and results in improved decision making by assessing levels of risk and uncertainty. Rock mechanical properties play the same role for geomechanical governing equations as petrophysical properties play for fluid flow governing equations and have the same heterogeneous characteristics as petrophysical properties. The effect of the spatial distribution of facies and associated uncertainty in petrophysical properties on production performance of SAGD and other recovery methods is well studied (Meddaugh et al., 2011; Gotawala and Gates, 2010; Rashid et al., 2010, to name a few). The effect of rock mechanical heterogeneity has been investigated on a macro scale for some geotechnical engineering problems (e.g. Elkateb, 2003). However, uncertainty in reservoir performance as a result of uncertainty in rock mechanical properties has not been investigated.

The objective of this chapter is to investigate the importance of considering heterogeneous models for geomechanical properties during coupled geomechanical flow simulation of SAGD. Considering heterogeneous models for both petrophysical and rock mechanical properties has an effect on critical performance indicators such as COP, SOR and VDP at the top of the reservoir; this effect is quantified and compared to industry standard practice of homogeneous rock mechanical properties.

Synthetic data, which is deemed representative of the typical sand/shale spatial distribution of the McMurray Formation in Alberta-Canada, is considered for this case study.

GEOMECHANICAL BEHAVIOR OF OILSAND

Dusseault and Morgenstern (1978) reported oilsand structure as interlocked structure (Figure 2-2). Several geomechanical lab tests have been performed to determine the stress strain behavior of oil sand under different operating conditions. For low confining stresses, oil sand exhibits strain softening and dilation after yielding, while at higher confining stresses it becomes stiffer (hardening) and compressible (Wan, 1991).

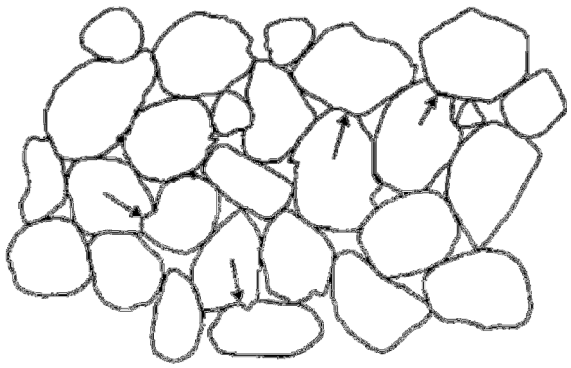

Figure 2-2 Interlocked structure of oil sand [after Dusseault and Morgenstern, 1978].

Critical state theory and associated critical state models, such as the Cam-Clay model would be appropriate for describing this kind of mechanical behavior. For simplicity, in this work an elastic-perfectly plastic Mohr-Coulomb failure

criterion is assumed. Before failure, oil sand behavior is controlled by elastic theory using bulk and shear modulus elastic parameters. After yielding, the material is assumed to behave perfectly plastic.

Dilation and associated volumetric strain are calculated based on the associated and non-associated flow rule. In the non- associated flow rule (used here), the potential function is not the same as the yield function. The potential function in the non-associated flow rule is described by the dynamic dilation angle to address change of dilation and associated volumetric strain.

GEOMECHANICAL BEHAVIOR OF SHALE

Inter bedded shale (IBS) behaves as a strain softening material similar to oil sand (Oldakowski, 2007; Oldakowski, 2008; Oldakowski, 2009). Dilation is observed for low confining stresses and decreases significantly at higher confining stresses. An elastic-perfectly plastic Mohr-Coulomb constitutive model with a non-associated flow rule for controlling dilation and associated volumetric strain is assumed for IBS like sand facies as well.

PERMEABILITY VARIATION OF OILSAND AS A RESULT OF GEOMECHANICS

Oldakowski (1994), Scott et al. (1994) and Touhidi-Baghini (1998) conducted a series of lab experiments to characterize the relationship between permeability changes and geomechanical response. In particular, an increase in absolute permeability of 30% to 50% may occur in cold regions of the reservoir in front of the growing steam chamber (Chalaturnyk, 1996).

The results of experimental work by Touhidi-Baghini, (1998) are used for updating the permeability of sand. When oil sand experiences contraction in the beginning of shearing, there is no change in absolute permeability. As contraction increases, shear induced dilation occurs and the permeability increase is a function of volumetric strain:

$$\ln \frac{K}{K_0} = C\, \varepsilon_v \tag{2-1}$$

In which:

K: updated Permeability

K_0: initial Permeability

ε_v: volumetric strain

Based on data analysis obtained from Touhidi-Baghini (1998), for vertical cores in Equation (2-1), C is 17.5 and for horizontal core it is 9.1.

Permeability variation of shale as a result of geomechanics

Series of lab experiments has been done to investigate effect of change in shale permeability as a result of steam chamber growth (Oldakowski, 2007; Oldakowski, 2008; Oldakowski, 2009, to name a few). In this study, it is assumed that when shale fails, permeability increases to 100 mD but remains constant after failure.

$$\text{Shale Permeability} = \begin{cases} \text{Constant} & \text{Before Failure} \\ 100\ \text{mD} & \text{After Failure} \end{cases} \tag{2-2}$$

POROSITY VARIATION OF OILSAND AND SHALE AS A RESULT OF GEOMECHANICS

Porosity for both shale and sand facies is updated via the following equation;

$$\Phi = \frac{\Phi_0 + \varepsilon_v}{1 + \varepsilon_v} \tag{2-3}$$

In which:

Φ: updated porosity

Φ_0: initial porosity

COUPLING FLOW AND GEOMECHANICS

Iterative coupling is considered to investigate the effect of geomechanics during SAGD. Temperature and pressure effect on stress redistribution, deformation of media, ground heave and change in inherent properties such as porosity and permeability. Schematic of iterative coupling is shown in Figure 2-3. STARS (CMG®) for flow simulation and FLAC (ITASCA®) for geomechanical simulation are used. Petrophysical properties, (porosity and permeability) are updated after each time step. In each time step STARS is run first and temperature and pressure profiles determined and transferred to FLAC (Figure 2-3). Volumetric strain is used to update porosity and permeability from Equations 2-1 through 2-3.

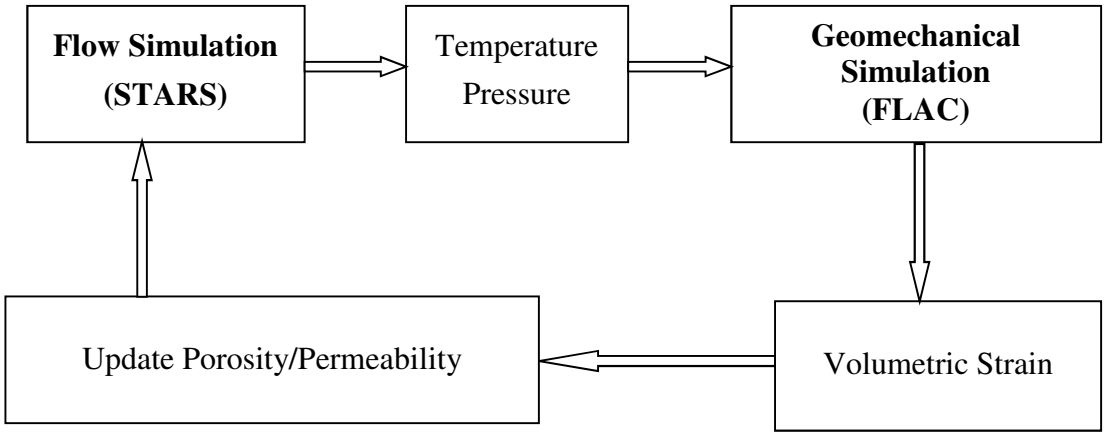

Figure 2-3 Iterative coupling process.

MODEL DESCRIPTION

To decrease boundary effects, model dimensions considered for geomechanical simulation are typically 3 to 4 times larger than the dimensions considered for flow analysis. In addition to the common reservoir section, an additional depth above and below the reservoir (over burden and under burden) and side burden are considered in the geomechanical model (Figure 2-4).The reservoir section is the only area considered for coupled geomechanical flow analysis, thus, a coarser gird is considered for the under, over and side burden. Table 2-1 provides the model dimension used in this study.

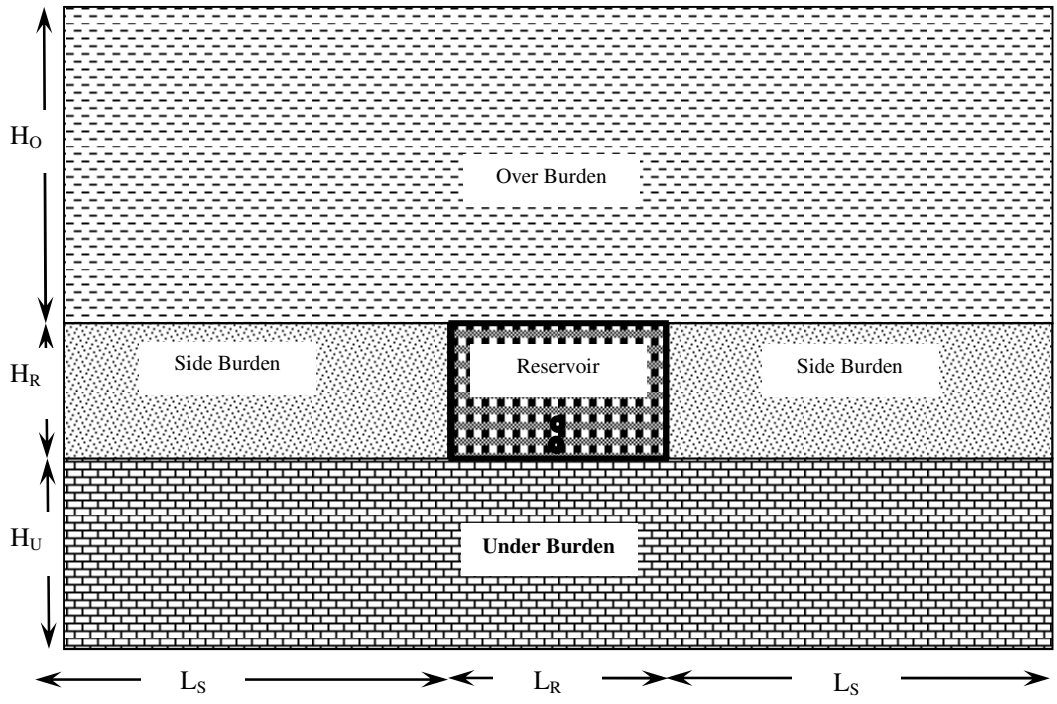

Figure 2-4 Model description.

Table 2-1 Model dimension and grid density information.

Section	Length (m)	Height (m)	Number of cells in X	Number of cells in Y
Underburden	400 ($2L_S+L_R$) *	50 (H_U)	70	5
Reservoir	100 (L_R*)	20 (H_R)	50	40
Sideburden (each)	150 (L_S)	20 (H_R)	10	40
Overburden	400 ($2L_S+L_R$)	140 (H_O)	70	10

* L_S and L_R are shown in Figure 2-4.

The boundary conditions are a fixed horizontal displacement on all sides and fixed vertical displacement at the bottom of the model. In situ stress configurations (i.e. magnitudes and directions) have a significant effect on the optimization of injection pressure to prevent cap rock instability, maximum dilatancy of reservoir, and well orientation to maximize SAGD performance. The selected minimum and maximum horizontal stresses, pore pressure and vertical stress are based on Collins, (2002) and summarized in Table 2-2. According to Azad, (2012) and Li, (2006), higher injection pressures result in larger geomechanical effects. By considering initial stress values (Table 2-2), 1500 KPa has been selected for the maximum steam injection pressure, which is assumed to be below the cap rock fracture gradient.

Table 2-2 Initial stress, pore pressure and temperature [After Collins (2002)].

Parameter	Value
Reservoir Depth	150 m
σ_h/σ_v	1
σ_H/σ_v	1.5
Initial reservoir pressure	650 KPa
Initial reservoir temperature	10 ˚C

Well spacing (distance between injector and producer) of 5 m, vertical to horizontal permeability ratio of 0.5, steam quality of 95%, initial reservoir pressure of 650 kPa, initial reservoir temperature of 10°C, preheating period of 100 days, and well radius of 0.1 m are assumed. Relative permeability curves and variation of oil viscosity by temperature are shown in Figure 2-5.

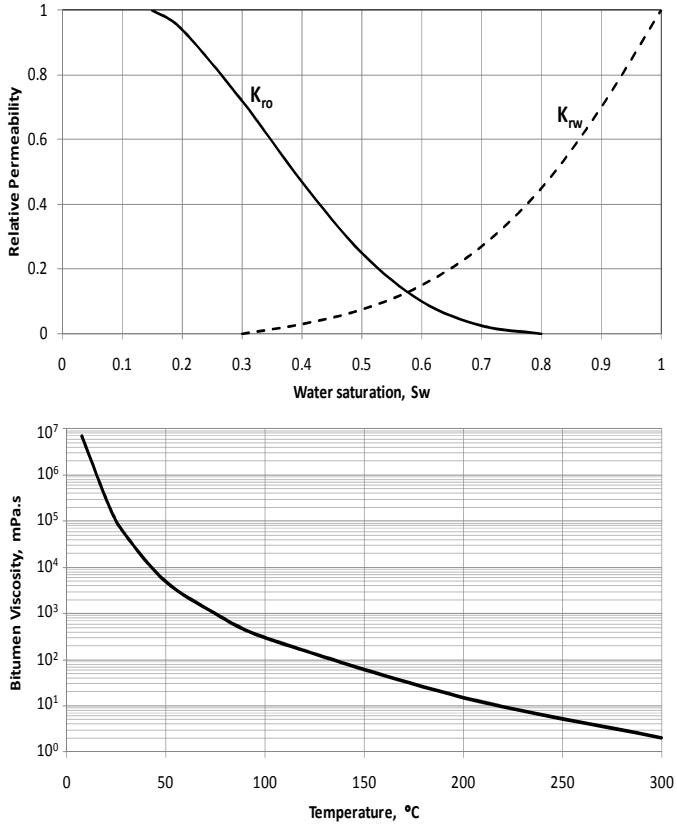

Figure 2-5 Relative permeability (top) and variation of viscosity by temperature (bottom) [after Chalaturnyk (1996)].

PETROPHYSICAL AND ROCK MECHANICAL PROPERTIES

The focus of this study is to investigate the effects of heterogeneous geomechanical property models on reservoir response using coupled geomechanical flow simulation. Porosity, permeability and saturations are required for flow simulation and elastic (bulk and shear modulus) and rock strength parameters (friction angle, dilation angle and cohesion) are required for geomechanical simulation.

The reservoir is the only area in the model (Figure 2-4) common between the two simulators. Multiple representative facies and property models, typical of the McMurray Formation are built to assess the effect of heterogeneity in geomechanical properties on reservoir performance. Sequential indicator simulation (SIS) is used to build several sand/shale models with 20% shale. Unconditional sequential Gaussian simulation (SGS) with a specified mean and standard deviation for each property (Tables 2-3 and 2-4) is used to generate the required property models. Figure 2-6 shows one facies, petrophysical and rock mechanical property models used for coupled geomechanical flow simulation.

Table 2-3 Mean, SD, minimum and maximum cut-offs of attributes considered for oil sand.

Property	Mean	Standard Deviation (SD)	Minimum Cut-Off	Maximum Cut-Off
Bulk Modulus (MPa)	700	80	500	900
Shear Modulus (MPa)	320	30	250	400
Friction angle (˚)	60	7	40	75
Dilation angle (˚)	20	3	15	25
Horizontal Permeability (mD)	4000	450	2500	5000
Porosity	0.32	0.04	0.25	0.4
Oil Saturation	0.85	0.05	0.75	1.00

Table 2-4 Mean, SD, minimum and maximum cut-offs of attributes considered for shale.

Property	Mean	Standard Deviation (SD)	Minimum Cut-Off	Maximum Cut-Off
Bulk Modulus (MPa)	300	50	150	450
Shear Modulus (MPa)	140	20	80	180
Friction angle (˚)	30	7	10	50
Dilation angle (˚)	7	2	4	10
Cohesion (kPa)	550	50	400	700
Horizontal Permeability (mD)	0.0001	0.0001	0.00005	0.0002
Porosity	0.01	0.005	0.005	0.02
Oil Saturation	0.01	0.005	0.005	0.02

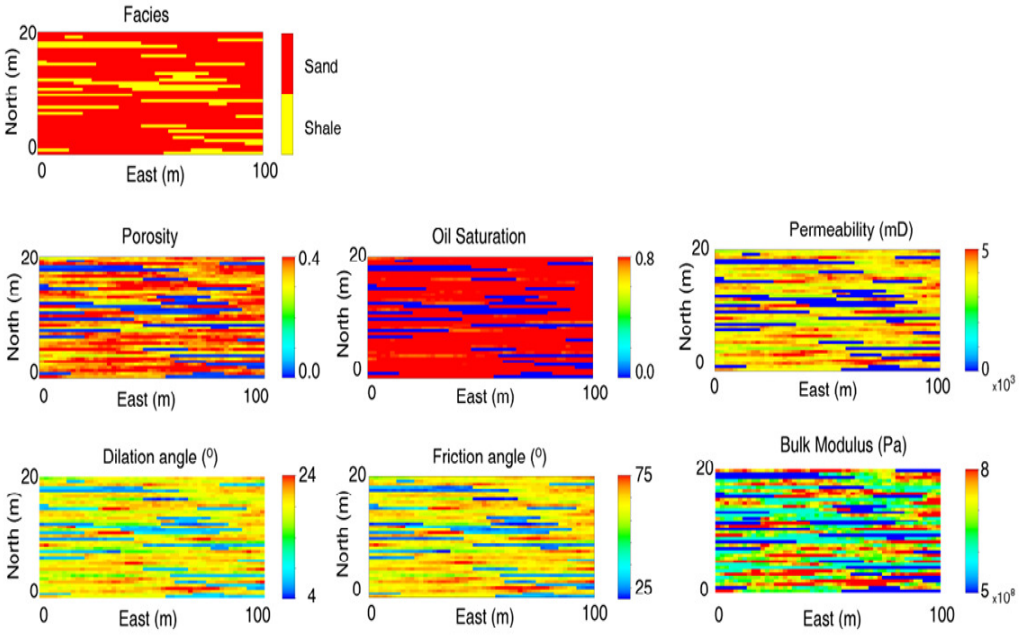

Figure 2-6 One realization.

The under, over and side burdens are considered homogeneous and elastic. Rock mechanical properties considered for these sections are summarized in Table 2-5. In addition to the rock mechanical properties required for geomechanical simulation, other constants are required for flow simulation (Table 6). The

information provided in Tables 2-5 and 2-6 are obtained from Chalaturnyk, (1996) and Li, (2006).

Table 2-5 Rock parameters used in geomechanical simulator [after Chalaturnyk, (1996) and Li, (2006)].

Zone	Parameter	Value
Overburden	Bulk Density (Kg/m^3)	2200
	Bulk Modulus (MPa)	208
	Shear Modulus (MPa)	96.2
	Linear Thermal Expansion coefficient ($^\circ K^{-1}$)	2×10^{-5}
Side Burdens	Bulk Density (Kg/m^3)	2200
	Bulk Modulus (MPa)	620
	Shear Modulus (MPa)	286
	Linear Thermal Expansion coefficient ($^\circ K^{-1}$)	2×10^{-5}
Under Burden	Bulk Density (Kg/m^3)	2200
	Bulk Modulus (MPa)	4167
	Shear Modulus (MPa)	1923
	Linear Thermal Expansion coefficient ($^\circ K^{-1}$)	2×10^{-5}

Table 2-6 Rock parameters used in flow simulator [after Chalaturnyk (1996) and Li (2006)].

Parameter	Value
Rock Compressibility (1/KPa)	5×10^{-6}
Rock Expansion Coefficient ($^\circ C^{-1}$)	3.84×10^{-5}
Rock Heat Capacity (KJ/Kg$^\circ$K)	1865
Rock Thermal Conductivity (W/m$^\circ$K)	1.736

In Appendix A one STARS input data file (Appendix A-1) and one FLAC input data file (Appendix A-2) are shown. Porosity and permeability files in STARS input data file are not fixed and updated based on geomechanical effect on these properties at the end of each time step. List of all other parameters which are not listed in above Tables but required for flow and geomechanical simulations process could be found in Appendix A-1 and A-2 respectively.

RESULTS

Permeability/porosity variations of different realizations

Changes in porosity and permeability due to geomechanical responses impact reservoir performance, i.e. COP and SOR. Figure 2-7 shows steam chamber growth for two realizations which result in minimum and maximum range of uncertainties for COP and SOR.

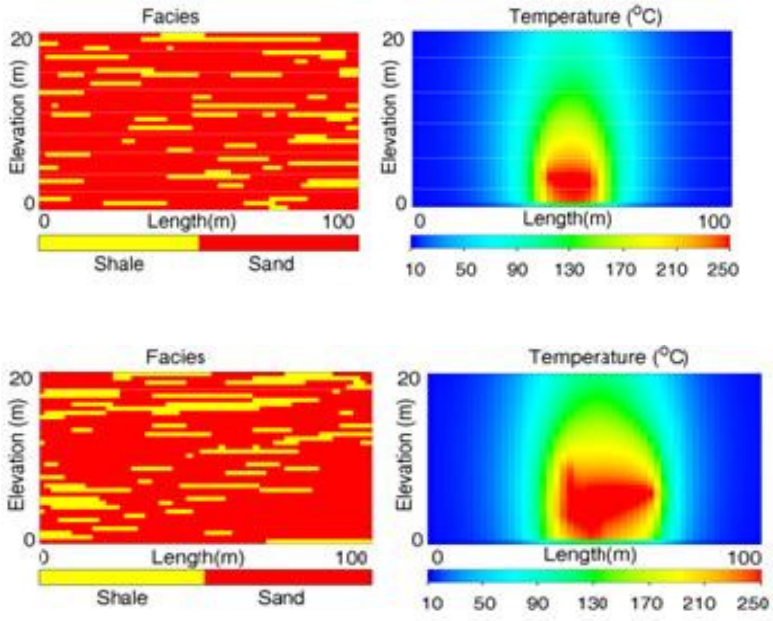

Figure 2-7 Facies (left) and steam chamber after 1000 days (right) for minimum (top) and maximum (bottom) range of COP uncertainties

The spatial distribution of low permeability shale effects the propagation of the steam chamber. Change in temperature and pressure fronts should be considered for geomechanical simulation. Considering heterogeneous petrophysical properties is a common approach in oil and gas industry however considering comprehensive geological models, which include both petrophysical and rock mechanical properties, is not common for coupled geomechanical flow simulation of SAGD. In the following section the effect of geomechanical parameter heterogeneity on ranges of uncertainties for COP, SOR and VDP is investigated.

Effect of considering heterogeneous geomechanical properties

To investigate how heterogeneity in geomechanical parameters affects SAGD performance, two cases for property models are considered:

a) Heterogeneous petrophysical and rock mechanical properties

b) Heterogeneous petrophysical and homogeneous rock mechanical properties (industry standard)

To assess the effect of heterogeneous properties on flow response it is necessary to analyze several realizations. In Figures 2-8 through 2-10 the minimum and maximum ranges of COP, SOR and displacement profiles obtained from simulating 100 realizations of case a) and b) are compared. The COP, SOR and VDP uncertainty increase when considering heterogeneous flow and geomechanical properties (Figure 2-11).

Coupled geomechanical flow simulation should be considered with all variables modeled stochastically to properly assess the expected range of uncertainty in reservoir response.

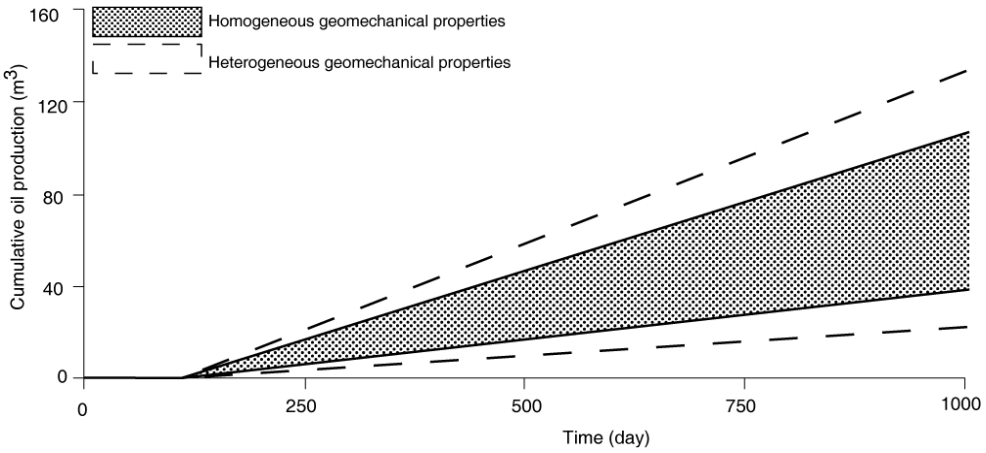

Figure 2-8 COP responses for case a) and case b); effect of considering heterogeneous geomechanical properties.

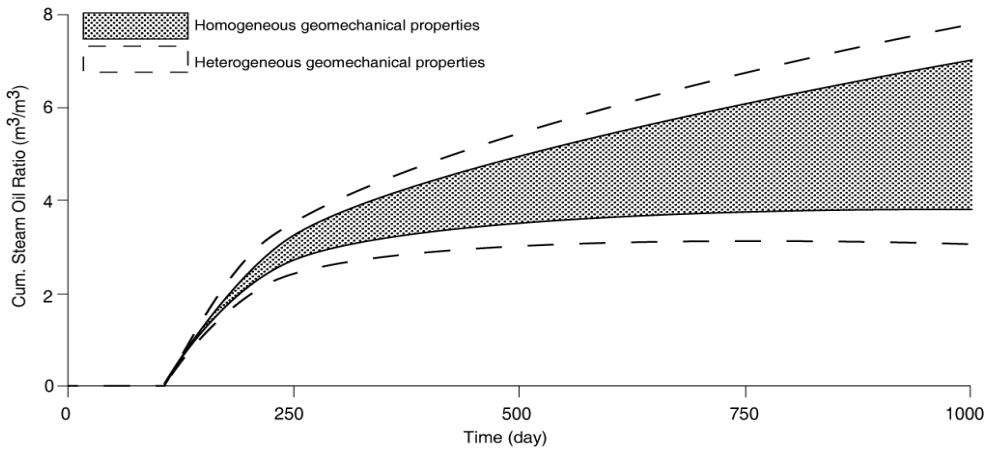

Figure 2-9 SOR responses for case a) and case b); effect of considering heterogeneous geomechanical properties.

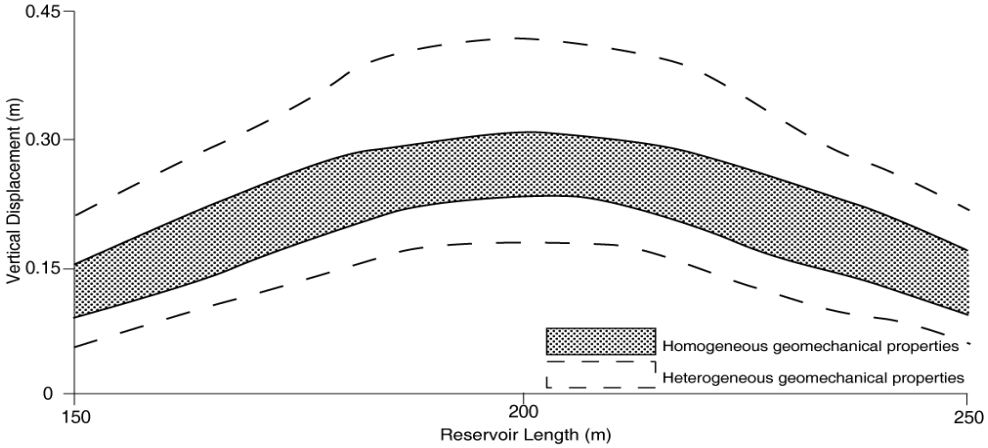

Figure 2-10 VDP responses for case a) and case b); effect of considering heterogeneous geomechanical properties.

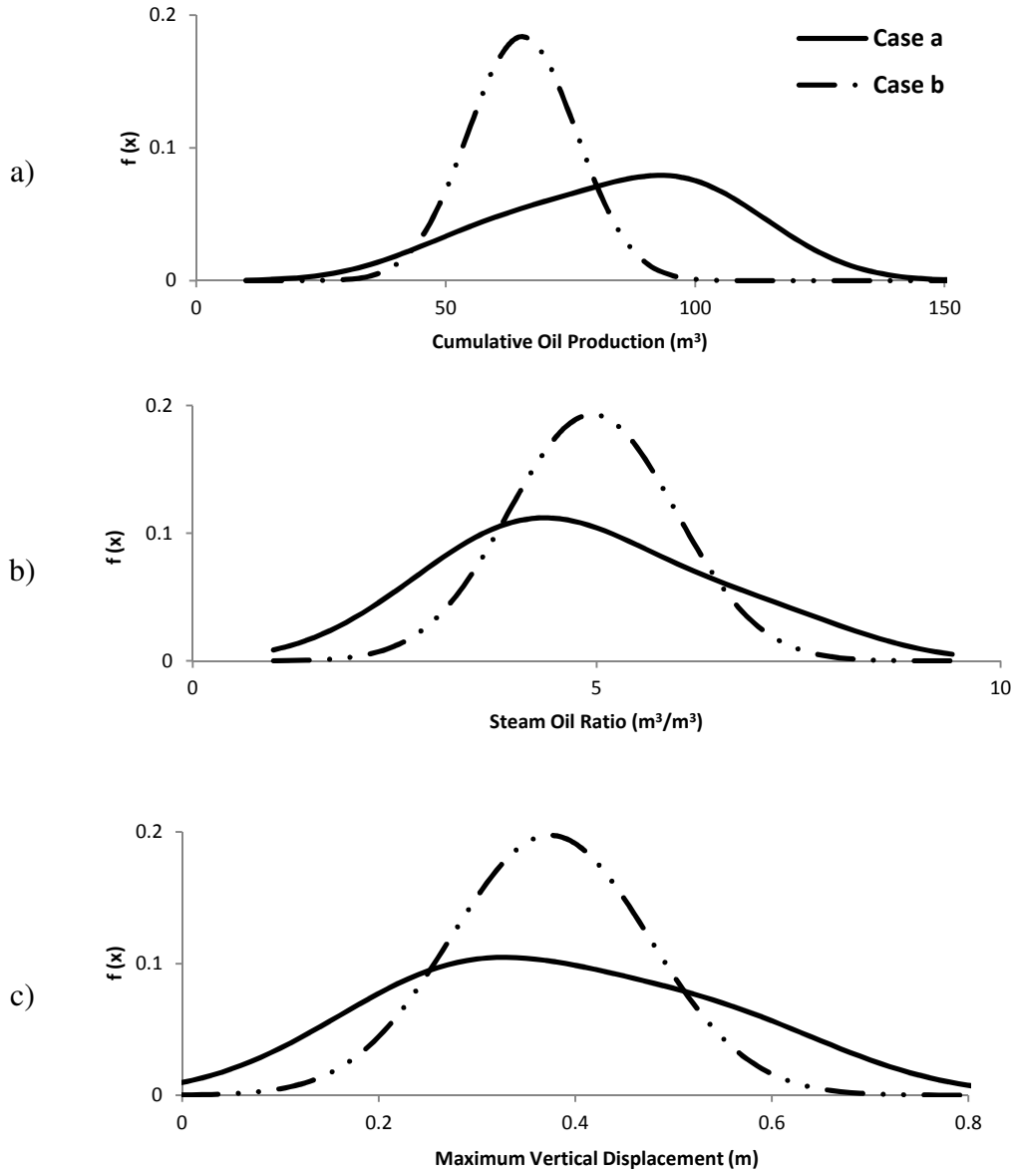

Figure 2-11 Smoothed Probability Distribution Functions of COP (a), SOR (b) and maximum vertical displacement (c).

DISCUSSION AND CONCLUSIONS

The impact of heterogeneous rock mechanical properties in coupled geomechanical flow simulation of SAGD was quantified. The range of COP,SOR and VDP considering heterogeneous models for petrophysical and rock mechanical properties was compared to the range of uncertainties obtained considering the industry standard practice of heterogeneous petrophysical and

homogeneous rock mechanical properties. The difference between these ranges is attributed to the effect of considering rock mechanical heterogeneity. The main conclusions obtained from this are:

- The effect of heterogeneous rock mechanical models when assessing SAGD performance, COP and SOR, should not be ignored.
- No general correlation could be made between range of uncertainties of two cases in which rock mechanical properties consider as homogeneous and heterogeneous models. To investigate uncertainty analysis in more accurate manner it is necessary to consider both petrophysical and rock mechanical property models as heterogeneous models.
- The effect of heterogeneous petrophysical models on SAGD performance, COP and SOR, is larger than the effect of heterogeneous rock mechanical models. This is expected as porosity and permeability directly relate to expected oil production.
- The VDP is more sensitive to heterogeneous rock mechanical models. This is expected as VDP is directly related to rock mechanical variables.
- In the case of investigating coupled geomechanical flow simulation of SAGD both flow and geomechanical responses were analyzed. Heterogeneous property models for both groups of parameters should be considered in order to properly assess the full range of uncertainty expected in SAGD performance.

It is recommended that multiple realizations spanning the uncertainty in geomechanical properties are jointly processed with similar petrophysical property models. There are computational restrictions in domain size when considering geomechanical simulation at the same scale as current flow simulation; regardless, it is important to understand the consequences of assuming a layer-cake model for geomechanical variables, the effect of geomechanical properties on SAGD performance prediction is not negligible.

REFERENCES

Azad, A. 2012. Rapid SAGD Simulation Considering Geomechanics for Closed Loop Reservoir Optimization. PhD dissertation, University of Alberta, Edmonton, Canada.

Butler, R. 1998. SAGD Comes of AGE. Journal of Canadian Petroleum Technology. 37(7): 9-12.

Chalaturnyk, R.J. 1996. Geomechanics of the Steam-Assisted Gravity Drainage Process in Heavy Oil Reservoirs. PhD dissertation, University of Alberta, Edmonton, Canada.

Collins, P.M. 2002. Injection Pressures for Geomechanical Enhancement of Recovery Process in the Athabasca Oil Sands. Proceeding of SPE International Thermal Operations and Heavy Oil Symposium and International Horizontal Well Technology Conference, Calgary, Canada, SPE No. 79028.

Dusseault, M., and N. Morgenstern. 1978. Shear strength of Athabasca oil sand. Canadian Geotechnical Journal. 15: 216-238.

Du, J. and Wong, R.C.K. 2005. Development of a Coupled Geomechanics-Thermal Reservoir Simulator Using Finite Element Method. Proceeding of Canadian International Petroleum Conference (CIPC), Calgary, Canada, 2005-027.

Elkateb, Tamer. 2003. Quantification of Soil Heterogeneity. PhD dissertation, University of Alberta, Edmonton, Canada.

Espinoza, E.E. 1983. A New Formulation for Numerical Simulation of Compaction, Sensitivity Studies for Steam Injection. Proceeding of SPE Reservoir Simulation Symposium, San Francisco, USA, SPE No. 12246.

Flach, P.D. 1984. Oil Sands Geology – Athabasca Deposit North, Alberta Research Council Bulletin 46, 31 p.

Gotawala, D. R. and Gates, I. D. 2010. On the Impact of Permeability Heterogeneity on SAGD Steam Chamber Growth. Natural Resources Research. 19(2):151-164.

Hein, F.J., Cotterill, D.K. and Berhane, H. 2000. An Atlas of Lithofacies of the McMurray Formation Athabasca Oilsands Deposit, North Alberta: Surface and Subsurface, Alberta Geological Survey, Earth Sciences Report.

Hein, F.J., and Dolby, G. 2001. Regional lithostratigraphy, biostratigraphy and facies models, Athabasca oil sand deposit, northeast Alberta. Canadian Society of Petroleum Geologists, Program with Abstracts, Rock the Foundation Convention, Abstract 25.

Li, P. 2006. Numerical Simulation of the SAGD Process Coupled With Geomechanical Behaviour. PhD dissertation, University of Alberta, Edmonton, Canada.

Meddaugh, W., Osterloh, W., Toomey, N., Bachtel, S. and Champenoy, N. 2011. Impact of Reservoir Heterogeneity on Steamflooding, Wafra First Eocene Reservoir, Partitioned Zone (PZ), Saudi Arabia and Kuwait. Proceeding of SPE Heavy Oil Conference and Exhibition, Kuwait City, Kuwait, SPE No. 150606.

Minkoff, S.E., Stone, C.M. Arguello, G., Bryant, S., Eaton, J., Peszynska, M. and, Wheeler, M. 1999. Staggered in Time Coupling of Reservoir Flow Simulation and Geomechanical Deformation: Step 1 – One Way Coupling. Proceeding of SPE Reservoir Simulation Symposium, Houston, USA, SPE No. 51920.

Oldakowski, K. 1994. Absolute Permeability of Oil Sands. PhD dissertation, University of Alberta, Edmonton, Canada.

Oldakowski, K. 2007. Permeability Changes of Inter-bedded Shale during SAGD Operation- Part I. AACI Report 0708-2.

Oldakowski, K. 2008. Permeability Changes of Inter-bedded Shale during SAGD Operation- Part II. AACI Report 0708-12.

Oldakowski, K. 2009. Permeability Changes of Inter-bedded Shale during SAGD Operation- Part III. AACI Report 0809-13.

Rashid, B., Bal, A., and Williams, G. 2010. Quantifying the Impact of Permeability Heterogeneity on Secondary Recovery Performance. Proceeding of SPE Annual Technical Conference and Exhibition, Florence, Italy, SPE No. 135125.

Scott, J.D., Proskin, S.A. and D.P. Adhikary. 1994. Volume and permeability changes associated with steam stimulation in an oil sands reservoir. Journal of Canadian Petroleum Technology. 33(7): 44-52.

Settari, A. and Mourits, F.M. 1998. A Coupled Reservoir and Geomechanical Simulation System. SPE Journal 3(3): 219-226.

Touhidi-Baghini, A. 1998. Absolute Permeability of McMurray Formation Oil Sands at Low Confining Stresses. PhD dissertation, University of Alberta, Edmonton, Canada.

Tran, D., Nghiem, L. and Buchanan, L. 2005. An Overview of Iterative Coupling between Geomechanical Deformation and Reservoir Flow. Proceeding of SPE/PS-CIM/CHOA International Thermal Operations and Heavy Oil Symposium, Calgary, Canada, SPE No. 97879.

Tran, D., Nghiem, L. and Buchanan, L. 2005. Improved Iterative Coupling of Geomechanics With Reservoir Simulation. Proceeding of the SPE Reservoir Simulation Symposium, The Woodlands, USA, SPE No. 93244-MS.

Tran, D., Nghiem, L. and Buchanan, L. 2009. Aspects of Coupling between Petroleum Reservoir Flow and Geomechanics. Proceeding of 43rd U.S. Rock Mechanics Symposium & 4th U.S. - Canada Rock Mechanics Symposium, Asheville, North Carolina, ARMA No. 09-89.

Wan, R. G. 1991. A Constitutive Model for the effective Stress-Strain Behaviour of Oil Sands. Journal of Canadian Petroleum Technology. 30(4): 89-98.

Yin, S., Dusseault, M.B. and Rothenburg, L. 2009. Thermal Reservoir Modeling in Petroleum Geomechanics. International Journal for Numerical and Analytical Methods in Geomechanics. 33: 449-485.

CHAPTER 3: RANKING OF GEOLOGICAL REALIZATIONS BASED ON GEOMECHANICAL RESPONSE OF SAGD[1]

ABSTRACT

Using coupled geomechanical flow simulation to predict steam assisted gravity drainage (SAGD) performance requires a balance between computational time and grid resolution. It has been shown that the heterogeneity of rock mechanical properties is important for performance prediction; however, coupled geomechanical flow simulation requires significant computational time for fine grids. A methodology for upscaling elastic properties is proposed. Coarser grids can then be used in geomechanical simulation allowing for the processing of multiple realizations to explore uncertainty in reservoir response.

Accurately homogenizing elastic properties to determine an equivalent elastic media (EEM) that results in the same model responses is explored. The proposed methodology is to minimize the difference in the model response (vertical displacement profile) between the heterogeneous model and a homogeneous value; however, it is not possible to calculate this equivalent value for all geostatistical realizations necessary to understand the uncertainty in the reservoir, often 100 realizations are considered. A ranking methodology is used to predict the geomechanical response, elastic deformation only, of each realization which mimics the SAGD process and quickly predicts the expected geomechanical response of the realization. The realizations are ranked and specific quantiles (often the P_{10}, P_{50} and P_{90}) can be analyzed with the proposed EEM methodology or with full geomechanical simulation depending on model size.

Examples are presented that are representative of the complex sand/shale configuration of the McMurray Formation in Alberta-Canada. The ranking methodology has a correlation of 0.87 with the geomechanical response. While the ranking predicts which realizations will have more or less deformation, the magnitude of deformation is not predicted. Geomechanical simulation and EEM analysis is required after selecting the desired realizations based on the ranking.

[1] A version of this chapter has been sent for publishing in SPE Reservoir Evaluation and Engineering-Reservoir Engineering.

INTRODUCTION

Alberta's oil sands contain the largest crude bitumen resource in the world, having approximately 259 billion cubic meters of oil in place (AEUB, 2003). About 20% of these deposits can be surface mined as the resource is shallow resulting in a significant resource that can only be economically produced using in situ recovery methods.

The most common in situ recovery technology is the SAGD process. This recovery process was field tested at the Underground Test Facility (UTF) near Fort McMurray-Alberta through different phases of pilot operation and is now in a commercial stage of production in Western Canadian oil sands (Edmunds et al., 1989; Komery et al., 1993; and Butler, 2001).

In this process, two horizontal wells separated by a small vertical distance are placed near the bottom of the formation. The top horizontal well is used to inject steam and the bottom well is used to collect the produced liquids, i.e. formation water, condensate, and oil.

Numerical flow simulation is used to optimize and predict SAGD reservoir performance. A geological model that captures the heterogeneity of the various sand and shale facies is required as they have very different flow and stress responses. There is insufficient well and seismic data to deterministically model these facies and multiple heterogeneous geological realizations are often used to explore potential uncertainty in flow simulation. This results in a probabilistic analysis where uncertainty in future reservoir production can be characterized and better reservoir management decisions made. Geostatistical techniques are used widely to produce these heterogeneous models. Structural, facies and property models are included in each geostatistical realization. Petrophysical properties of interest often include porosity, permeability and saturations, but of interest to the proposed work are geomechanical properties that affect reservoir performance.

Dusseault and Morgenstern (1978) showed that the oil sands in the McMurray Formation have an in-situ interlocked fabric configuration termed locked sands.

Absence of cohesion, high strength, high quartzose mineralogy, brittle and sharp failure behavior are characteristic of this type of material.

Geotechnical properties of oil sands including, stress-strain behavior, volume change as a function of stress change, permeability change as a function of volumetric strain and thermal properties of oil sands have been well studied (Agar et al. (1986), Kosar et al. (1987), Oldakowski (1994), Scott et al. (1994), Chalaturnyk (1996), Samieh and Wong (1996) and Touhidi-Baghini (1998)).

Often in SAGD an increase in reservoir fluid pressure due to steam injection leads to a decrease in effective stress. Moreover, increases in reservoir temperature results in thermal expansion and an increase in confining stresses. These pressure and temperature effects create complex fluid flow and geomechanical interactions. Considering flow simulation alone is insufficient to characterize reservoir performance; it is necessary to also consider the geomechanical response of the reservoir to better predict fluid flow, specifically, coupled geomechanical flow simulation should be implemented to better understand the complex interactions between flow and geomechanical effects for reservoirs in the McMurray Formation. Numerical studies in the field of coupled geomechanical flow simulation (Chalaturnyk (1996), Settari et al. (2001), Li (2006), Du and Wong (2007), Azad (2012), to name a few) have confirmed that during SAGD geomechanics play a significant role in reservoir performance.

Khajeh et al. (2011) showed that considering heterogeneous geomechanical properties has considerable effect on predicted reservoir performance; to obtain an accurate uncertainty analysis in coupled geomechanical flow simulation of SAGD, geomechanical properties should be modeled stochastically. A comprehensive geological model consisting of petrophysical and rock mechanical properties as well as the in situ stress state is termed a mechanical earth model (MEM) and is required for coupled geomechanical flow simulation of SAGD.

The McMurray Formation contains two main facies, sand and shale, which have considerably different elastic properties. Considering coupled simulation of the

high resolution heterogeneous models is recommended; however, it is common practice to consider coarser grids for computational reasons.

In the McMurray Formation, the predominance of sand facies usually results in the geomechanical properties of sand being chosen to represent the EEM of the formation. However, the low percentile of shale often significantly affects the geomechanical response of the reservoir but this is rarely considered in the determination of a representative EEM for a given reservoir. Two different techniques for determination of EEM could be considered; mixing rule averaging and analytical EEM determination. With the mixing rules, the EEM is determined based largely on the percentile of sand/shale facies.

Numerous researches have been done in the field of analytical homogenization of elastic properties. Mackenzie (1950) used a self-consistent model to obtain the EEM for three phase material. In the self-consistent model one of the phases is the as-yet-unknown and EEM value are identified when equating the displacements at the boundaries of heterogeneous models with the homogeneous models submitted to the same load. Hashin (1955 and 1958), developed another homogenization technique based on concept of elastic energy. Hashin applied this technique to rigid spherical materials (Hashin, 1955) and elastic spherical material (Hashin, 1958). Using a two phase self-consistent model, Hill (1965) calculated the elastic moduli of two phase composite materials. The materials studied by Hill (1965) differed from the materials studied by Mackenzie because it no longer assumes a surrounding phase. Budiansky (1965) extended the model proposed by Hill (1965) to multiphase materials. Salamon (1968) derived five elastic coefficient of homogeneous transversely isotropic medium equivalent to perfect horizontally layered rock. Although different assumptions are considered in these analytical homogenization approaches, a common element is that they consider a simplified (often stratified) facies configuration which is not appropriate for the complex facies configurations characteristic of the McMurray Formation.

A second issue with geomechanical simulation is that even at a coarse resolution (i.e. after the proposed upscaling is applied) computational time required to

simulate multiple realizations is still excessive. A common solution to this is the raking of the upscaled realizations and selecting a subset of the models to process. Ranking is often performed with flow simulation as a balance between the geostatisticians desire to process many realizations to accurately explore the uncertainty response in the reservoir must be balanced against the reservoir engineers reluctance to process more than a few realizations for computational reasons. Ranking methodologies can be broadly classified in two categories; static and dynamic measures.

Statistical measures include: calculation of the net to gross ratio, net pore volume or average permeability (Deutsch and Srinivasan, 1996); volumetric measures such as calculation of original oil in place (OOIP) or net oil in place (McLennan and Deutsch, 2005); statistical measures of global connectivity (Deutsch and Srinivasan, 1996); and statistical measure of local connectivity, (McLennan and Deutsch, 2005; Fenik et al., 2009; Wilde and Deutsch, 2012).

Dynamic ranking measures (Saad et al., 1996; Gilman et al., 2005; and Ates et al., 2005 to name a few) include; random walk, time of flight, tracer and streamline simulation. Applied to flow simulation, this type of dynamic measure is often a simplification of full numerical flow simulation where a simplification of flow-physics is considered. When used in the appropriate conditions, dynamic ranking measures often outperform static measures but are difficult to implement; simple static ranking measures are usually used in practice. To the authors' knowledge, there are not ranking measures available for the ranking of geomechanical property realizations for SAGD applications; this is a major focus of the proposed work.

In the following sections, methodologies used for determination of EEM, i.e. mixing rule, analytical and proposed numerical approach, are explained first. And proposed ranking methodology is explained first. Applicability of proposed numerical technique and ranking technique are investigated after that. Conclusions and discussion section comes at the end.

METHODOLOGY: DETERMINATION OF EEM

Mixing rule technique

The averaged shear modulus using a linear averaging technique (mixing rule) is obtained from:

$$G^* = \sum_{i=1}^{N} c_i G_i \tag{3-1}$$

In which;

G^*: Homogenized shear modulus

c_i: Proportion of each facies

G_i: Shear modulus of each facies.

While there is no theoretical reasoning for performing a simple averaging of the properties to determine the EEM, this is a very simple technique that is considered to compare to the proposed methodology as well as to the analytical techniques considered.

Analytical technique

The analytical approach developed by Budiansky (1965) was adopted for this study. In this approach the composite materials are assumed to be isotropic, elastic and spatial distributions of the phases are assumed such that, in general, the composite material is homogeneous and isotropic. The spatial distribution of the materials is not considered and EEM is a function of the initial elastic value and volume fraction of each material. The material is imagined to consist of contiguous, irregular grains of the constituent materials.

The averaged shear modulus in this approach is:

$$\frac{1}{G^*} = \frac{1}{G_N} + \sum_{i=1}^{N-1} \left(1 - \frac{G_i}{G_N}\right) \frac{c_i}{G^* + \beta^*(G_i - G^*)} \tag{3-2}$$

c_i is the volume fraction of each material and $\boldsymbol{\beta}^*$ is:

$$\beta^* = \frac{2(4-5\nu^*)}{15(1-\nu^*)} \tag{3-3}$$

In Equation 3-3, ν* is the poisson ratio of composite material.

Proposed numerical technique

To obtain EEM numerically, an error function, which is representative of the difference between the fine scale model VDP response and the VDP obtained from the homogenized value, is defined as:

$$\text{obj}(\mathbf{u}) = \sum_{i=1}^{n} (z(\mathbf{u}_i) - z^*(\mathbf{u}_i))^2 \tag{3-4}$$

Where z (u_i) is the vertical displacement at location u_i along the top of reservoir using a homogenized EEM and $z^*(\mathbf{u}_i)$ is the value of vertical displacement on the top of the reservoir obtained from the fine scale model. The numerically determined EEM is the value which minimizes obj (**u**). A binary search is used to find EEM numerically.

PROPOSED RANKING TECHNIQUE: GEOMECHANICAL RANKING (GR)

The main objective of GR is to be able to quickly predict the VDP of a given upscaled realization without performing the computationally demanding full geomechanical simulating. Specifically, the VDP_{GR} is predicted with the goal of best matching the true VDP found using geomechanical simulation. The procedure for determination of VDP_{GR} is explained using simplified schematics Figures 3-1 through 3-4.

It is assumed that, at each point on the top of the reservoir the vertical displacement is a combination of the displacement the stack of cells in the column below that point (shown by n_i in Figure 3-1). For each cell in column n_i, i ϵ [1, n_H], there are various sand/shale facies. Each cell in each n_i is in a different position with respect to the injector and the potential location of the steam chamber. Different elastic deformation is expected in different cells depending on

when the steam chamber reaches that location. Discounting factors are introduced to mimic the strength of the steam chamber when it reaches different locations in the model. These factors are applied to the deformation in each cell before the summation in Equation 3-8 is applied.

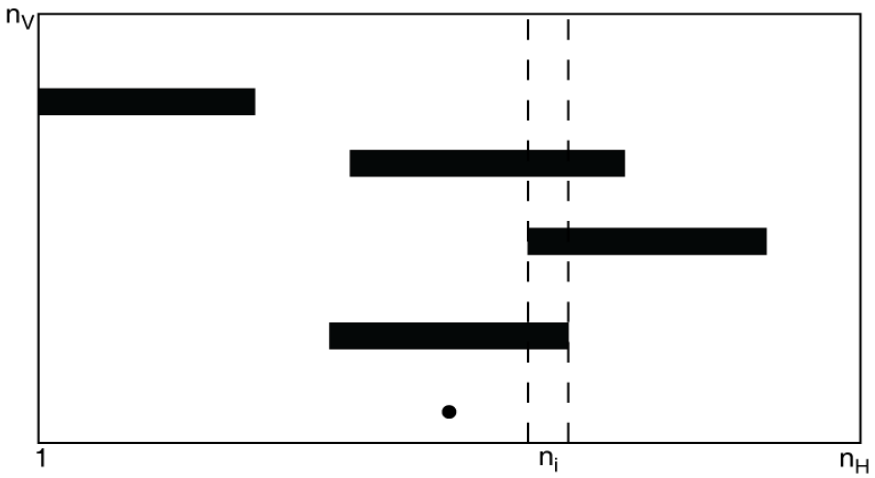

Figure 3-1 Small section of a typical deposit showing sand (white) and shale (black) facies consisting of n_H columns and n_V rows. Injector shown as a circle.

Angle of tolerance, distance to the injector and the number of direction changes (steps) are the three discounting factors defined to investigate different parameters which may have an effect on deformation. Most of these parameters are already defined by Wilde and Deutsch (2012). The following sections describe each of these discounting factors.

Number of steps:

In SAGD, temperature and pressure are the drivers for deformation. Propagation of the steam chamber is highly dependent on connectivity of the sand facies and the location of barriers (shale facies) which prohibit continuous steam chamber propagation. The first consideration in defining the discounting factors is the number of direction changes the steam chamber must take to reach the model location from the injector, this considers the role of barriers (shale facies) in this proxy model (Figure 3-2). This factor considers that it takes longer for the steam to go around layers of shale and there could be less steam that reaches areas of the reservoir if direction changes are required. In Figure 3-2, gray zones are reached

first by the steam chamber and more weight should be considered for the deformation of cells inside of this zone (step1). The hatched zone in Figure 3-2 is discounted more, and so on. The same procedure is repeated for each change of direction (shown by dotted area in Figure 3-2). White zones in Figure 3-2 are never reached and therefore they are not considered to deform.

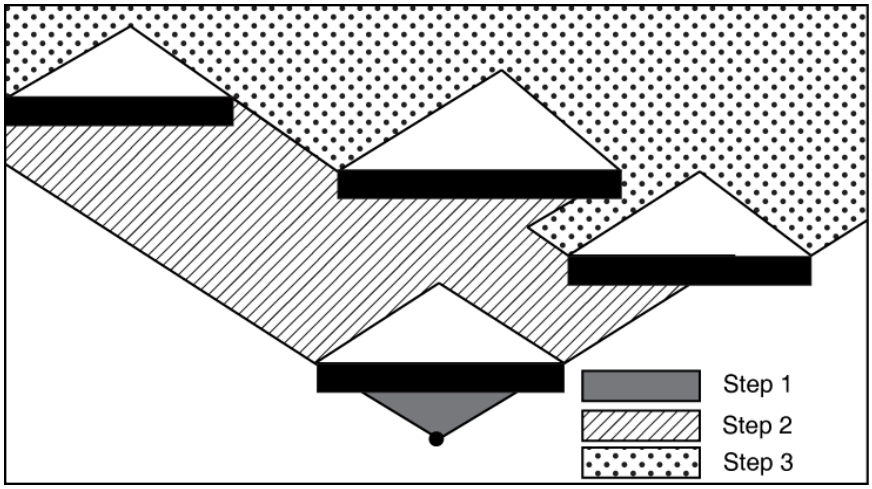

Figure 3-2 Schematic of number of steps-discounting factor (F_s).

Calculation of the step discounting factor (F_s) for each cell in the model is:

$$F_{s_{i,j}} = 1 - r\, S_{i,j} \tag{3-5}$$

Where r is a non-negative calibration parameter which can be calibrated based on running multiple realizations and comparing the VDP's. $S_{i,j}$ is the number of steps or direction changes to reach the producer from location $\mathbf{u}_{i,j}$. Considering r=1 results in equal weighting for all steps.

Angle from vertical:

The angle made between the location of the cell and the injector, measured from vertical, is also considered (F_a). Schematic of this discounting factor is shown in Figure 3-3. In this Figure, cell 2 has larger angle (α_2) and is likely to be reached by a weaker portion of the steam chamber and at a later time than cell 1 (α_1).

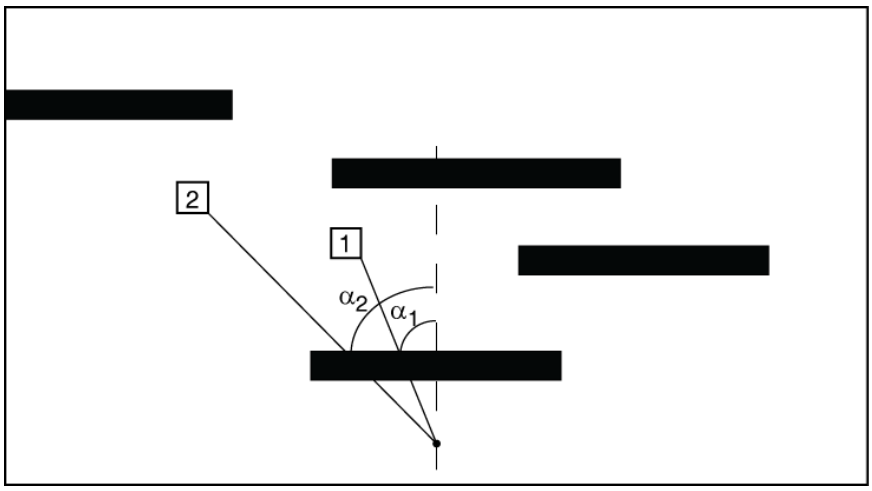

Figure 3-3 Schematic of angle from vertical-discounting factor (Fa).

F_a for cell (i, j) is calculated as:

$$F_{a_{i,j}} = 1 - t\, a_{i,j} \tag{3-6}$$

Where t is non-negative parameter which should be calibrated VDP's and $a_{i,j}$ is the angle between location $\mathbf{u}_{i,j}$ and the injector.

Distance:

Length of path from steam chamber to location of each cell is another discounting factor considered. This is illustrated in Figure 3-4. Point A is closer to the injector and would be reached first, causing more overall deformation for this location in the model.

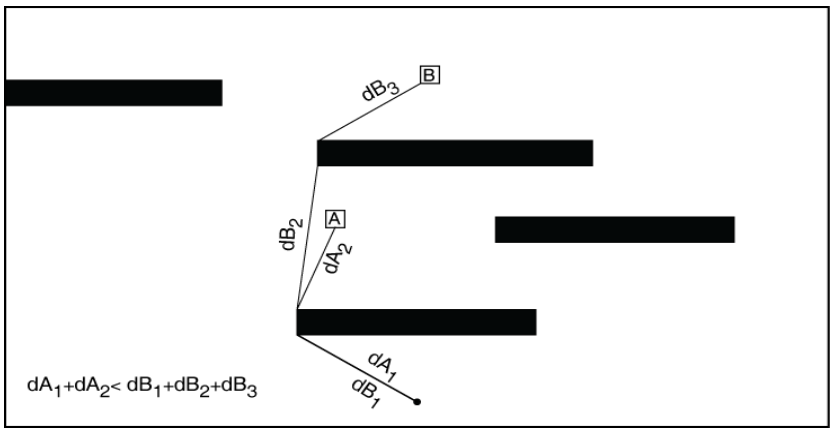

Figure 3-4 Schematic of distance-discounting factor (F_d).

Distance-discounting factor ($F_{d_{i,j}}$) is calculated as:

$$F_{d_{i,j}} = \left(\frac{d_{i,j}}{d_{max}}\right)^{\omega} \tag{3-7}$$

Where $d_{i,j}$ is length of distance from cell (i,j) to injector and d_{max} is maximum observed distance. ω is a calibrated parameter which should be calibrated based on VDP's obtained from coupled geomechanical flow simulation process.

Finally, $VD_{GR}(n_i)$, the vertical displacement for a stack of cells in column n_i (Figure 3-1), is calculated by:

$$VD_{GR}(n_i) = \sum_{j=1}^{n_V} F_{si,j}.F_{a_{i,j}}.F_{d_{i,j}}.[I_S.C_S.Disp_S + I_{Sh}.C_{Sh}.Disp_{Sh}] \tag{3-8}$$

For each cell in stack of cells in column n_i:

$$I_S: \begin{cases} 1 & \text{if the cell is sand and seen from the well location} \\ 0 & \text{if the cell is shale} \end{cases},$$

$$I_{Sh}: \begin{cases} 1 & \text{if the cell is shale} \\ 0 & \text{if the cell is sand} \end{cases},$$

C_S and C_{Sh}: Deformation characteristics of sand and shale respectively. These calibration parameters are considered due to significant differences in sand and shale elastic properties which effects deformation as a result of stress redistribution.

$Disp_S$ and $Disp_{Sh}$: Displacement of sand and shale facies as a result of temperature and pressure propagation during SAGD process.

Repeating this procedure for all columns of Figure 3-1, results in the overall VDP_{GR}. The maximum displacement for each realization is used as the ranking criteria and compared with maximum value of the VDP obtained from coupled geomechanical flow simulation of each realization. The average VDP could also be used if that is more indicative of the response of interest, but here we are interested in the maximum displacement.

Example:

Figure 3-5 shows one facies realization generated with sequential indicator simulation and is typical of the McMurray Formation, with 100m horizontal and 20m vertical. The VDP obtained through numerical simulation after 1000 days is shown in Figure 3-5. The objective of GR technique is to find geometrical characteristics of the realization which correlates with the VDP of the simulated response. Using appropriate parameters (Equation 3-8) result in determination of VDP_{GR}, dashed line in below graph. Using appropriate parameters used in Equation 3-8 result in determination of VDP_{GR}, dashed line in below graph. Calibrated parameters should be determined by considering range of values for each of variable used in Equation 3-8 and select the most optimized set of parameters which results in the best match with VDP obtained from numerical simulation. Parameters which have been used for determination of VDP_{GR} in the following graph are; $C_S = 0.0015$, $C_{Sh} = 0.01$, $F_{si,j} = 0.7$, $F_{ai,j} = 0.2$ and $\omega = 0.5$. ω is distance exponent (Equation 3-6). Tolerance of angle is considered as 80° and discounting factor for step 1, step 2 and other steps are considered as 1, 0.5 and 0 respectively.

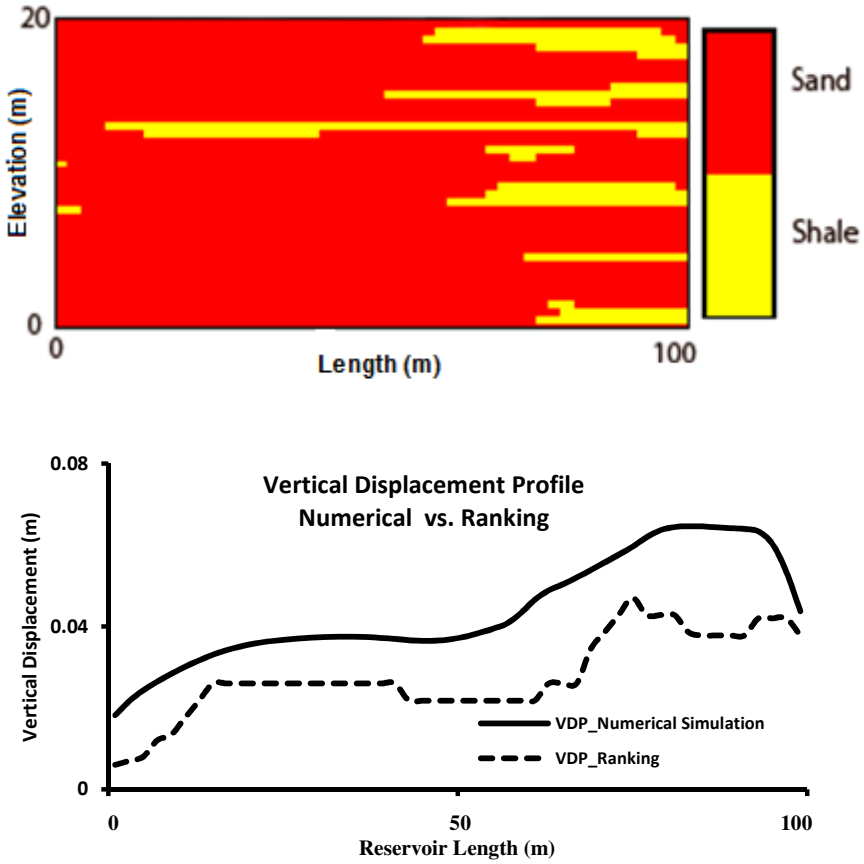

Figure 3-5 one spatial facies configuration (above), numerically determined VDP (below-solid line) and estimated VDP through GR ranking (below-dashed line).

MODEL DESCRIPTION

To decrease boundary effects, the dimensions of a model considered for geomechanical analysis is usually 3 to 4 times larger than dimensions of the model considered for flow analysis (Wood, 2004). In addition to the common reservoir section between the two simulators, additional depth above and below the reservoir (overburden and underburden) and sideburden is considered in the geomechanical model (Khajeh et al., 2011) (Figure 3-6). As the reservoir is the only section which is considered for coupled geomechanical flow analysis, a coarser gird was considered for the regions surrounding the reservoir. The same grid density and model dimension that was used in Khajeh et al. (2011) is used for this work as well. Table 3-1 provides grid density and model dimension of the model area. Fixed horizontal displacement for all sides of the model and fixed

vertical displacements at the bottom of the model are considered (Khajeh et al., 2011). In-situ stress configuration (i.e. magnitudes and directions) has a significant impact on geomechanical response and affects the optimization of injection pressure to prevent cap-rock instability, the maximum dilatancy of the reservoir, and the selection of drilling direction to maximize SAGD performance. The magnitudes selected for minimum and maximum horizontal stresses, pore pressure and vertical stress are based on Collins (2002) and are given in Table 3-2. Injection pressure of 1500 KPa has been considered for steam injection pressure.

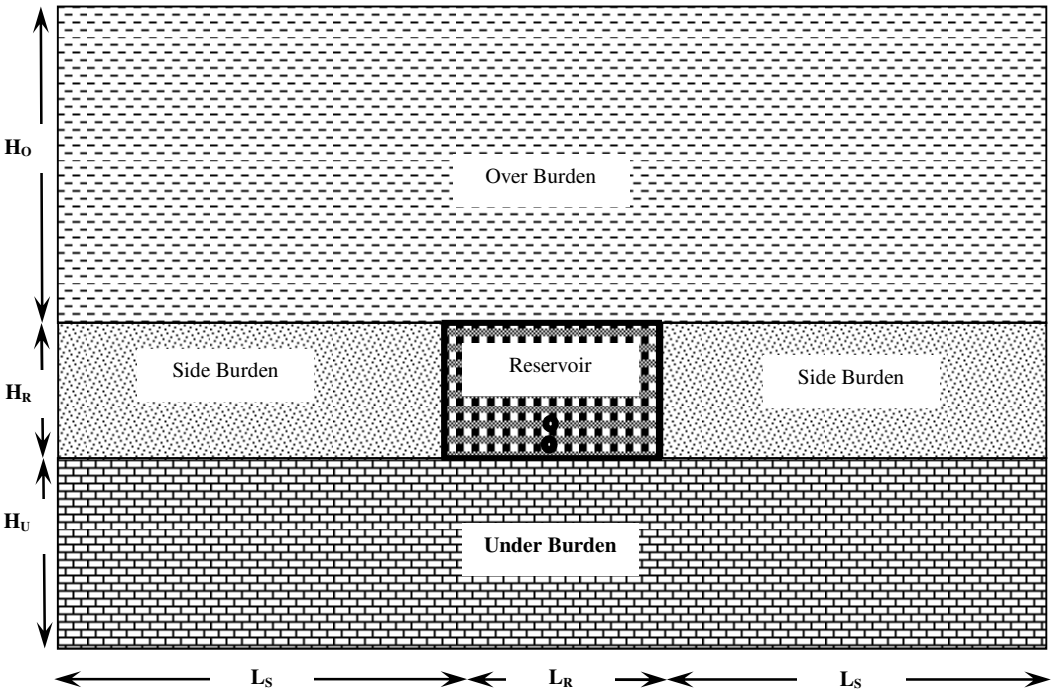

Figure 3-6 Model description (after Khajeh et al, 2011).

Table 3-1 Model dimension and grid density information (After Khajeh et al., 2011).

Section	Length (m)	Height (m)	Number of cells in X	Number of cells in Y
Underburden	400 ($2L_S+L_R$) *	50 (H_U)	70	5
Reservoir	100 (L_R)	20 (H_R)	50	40
Sideburden (each)	150 (L_S)	20 (H_R)	10	40
Overburden	400 ($2L_S+L_R$)	140 (H_O)	70	10

* **L_S and L_R are shown in Figure 3-5.**

Table 3-2 Initial stress, pore pressure and temperature [After Collins (2002)]

Parameter	Value
Reservoir Depth	150 m
$\sigma_h/\ \sigma_v$	1
$\sigma_H/\ \sigma_v$	1.5
Initial reservoir pressure	650 KPa
Initial reservoir temperature	10 ˚C

Well spacing (distance between injector and producer) of 5 m, steam quality of 95%, preheating period of 100 days, and well radius of 0.1 m are assumed. Relative permeability curves and variation of oil viscosity by temperature are shown in Figure 3-7.

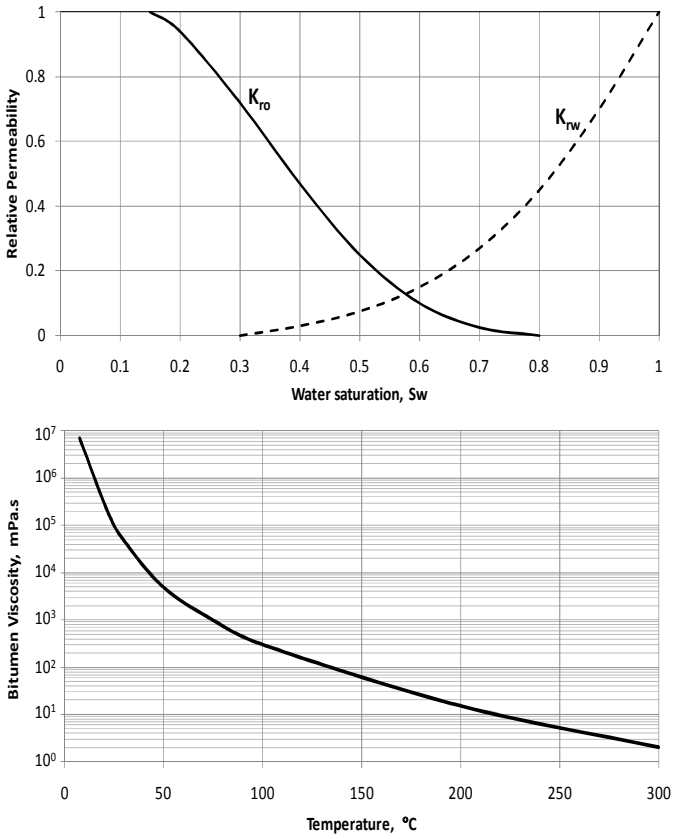

Figure 3-7 Relative permeability (top) and variation of viscosity by temperature (bottom) [after Chalaturnyk (1996)].

PETROPHYSICAL AND ROCK MECHANICAL PROPERTIES

Linear elastic deformation is considered for all model regions (Figure 3-6). Table 3-3 lists elastic properties considered for over, side and underburden. The reservoir section is the only region which is common between the two simulators. Different petrophysical (porosity, permeability and oil saturation) and elastic properties (bulk and shear modulus) are considered for sand and shale (Table 3-4). Additional rock mechanical properties are required for flow simulation and are summarized in Table 3-5. Linear thermal expansion coefficient of 2×10^{-5} ($^{\circ}K^{-1}$) and bulk density of 2200 (kg/m^3) are considered for all regions shown in Figure 3-6. Parameters in Table 3 through Table 3-5 are selected based on previous studies (Chalaturnyk 1996; Li 2006).

Table 3-3 Elastic properties considered for over, under and side burdens.

Zone	Parameter	Value
Overburden	Bulk Modulus (MPa)	208
	Shear Modulus (MPa)	96.2
Sideburden	Bulk Modulus (MPa)	620
	Shear Modulus (MPa)	286
Underburden	Bulk Modulus (MPa)	4167
	Shear Modulus (MPa)	1923

Table 3-4 Petrophysical and elastic properties considered for sand and shale facies.

Property	Sand	Shale
Bulk Modulus (MPa)	900	150
Shear Modulus (MPa)	415	69
Permeability (mD)	3000	1
Porosity	0.3	0.01
Oil Saturation	0.85	0.05

Table 3-5 Rock parameters used in flow simulator

Parameter	Value
Rock Compressibility (1/kPa)	5×10-6
Rock Expansion Coefficient ($^{\circ}C^{-1}$)	3.84×10-5
Rock Heat Capacity (kJ/kg˚K)	1865
Rock Thermal Conductivity (W/m˚K)	1.736

FACIES MODEL

Three different facies models are considered (Figure 3-8) (1) Layer cake model (2) randomly distributed model (3) spatially correlated (sequential indicator simulation) model. The layer cake and randomly distributed models are not realistic but are included to show that the analytical methods perform well in these cases but are insufficient for a realistic model such as the spatially correlated model.

The shale proportion in the reservoir is assumed to be 20% for all models. 100 realizations are generated for each type of model; the SIS model is generated with a nugget effect of 0, a spherical variogram with horizontal variogram range (R_H) of 50 m and vertical variogram range (R_V) of 2 m. These models represent the reservoir section (Figure 3-6) other areas of the model are populated with homogeneous properties. Sequential indicator simulation (SIS) as implemented in GSLIB (Deutsch, 1998) is used to generate the necessary realizations. Figure 3-8 shows the layer cake model, one of the spatially correlated realizations and a randomly distributed model and corresponded steam chambers of these facies during SAGD process after 1000 days. Note that the horizontal shale layers in the layer cake model and the correlated model have a significant effect on the propagation of the steam chamber.

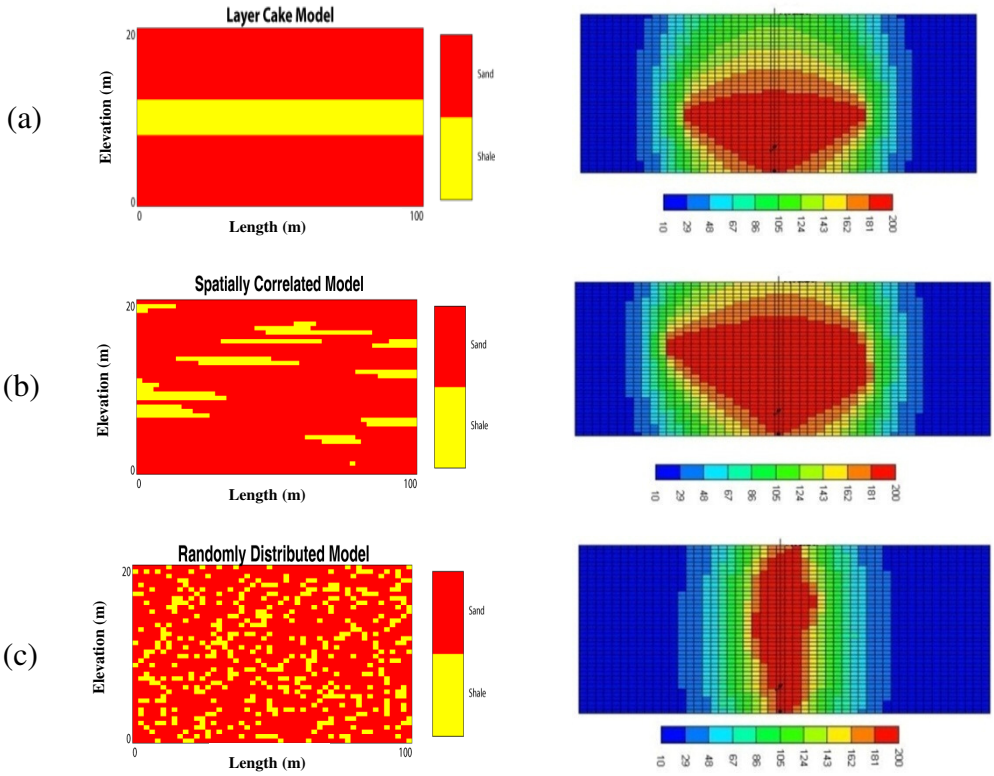

Figure 3-8 Three facies configuration with corresponded steam chambers
a) Layer cake, b) Spatially correlated realization and c) Randomly distributed.

RESULTS

EEM and corresponded VPD

The VDP's obtained from the numerical, the Budiansky, and the mixing rule approaches are compared for the three different models discussed previously (Figures 3-9 to 3-11). Table 3-6, shows corresponding EEM values for these models obtained from different approaches.

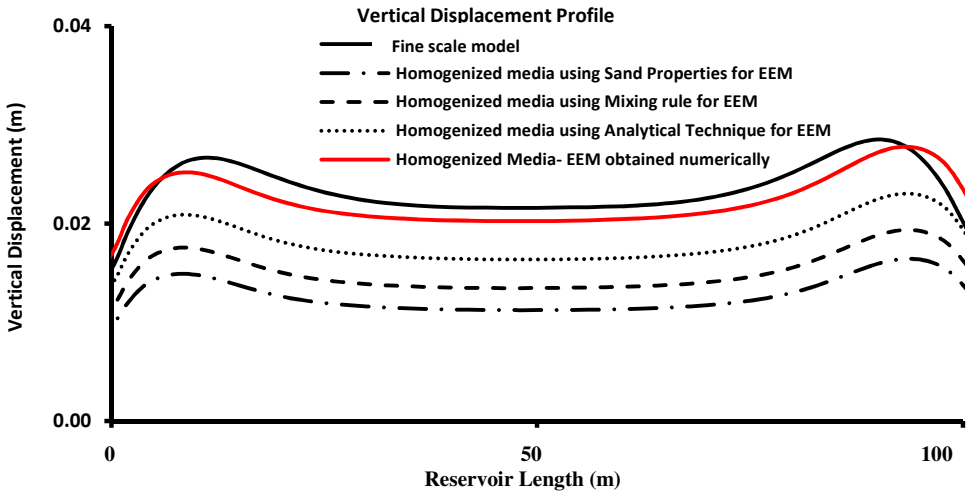

Figure 3-9 VDP's of the heterogeneous fine scale model and homogenized media using different approaches to obtain EEM (Layer cake model).

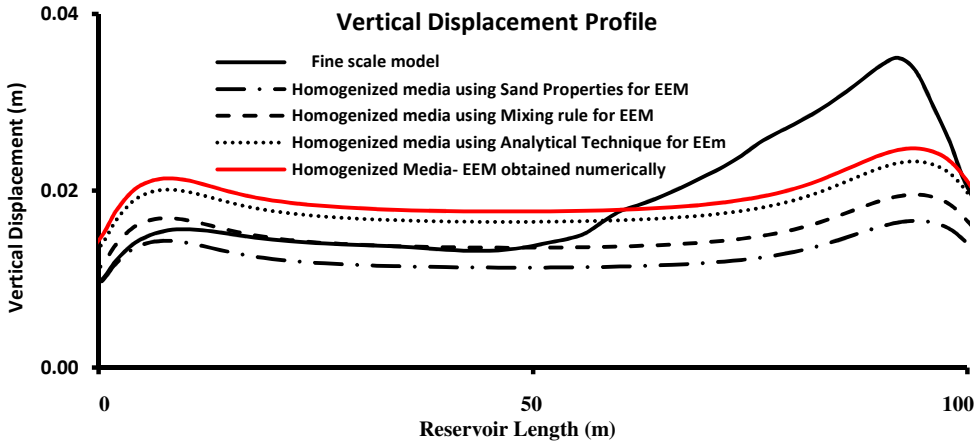

Figure 3-10 VDP's of the heterogeneous fine scale model and homogenized media using different approaches to obtain EEM (Spatially correlated model).

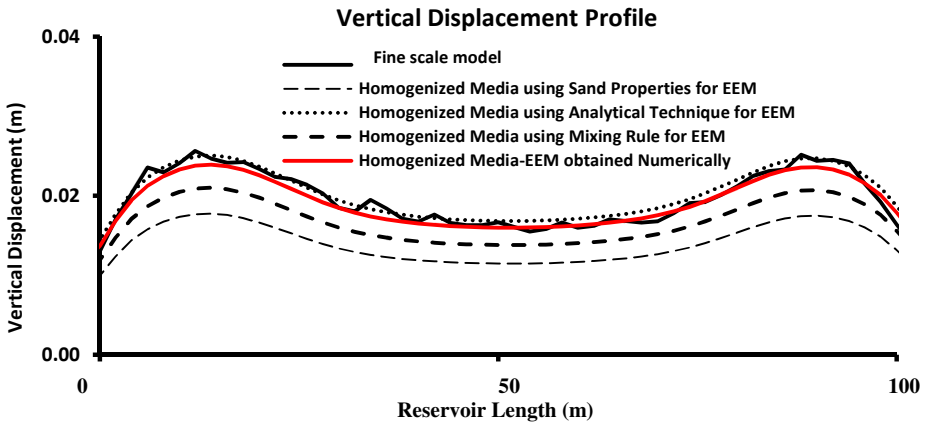

Figure 3-11 VDP's of the heterogeneous fine scale model and homogenized media using different approaches to obtain EEM (Randomly distributed model).

Table 3-6 Homogenized EEM values obtained from different approaches for three different models.

Homogenized Bulk Modulus [MPa]			
	Layer Cake Model	Spatially Correlated Model	Randomly Distributed Model
Sand Properties	900	900	900
Mixing Rule	750	750	750
Budiansky	617	617	617
Numerical Technique	**500**	**560**	**650**

In Table 3-7 error corresponded to different techniques for three different facies configuration (Figure 3-8) are shown. Errors in this Table are calculated by using Equation 3-9.

$$\text{Error}(\%) = \frac{\sum_{i=1}^{n} \left| 1 - \frac{\text{VDP}_{\text{Homogenized model}}}{\text{VDP}_{\text{Heterogeneous model}}} \right|}{n} \times 100 \qquad (3\text{-}9)$$

In which n is the number of points in VDP of homogenized and heterogeneous models.

Table 3-7 VDP error corresponded to homogenized EEM values obtained from different approaches for three different models.

	Error (%)		
	Layer Cake Model	Spatially Correlated Model	Randomly Distributed Model
Sand Properties	66.2	35.6	9.1
Mixing Rule	49.6	20	5
Budiansky	30.8	12.8	1.7
Numerical Technique	**5.3**	**3.1**	**0.7**

The most common practice used currently is to assume the reservoir acts as if it is made entirely of sand as this is the most dominant facies; however, this results in the largest mismatch. Although choosing the analytical approach results in a lower error in comparison with the other techniques, the results obtained from all three alternative approaches underestimate the displacement obtained from the fine scale model. The numerical approach provides a reasonable estimate of the overall VDP even if some local accuracy is lost; this loss is expected as in the EEM approach the entire model is homogenized. The numerically determined EEM value for spatially correlated model (560 MPa) is between layer cake model EEM (500 MPa) and randomly distributed model (650 MPa).

The EEM for each of the 100 realizations are calculated with the proposed numerical approach. The distribution of EEM values is shown Figure 3-12.

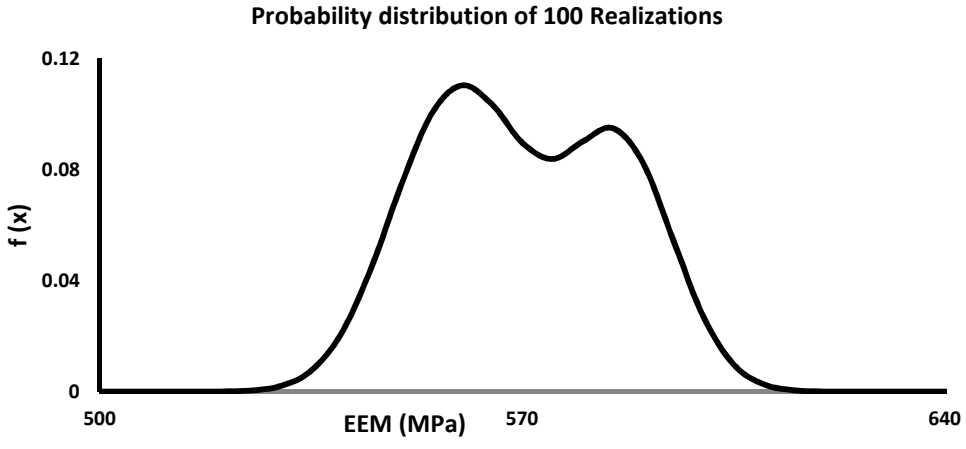

Figure 3-12 Smoothed probability distribution function for EEM values of 100 realizations.

Two important parameters have effect on changes in VDP's and accordingly on EEM values representative of geological realizations. The first one is that the shale facies have lower permeability/porosity in comparison to sand and behaves like barriers and has an effect on the propagation of the steam chamber. On the other hand, since shale is considerably softer in comparison to sand, with the same loading conditions, elastic deformation of shale is higher than the elastic deformation of sand. After a long time period (1000 days in this study) pressure is distributed uniformly in the media. So, in regions of higher shale content, vertical displacement (elastic deformation) is larger.

Ranking of geological realizations based on expected geomechanical response

As shown in Figure 3-12, it is not appropriate to assign a single EEM value to a single reservoir as there is considerable uncertainty depending on the facies configurations. Rather, a range of EEM values should be determined that characterize the uncertainty in the reservoir; while running the full geomechanical simulation on all realizations, as was done for Figure 3-12, is preferred, it is not always feasible in practice. Moreover, the numerical determination of EEM is more precise but requires running a geomechanical simulation for the fine scale model and then minimization or error based on VDP obtained from fine scale model which is computationally expensive.

Ranking is often applied to select a subset of realizations in order to approximate the range of uncertainty seen in the system without having to simulate all of the realizations. For example, the P_{10}, P_{50} and P_{90} realizations could be identified with a proxy model and assumed to represent the true range of uncertainty if the proxy model is reasonable.

The proposed GR technique is applied to the 100 realizations. VDP_{true} obtained from coupled geomechanical flow simulation is compared with the VDP_{GR} obtained from the GR technique. Maximum values of displacement in each VDP_{GR} obtained from each realization is used as the ranking criteria and compared with value determined from running coupled geomechanical flow simulation on the fine scale model; note that this is not often done in practice, but

all 100 realizations were simulated for this study to explore the effectiveness of the ranking measure. The discounting factors (Cs, C_{sh}, $F_{si,j}$, $F_{ai,j}$,ω) considered in Equation 3-8 require calibration using the 100 simulated realizations. Each parameter is optimized independently. The best set of parameters which results in best correlation ranking are considered to be calibrated. These calibrated parameters are already mentioned in example section (Figure 3-6). The ranking measure is highly correlated (0.87) to the reservoir response (Figure 3-13).

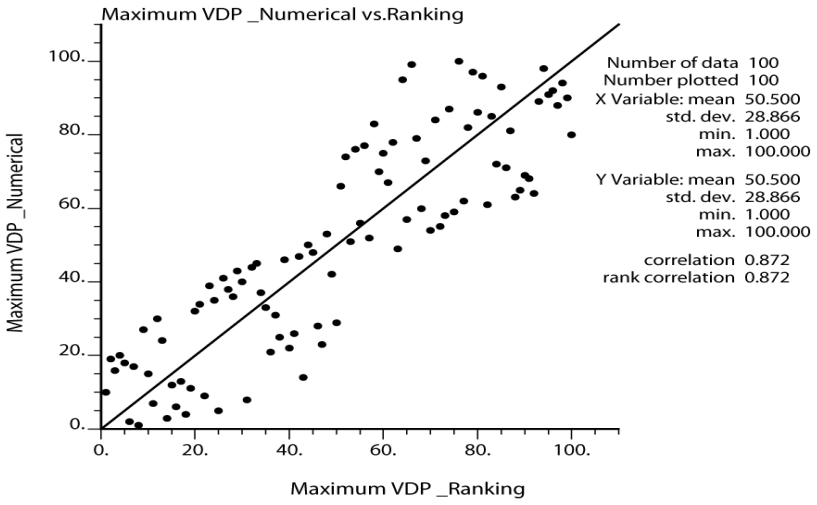

Figure 3-13 Ranked scatter plot: Maximum value of VDP obtained from coupled geomechanical flow simulation vs. maximum value of VDP obtained from GR technique

DISCUSSION AND CONCLUSIONS

In this study, the efficiency of existing approaches to determine homogenized EEM for SAGD were assessed. The currently used technique of considering the properties of sand to be representative of the reservoir was found to be inappropriate for elastic deformation. The proposed numerical approach resulted in EEM values that were more similar to the true response (by design). In the three facies configurations considered, it was shown that using sand properties as the homogenized media resulted in VDP's that depart the most from the fine scale model response. The Budiansky technique was only appropriate for cases where there was no spatial correlation in the facies.

The uncertainty in EEM was explored considering multiple realizations and the full numerical upscaling approach. This is not practical for application to existing reservoirs as it requires the full geomechanical simulation of many realizations. Rather, a geomechanical proxy model was proposed that was able to effectively predict elastic deformation after calibration. Calibration would be performed on a fairly large number of realizations if possible, but these calibrated parameters could be used in future modeling of similar domains. The proxy model can be used to rank realizations and select a few representative models for full simulation. This would provide a reasonable range of EEM values to use in full coupled flow-geomechanical simulation.

REFERENCES

Agar, J.G., Morgenstern, N.R. and Scott, J.D. 1986. Shear strength and stress-strain behavior of Athabasca oil sand at elevated temperatures and pressures. Canadian Geotechnical Journal. 24: 1-10.

Alberta Energy and Utilities Board, (AEUB). 2003. Statistical Series 2003-98, Calgary, Canada.

Ates, H., Bahar, A., El-Abd, S., Charfeddine, M., Kelkar, M. and Datta-Gupta, A. 2005. Ranking and upscaling of geostatistical reservoir models by use of streamline simulation: A field case study. Proceeding of Middle East Oil Show, Bahrain, SPE No. 81497-MS.

Azad, A. 2012. Rapid SAGD Simulation Considering Geomechanics for Closed Loop Reservoir Optimization. PhD dissertation, University of Alberta, Edmonton, Canada.

Budiansky, B. 1965. On the elastic moduli of some heterogeneous materials. Journal of the Mechanics and Physics of Solids 13:223–227.

Butler, R. M. 2001. Some Recent Developments in SAGD. Journal of Canadian Petroleum Technology. 40(1): 18-22.

Chalaturnyk, R.J. 1996. Geomechanics of the Steam-Assisted Gravity Drainage Process in Heavy Oil Reservoirs. PhD dissertation, University of Alberta, Edmonton, Canada.

Collins, P.M. 2002. Injection Pressures for Geomechanical Enhancement of Recovery Process in the Athabasca Oil Sands. Proceeding of SPE International Thermal Operations and Heavy Oil Symposium and International Horizontal Well Technology Conference, Calgary, Canada, SPE No. 79028.

Deutsch, C. and Srinivasan, S. 1996. Improved Reservoir Management through Ranking Reservoir Models. Proceeding of SPE/DOE Improved Oil Recovery Symposium, Tulsa, SPE No. 35411.

Du, J. and Wong, R.C.K. 2007. Coupled geomechanics-reservoir simulation of UTF phase A project using a full permeability tensor. Proceeding of the Petroleum Society's 8th Canadian International Petroleum Conference, 1-16.

Dusseault, M. and Morgenstern, N.R. 1978. Shear strength of Athabasca oil sand. Canadian Geotechnical Journal 15: 216-238.

Edmunds, N.R., Haston, J.A, and Best, D.A. 1989. Analysis and implementation of steam assisted gravity drainage process at the AOSTRA UTF. Proceeding of Insitu recovery, Calgary, Canada, 223-238.

Fenik, D.R., Nouri, A. and Deutsch, C.V. 2009. Criteria for ranking realizations in the investigation of SAGD reservoir performance. Proceeding of the Canadian International Petroleum Conference (CIPC), Calgary, Canada.

Gilman, J., Meng, H., Uland, M., Dzurman, P. And Cosic, S. 2005. Statistical ranking of stochastic geomodels using streamline simulation: a field application. Proceeding of SPE Annual Technical Conference and Exhibition, San Antonio, USA, SPE No. 77374.

Hashin Z. 1958. The moduli of an elastic solid, containing spherical particles of another elastic material. Proceedings of IUTAM Symposium on Non-homogeneity in Elasticity and Plasticity, Warsaw, Poland,17:463–478.

Hashin, Z. 1955. The moduli of an elastic solid reinforced by rigid particles. Bulletin of the Research Council of Israel. 5C:46–59.

Hill, R. 1965. A self-consistent mechanics of composite materials. Journal of the Mechanics and Physics of Solids. 13:213–222.

Khajeh, M., Chalaturnyk, R. and Boisvert, J. 2011. Impact of Heterogeneous Geomechanical Properties on Coupled Geomechanical-Flow Simulation of SAGD. Proceeding of SPE Reservoir Characterization and Simulation, Abu Dhabi- UAE, SPE No. 148338-PP

Conference and Exhibition, Abu Dhabi, UAE, 9–11 October.Komery, D.P., O'Rourke, J.C., and Chambers, J.I. 1993. AOSTRA underground test facility (UTF) Phase B implications for commercialization. Proceeding of AOSTRA/CANMET oil sands our petroleum future , Edmonton, Canada.

Kosar, K.M., Scott, J.D. and Morgenstern, N.R. 1987. Testing to determine the geotechnical properties of oil sands. Proceeding of the 38th Annual Technical Meeting of the Petroleum Society of CIM, Calgary, Canada, 995-1010.

Li, P. 2006. Numerical Simulation of the SAGD Process Coupled With Geomechanical Behaviour. PhD dissertation, University of Alberta, Edmonton, Canada.

Mackenzie, J. 1950. The elastic constants of a solid containing spherical holes. Proceedings of the Royal Society London. 63(1): 2–11.

McLennan, J. and Deutsch, C. 2005. Ranking geostatistical realizations by measures of connectivity. Proceeding of SPE international thermal operations and heavy oil symposium, Calgary, Canada, SPE No. 98168.

Oldakowski, K. 1994. Absolute Permeability of Oil Sands. PhD dissertation, University of Alberta, Edmonton, Canada.

Saad, N., Maroongroge, V. and Kalkomery, C. 1996. Ranking geostatistical models using tracer production data. Proceeding of European 3D Reservoir Modelling Conference, Stavanger, Norway, SPE No. 35494.

Salamon, M. 1968. Elastic moduli of a stratified rock mass. Journal of Rock Mechanics and Mining Sciences. 5:519–527.

Samieh, A.M. and Wong, R.C.K. 1997. Deformation of Athabasca oil sand at low effective stresses under varying boundary conditions. Canadian Geotechnical Journal. 34: 985–990.

Scott, J.D., Proskin, S.A. and D.P. Adhikary. 1994. Volume and permeability changes associated with steam stimulation in an oil sands reservoir. Journal of Canadian Petroleum Technology. 33(7): 44-52.

Settari, A., Walters, D.A. and Behie, G.A. 2001. Use of coupled reservoir and geomechanical modelling for integrated reservoir analysis and management. Journal of Canadian Petroleum Technology. 40(12): 55-61.

Touhidi-Baghini, A. 1998. Absolute Permeability of McMurray Formation Oil Sands at Low Confining Stresses. PhD dissertation, University of Alberta, Edmonton, Canada.

Wilde, B.J. and Deutsch, C.V. 2012. Calculating and improved connected hydrocarbon volume with line-of-sight for ranking realizations by SAGD performance. Proceeding of 14th annual meeting of Centre for Computational Geostatistics (CCG), university of Alberta, Edmonton, Canada, Paper No. 205.

Wood, D.M 2004. Geotechnical Modeling. Spon Press, Taylor & Francis. 488 p.

.

CHAPTER 4: NUMERICAL LOCAL UPSCALING OF ELASTIC PROPERTIES[1]

ABSTRACT

Upscaling elastic geomechanical properties is important for reducing the computational requirements of geomechanical simulation while honoring local heterogeneities in rock properties. Elastic properties are often considered homogeneous during simulation; however, there is increasing interest in understanding the effect of heterogeneity on geomechanical simulation. These heterogeneous models are usually fine scale models generated by geostatistical techniques. Although geomechanical simulation of the high resolution property models is preferred, simulation with the fine scale model is not often computationally feasible for full–field, coupled geomechanical flow simulation. Upscaling from fine scale/high resolution property models to coarser scale/low resolution models allows for the generation of realistically sized numerical models. A novel local numerical upscaling technique is proposed to describe the macroscopic elastic behavior of complex heterogeneous media. This numerical technique is not restricted to specific geologies as most existing analytical techniques are. Moreover, transversely isotropic deformation is considered rather than the usual assumption of isotropic deformation. This technique is compared to conventional analytical techniques and is shown to produce superior results when assessing the upscaling error of a synthetic facies model. The geomechanical responses (volumetric strain and shear strain) of the coarse upscaled models are more similar to the response of the fine scale model using the proposed technique.

[1] A version of this chapter has been sent for publishing in Petroleum Science and Engineering.

INTRODUCTION

The main objective of geomechanical simulation is to predict the deformation behavior of geo-materials when loads are applied. Rock mechanical properties, both elastic and rock strength parameters, are critical input parameters. Subsurface rocks are composed of different materials having different mechanical properties. The mechanical properties of these composite rock materials may vary on a scale that is much smaller than the size of the cells used in numerical geomechanical simulation. To capture small scale heterogeneities, fine scale cells are usually considered in geostatistical modeling. Mechanical earth models (MEM's) are comprehensive geological models which include in-situ stress magnitudes/directions and also heterogeneous maps of rock mechanical properties. However, layer cake geo-models with constant elastic and rock strength properties dominate the geomechanical field. Rather, the use of heterogeneous MEM's are proposed in order to account for known rock heterogeneity and to better predict the geomechanical response of an area of interest. Coupled geomechanical flow simulations is of interest for several applications including geomechanical effects during thermal recovery processes (e.g., SAGD process) and cap rock integrity investigation. Comprehensive geological models used for these kinds of simulations include both heterogeneous maps of petrophysical properties, including porosity and permeability, and rock mechanical properties, including elastic and rock strength properties.

The consideration of heterogeneous geostatistical models for petrophysical and rock mechanical properties allows for the quantification of uncertainty in flow and geomechanical responses. The limiting factor in considering multiple realizations and fine scale heterogeneous property models is the CPU requirements of the geomechanical simulator (e.g. FLAC). This is the main motivation for considering upscaling. It is desirable to move from a high resolution/fine scale geological model that fully captures known heterogeneities to a low resolution/coarse scale model that responds in the same way as the fine scale geological models but can be simulated in a reasonable timeframe. As a

result, upscaling is considered as an intermediate step between geological modeling and geomechanical simulation.

Power law averaging (Deutsch, 1989) could be used for upscaling of elastic properties, but there is little theoretical justification for its use in upscaling geomechanical properties. Analytical upscaling of fine scale elastic mechanical parameters has been discussed by many researchers (Mackenzie, 1950; Hashin and Shtrikman, 1962, 1963; Backus, 1962; Hill, 1963; Budiansky, 1965; Salomon, 1968; Rijpsma and Zijl, 1998, to name a few). Mackenzie (1950) used a self-consistent model to determine the equivalent elastic media (EEM) of a material composed of three phases surrounding each other. Hashin and Shtrikman (1962, 1963) determined upper and lower bounds for the EEM, which were derived from a variational principle. Their results are valid only for statistically isotropic fine scale parameter distributions. Backus (1962) developed an upscaling technique applicable for perfectly layered rocks. Considering perfectly layered fine structure Backus (1962) derived an upscaled compliance matrix with five linearly independent parameters describing the elastic behavior of the equivalent homogeneous rock. The materials studied by Hill (1963) differed from the materials studied by Mackenzie (1950) because it no longer assumes a surrounding phase. Budiansky (1965) extended the model proposed by Hill (1963) to multiphase materials but still he assumed isotropic deformation. Salamon (1968) extended work done by Backus (1962) by describing transversely isotropic behavior. Rijpsma and Zijl (1998) introduce the concept of imperfectly layered rock types. By imperfectly layered rocks, they meant rock materials with fine scale parameters that vary smoothly in the horizontal direction and strongly in the vertical direction.

Numerical techniques for upscaling elastic properties are not common. Elkateb (2003) proposed a mathematical expression for the determination of equivalent elastic media (EEM) for a simplified layer cake model with isotropic elastic deformation. However, the deformation behavior of many materials depends on orientation. That is, the stress-strain response of a sample taken from the material

in one direction is different if the sample were taken in a different direction. In this case, the assumption of isotropic deformation may result in significant error.

Although different assumptions are considered in these approaches, complex facies distributions (Figure 4-1a) and anisotropic deformation (Figure 4-1b) that are common to many SAGD operations have not been considered in previous elastic property upscaling techniques.

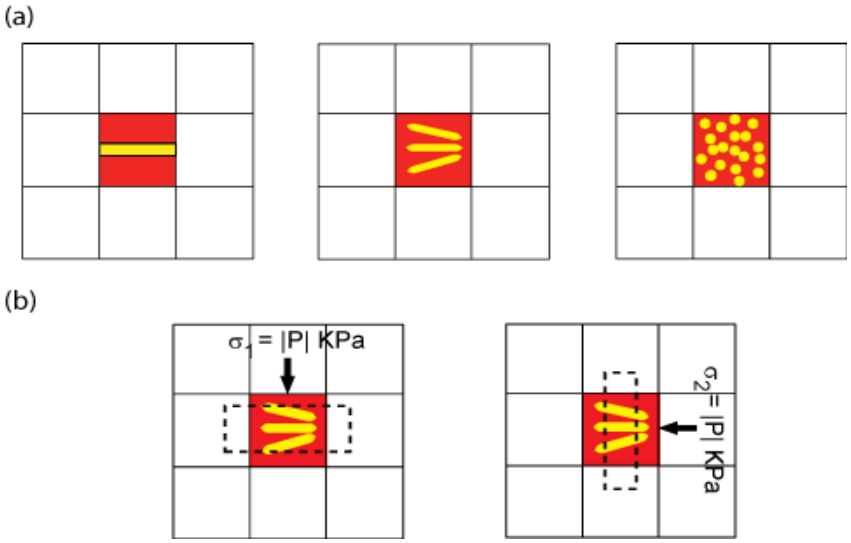

Figure 4-1 (a) Three different distributions of facies with the same proportion for each facies. (b) Anisotropic deformation.

A novel numerical upscaling technique for elastic geomechanical properties is proposed. Both complex facies configuration and anisotropic deformation are considered in developing the proposed approach.

Proposed numerical upscaling technique for upscaling of elastic properties in this work has similar concept as local upscaling of permeability (Durlofsky, 1991; Pickup et al., 1994; and Durlofsky, 2005).

In local upscaling technique, the solution of the governing physical equations (i.e. fine scale pressure equation for flow) with an assumed boundary condition for the fine grid blocks that are contained in a single coarse cell (Figure 4-2a) is considered. The cells surrounding the coarse block of interest are ignored. Different boundary conditions are often considered with constant pressure and no flow boundaries (Figures 4-2b and 4-2c). Effective properties (i.e. permeability)

in different directions are obtained. From the configurations shown in Figure 4-2b and 4-2c, effective properties in the horizontal and vertical directions (i.e. K^*_x and K^*_y) can be calculated.

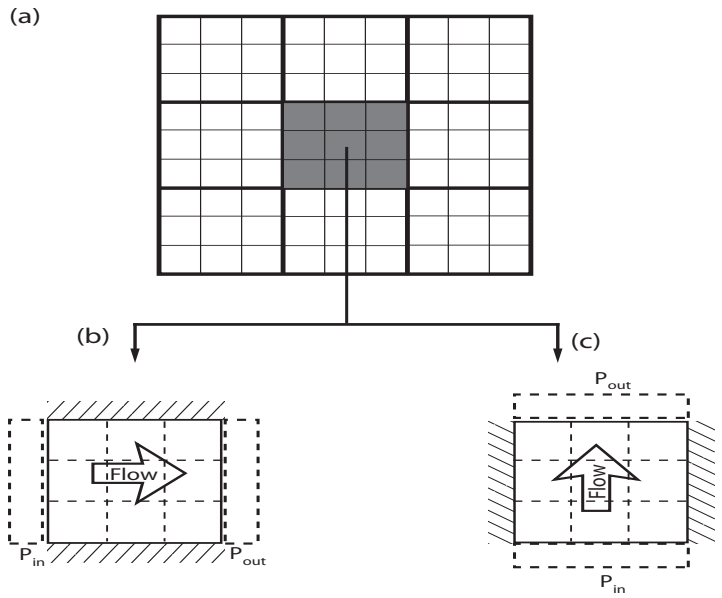

Figure 4-2 Schematic of pure local upscaling (After Durlofsky, 1991).

The methodology is demonstrated on a synthetic 2D model based on sand/shale distributions typical of the McMurray oil sands deposit located in northern Alberta, Canada. To assess the accuracy of the proposed methodology, conventional averaging techniques based on power law averages and Budiansky`s (1965) approach are compared.

In Budiansky`s approach, the composite materials are assumed to be isotropic and elastic. No specific spatial distribution of the materials is considered and spatial distributions of the phases are assumed such that, in general, the composite material is homogeneous and isotropic. EEM is a function of the initial elastic value and volume fraction of each material. The material is imagined to consist of contiguous, irregular grains of the constituent materials. No specific consideration of spatial distribution of facies in Budiansky technique is the main reason for selecting this analytical upscaling approach. Considering a simplified facies configuration, usually a layer cake model, is the most common element of the

other discussed upscaling technique which is not suitable for complex facies configuration like shale/sand facies of McMurray Formation.

The averaged shear modulus in Budiansky`s approach is:

$$\frac{1}{G^*} = \frac{1}{G_N} + \sum_{i=1}^{N-1} \left(1 - \frac{G_i}{G_N}\right) \frac{c_i}{G^* + \beta^*(G_i - G^*)} \tag{4-1}$$

where,

G^*: Shear modulus of coarse scale cell

G_i, G_N : Shear modulus of fine scale cells inside of each coarse scale cell

c_i : Volume fraction of each material and

β^* is:

$$\beta^* = \frac{2(4 - 5\nu^*)}{15(1 - \nu^*)} \tag{4-2}$$

Due to the importance of tracking shear strain and volumetric strain during SAGD thermal recovery process, these two geomechanical responses are considered as the geomechanical responses of interest and accuracy of proposed numerical upscaling technique is compared with other techniques by comparing the shear strain and volumetric strain obtained from geomechanical simulation of fine scale and upscaled models. During growth of the SAGD steam chamber, expansion of sand inside the reservoir is accompanied by shear strain. This shear strain may result in casing/wellbore failure. Growth of the SAGD steam chamber is accompanied by changes in pressure and temperature, leading to reservoir deformation and, thus, a change in the permeability of the formation. Change in permeability of formation is a function of the volumetric strain (Li, 2006; Adhikary, 1991; Oldakowski, 1994; and Touhidi-Baghini, 1998).

In the following section, first, theoretical background is reviewed briefly. Proposed numerical upscaling technique is explained in details after that. By considering synthetic two facies model, representative of sand/shale facies

configuration of the McMurray Formation, fine scale geomechanical simulations are compared with upscaled simulation results. Proposed numerical technique conventional power and Budiansky's approaches are used to move from fine scale elastic property models to coarse scale one. Results and discussion section comes at the end.

THEORETICAL BACKGROUND

Elastic deformation formulation could be found in numerous soil/rock mechanical engineering text books (Lekhnitskii (1981), Zoback (2007), Fjaer et al. (2008); to name a few). Hooke's Law is the main governing equation which is comprehensively used in classical theory of elasticity. The general form of Hooke's Law is:

$$\sigma_{ij} = A_{ijmn} e_{mn} \tag{4-3}$$

Where σ_{ij} is the 2nd order stress tensor, e_{mn} is the 2nd order strain tensor and A_{ijmn} is a general form of the 4th order elastic tensor. In the case of heterogeneous material, the characteristic tensor is described by Equation 4-4. Using more convenient notation, Hooke's Law is given by Equation 4-5.

$$A_{ijmn} = A_{ijmn}(x, y, z) \tag{4-4}$$

$$\begin{bmatrix} \sigma_x \\ \sigma_y \\ \sigma_z \\ \tau_{zy} \\ \tau_{zx} \\ \tau_{xy} \end{bmatrix} = \begin{bmatrix} A_{11} & A_{12} & A_{13} & A_{14} & A_{15} & A_{16} \\ A_{21} & A_{22} & A_{23} & A_{24} & A_{25} & A_{26} \\ A_{31} & A_{32} & A_{33} & A_{34} & A_{35} & A_{36} \\ A_{41} & A_{42} & A_{43} & A_{44} & A_{45} & A_{46} \\ A_{51} & A_{52} & A_{53} & A_{54} & A_{55} & A_{56} \\ A_{61} & A_{62} & A_{63} & A_{64} & A_{65} & A_{66} \end{bmatrix} \begin{bmatrix} e_x \\ e_y \\ e_z \\ e_{zy} \\ e_{zx} \\ e_{xy} \end{bmatrix} \tag{4-5}$$

Micro features commonly arise in natural and synthetic materials in such a way as to produce a stress-strain response with particular symmetries. The elastic characteristic matrix A_{ijmn} (or in contracted form, A_{ij}) can be simplified with reasonable symmetry assumptions. Orientations for which an anisotropic material

has the same stress-strain response can be determined by coordinate transformation. Transversely isotropic deformation is commonly assumed and specifies that a material possess an axis of symmetry of order n when the elastic moduli remains unchanged for rotations of 2π/n radians about the axis (Figure 4-3).

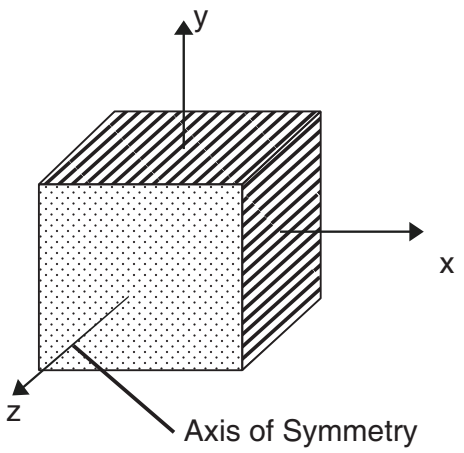

Figure 4-3 Plane of symmetry for transversely isotropic materials.

The elasticity stiffness matrix, assuming transverse isotropy, reduces to:

$$\begin{bmatrix} A_{11} & A_{12} & A_{13} & 0 & 0 & 0 \\ A_{21} & A_{11} & A_{23} & 0 & 0 & 0 \\ A_{31} & A_{32} & A_{33} & 0 & 0 & 0 \\ 0 & 0 & 0 & A_{44} & 0 & 0 \\ 0 & 0 & 0 & 0 & A_{44} & 0 \\ 0 & 0 & 0 & 0 & 0 & (A_{11} - A_{12})/2 \end{bmatrix}$$

Thus, the elasticity matrix for the transversely isotropic case reduces to having only five independent stiffness components. Further simplification of this system is obtained by assuming plane strain. If the dimension of the body in one direction, x_3, is considerably larger than the dimension of body in other two directions, it can be said that displacement in that direction would be zero. In other words:

$$U_1=u_1(x_1,x_2)$$
$$U_2=u_2(x_1,x_2) \qquad (4\text{-}6)$$

U_3=constant

As a result it can be assumed that:

$$e_{33}=e_{32}=e_{31}=0 \tag{4-7}$$

If the dimension of the body in one direction, x_3, is considerably smaller than the dimensions of the body in the other two directions, $\sigma_{33}= \sigma_{32}= \sigma_{33}= e_{32}=e_{31}= 0$ but e_{33} is not zero. In the proposed methodology, the plane strain condition is considered to reduce the dimensionality of the problem. Thus, Hooke's Law in the case of transverse isotropy and plane strain simplifies to:

$$\begin{bmatrix} e_{11} \\ e_{22} \\ 0 \\ e_{12} \end{bmatrix} = \begin{bmatrix} a_{11} & a_{12} & a_{13} & 0 \\ a_{21} & a_{22} & a_{23} & 0 \\ a_{31} & a_{32} & a_{33} & 0 \\ 0 & 0 & 0 & 1/2G' \end{bmatrix} \begin{bmatrix} \sigma_{11} \\ \sigma_{22} \\ \sigma_{33} \\ \sigma_{12} \end{bmatrix} \tag{4-8}$$

In terms of elastic properties, young modulus (E) and poisson's ratio (ν):

$$\begin{bmatrix} e_{xx} \\ e_{yy} \\ 0 \\ e_{xy} \end{bmatrix} = \begin{bmatrix} 1/E_x & -\nu_{yx}/E_y & -\nu_{zx}/E_z & 0 \\ -\nu_{xy}/E_x & 1/E_y & -\nu_{zy}/E_z & 0 \\ -\nu_{xz}/E_z & -\nu_{yz}/E_y & 1/E_z & 0 \\ 0 & 0 & 0 & 1/2G' \end{bmatrix} \begin{bmatrix} \sigma_{xx} \\ \sigma_{yy} \\ \sigma_{zz} \\ \sigma_{xy} \end{bmatrix} \tag{4-9}$$

where

E_i: young modulus in tension/compression

ν_{ij}: poisson ratio characterizing contraction in the direction of one axis when tension is applied in a different direction. For example, ν_{yx} is the ratio characterizing the contraction in x when tension is applied in y.

Assuming X-Z is the plane of symmetry:

$$E_x = E_z$$
$$\nu_{xz} = \nu_{zx} \quad (4\text{-}10)$$
$$\nu_{xy} = \nu_{zy}$$

By considering:

$$E_x = E_z = xm$$
$$E_y = ym$$
$$\nu_{xz} = \nu_{zx} = nux \quad (4\text{-}11)$$
$$\nu_{xy} = \nu_{zy} = nuy$$

Where;

xm: young modulus in the plane of symmetry

ym: young modulus in the plane perpendicular to the plane of symmetry

nux: poisson ratio for the normal strain in the x-direction (in the plane of isotropy) related to the normal strain in the z-direction due to uniaxial stress in the z-direction

nuy: poisson ratio for the normal strain in the y-direction (in the plane perpendicular to the plane of isotropy) related to the normal strain in the x-direction (in the plane of isotropy) due to uniaxial stress in the x-direction.

By knowing:

$$\nu_{xy}/E_x = \nu_{yx}/E_y \quad (4\text{-}12)$$

Equation 4-9 is simplified to:

$$\begin{bmatrix} e_{xx} \\ e_{yy} \\ 0 \\ e_{xy} \end{bmatrix} = \begin{bmatrix} 1/xm & -nuy/xm & -nux/xm & 0 \\ -nuy/xm & 1/E_y & -nuy/xm & 0 \\ -nux/xm & -nuy/xm & 1/xm & 0 \\ 0 & 0 & 0 & 1/2G' \end{bmatrix} \begin{bmatrix} \sigma_{xx} \\ \sigma_{yy} \\ \sigma_{zz} \\ \sigma_{xy} \end{bmatrix} \quad (4\text{-}13)$$

Five parameters are required to fully characterize the problem under the above assumptions: xm, ym, nux, nuy and G' (G_{xy}) which is the shear modulus between the plane of isotropy and the perpendicular plane. With good approximation, G' (G_{xy}) can be determined from Equation 4-14 (Lekhnitskii, 1981).

$$G_{xy} = \frac{E_x E_y}{E_x(1 + 2\nu_{xy}) + E_y} \tag{4-14}$$

PROPOSED METHODOLOGY FOR LOCAL UPSCALING OF ELASTIC PROPERTIES

The proposed numerical upscaling of elastic properties is similar to local upscaling of permeability, but is applied to elastic properties and geomechanical simulation. Conceptually, the numerical upscaling of elastic geomechanical properties is shown in Figure 4-4.

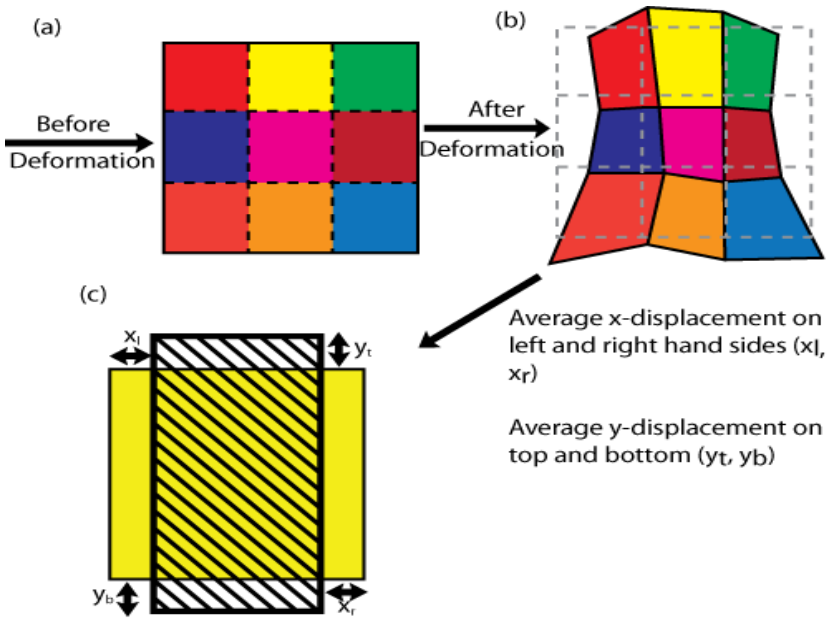

Figure 4-4 Schematic of local upscaling.

Each fine scale cell (Figure 4-4a) has its own elastic properties which could be different from the surrounding cells (heterogeneous media). Loading applied on the fine scale cells (Figure 4-4a) results in complex deformation (Figure 4-4b). After upscaling this system to a single block, the goal is to reproduce the average

fine scale deformation in the coarse scale block (Figure 4-4c). The coarse upscaled property (yellow color in Figure 4-4c) is the value that results in the average displacement had the fine scale model been deformed. The upscaling process reduces to determining the value of five parameters (Equations 4-13 and 4-14) for a coarse cell that results in the same average displacement as the fine scale model. The remainder of this section details each step of the upscaling process:

Step 1: Solve the transversely isotropic Hooke's law (Equation 4-13) for the boundary of the target coarse scale cell. In this step the strain tensor, (left-hand-side matrix in Equation 4-13), is calculated and the non-uniformly deformed body (Figure 4-4b) is obtained.

Step 2: Average the displacement on the border of the coarse scale body. In this step, the hatched black rectangle (Figure 4-4c) is obtained.

Step 3: Calculate the characteristic elastic parameters which result in the same stress and strain tensor applied on the uniformly deformed body. In this step, Equation 4-13 is solved again for the uniformly deformed body.

G' is determined from Equation 4-14, thus there are four unknowns determined from the uniform stress and strain tensors.

The number of equations obtained in a single loading configuration is less than the number of unknowns; therefore, it is not possible to determine all required values by applying one stress configuration. Two different initial boundary conditions are considered. Figure 4-5 shows the initial boundary conditions for the first (top) and second (bottom) loading scenarios. In addition to these two boundary conditions, an unsuccessful attempt at pure shear loading scenarios was conducted. The reasons for why pure shear did not provide valuable results remain unclear. However, it should still be considered as a candidate for initial loading and boundary conditions in future research.

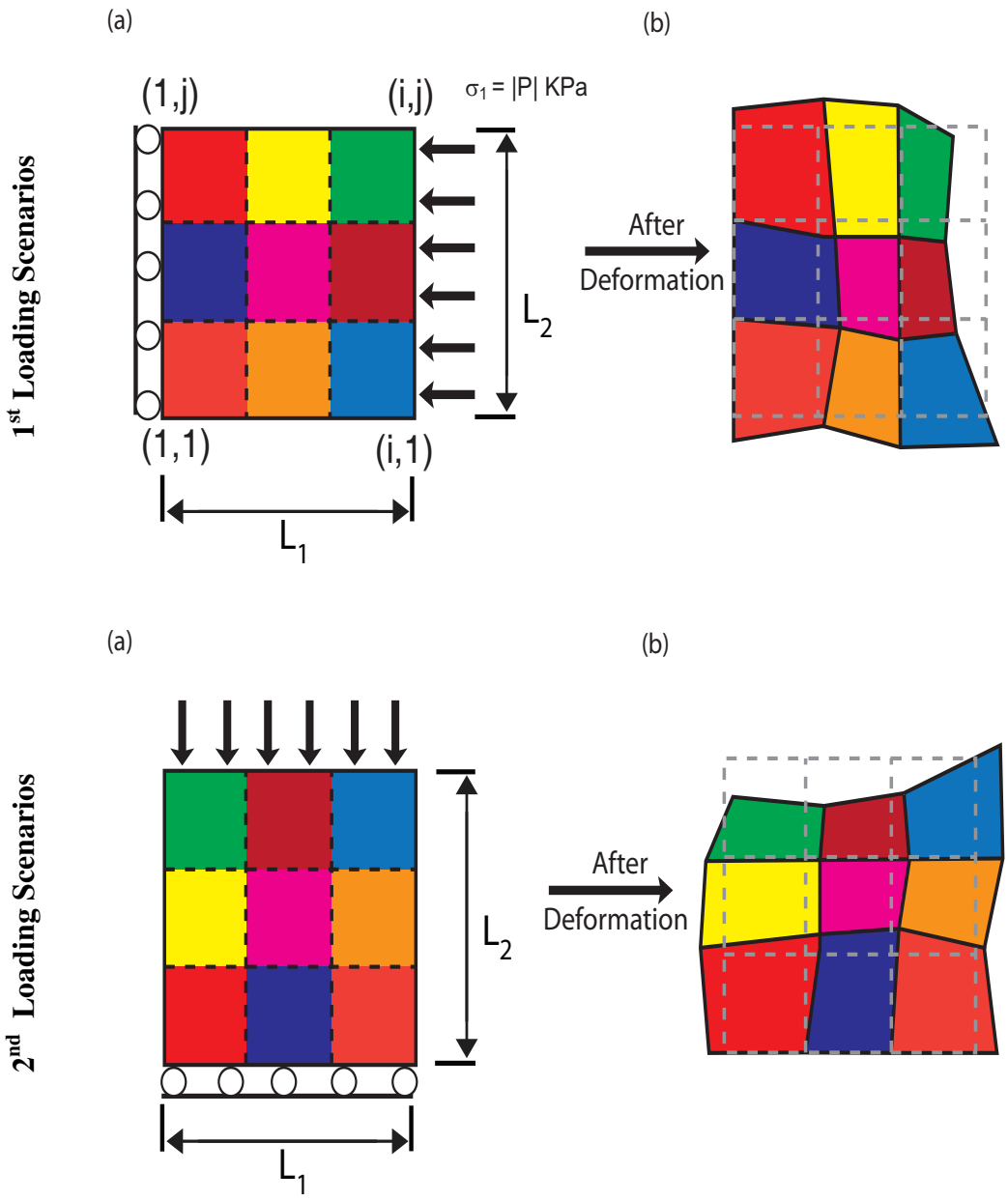

Figure 4-5 Initial loading conditions for loading scenarios.

where,

L_1: the initial length of coarse scale cell in the X direction.

L_2: the initial length of coarse scale cell in the Y direction.

i: the number of fine scale cells in the X direction of the coarse scale cell.

j: the number of fine scale cells in the Y direction of the coarse scale cell

Hooke's Law (Equations 15 and 16) are considered for the uniformly deformed body as a result of the first and second loading scenarios.

$$\begin{bmatrix} <e^1{}_{11}> \\ <e^1{}_{22}> \\ 0 \end{bmatrix} = \begin{bmatrix} 1/_{xm} & -nuy/_{xm} & -nux/_{xm} \\ -nuy/_{xm} & 1/_{E_y} & -nuy/_{xm} \\ -nux/_{xm} & -nuy/_{xm} & 1/_{xm} \end{bmatrix} \begin{bmatrix} <\sigma^1{}_{11}> \\ 0 \\ <\sigma^1{}_{33}> \end{bmatrix} \tag{4-15}$$

$$\begin{bmatrix} <e^2{}_{11}> \\ <e^2{}_{22}> \\ 0 \end{bmatrix} = \begin{bmatrix} 1/_{xm} & -nuy/_{xm} & -nux/_{xm} \\ -nuy/_{xm} & 1/_{E_y} & -nuy/_{xm} \\ -nux/_{xm} & -nuy/_{xm} & 1/_{xm} \end{bmatrix} \begin{bmatrix} 0 \\ <\sigma^2{}_{22}> \\ <\sigma^2{}_{33}> \end{bmatrix} \tag{4-16}$$

Where,

$<\sigma^1{}_{33}>$ and $<\sigma^2{}_{33}>$: the average σ_{33} as a result of the first and second loading configuration.

$<e^1{}_{11}>$, $<e^1{}_{22}>$ and $<e^2{}_{11}>$, $<e^2{}_{22}>$: the equivalent strain components for the uniformly deformed body for the first and second loading scenarios.

These can be obtained from:

$$\langle e_{11} \rangle = \frac{(\sum_{(i)} \mathrm{xdisp_l})/\mathrm{i} + (\sum_{(i)} \mathrm{xdisp_r})/\mathrm{i}}{L_1}$$

$$\langle e_{22} \rangle = \frac{(\sum_{(j)} \mathrm{ydisp_t})/\mathrm{j} + (\sum_{(j)} \mathrm{ydisp_b})/\mathrm{j}}{L_2} \tag{4-17}$$

Where,

$(\sum_{(i)} \mathrm{xdisp_l})/\mathrm{i}$: Average displacement of the fine scale cells on the left hand boundary of the coarse cell.

$(\sum_{(i)} \mathrm{xdisp_r})/\mathrm{i}$: Average displacement of the fine scale cells on the right hand boundary of the coarse cell.

$(\sum_{(j)} ydisp_t)/j$: Average displacement of fine scale cells on the top boundary of the coarse cell.

$(\sum_{(j)} ydisp_b)/j$: Average displacement of fine scale cells on the bottom boundary of the coarse cell.

From these loading configurations, the following system of equations (Equation 4-18 for the first loading scenario and Equation 4-19 for the second) is obtained.

$$\langle e_{11}^1 \rangle = \left(\frac{1}{xm}\right)\langle \sigma_{11}^1 \rangle + \left(\frac{-nux}{xm}\right)\langle \sigma_{33}^1 \rangle \quad (a)$$

$$\langle e_{22}^1 \rangle = \left(\frac{-nuy}{xm}\right)\langle \sigma_{11}^1 \rangle + \left(\frac{-nuy}{xm}\right)\langle \sigma_{33}^1 \rangle \quad (b) \quad (4\text{-}18)$$

$$0 = \left(\frac{-nux}{xm}\right)\langle \sigma_{11}^1 \rangle + \left(\frac{1}{xm}\right)\langle \sigma_{33}^1 \rangle \quad (c)$$

$$\langle e_{11}^2 \rangle = \left(\frac{-nuy}{xm}\right)\langle \sigma_{22}^2 \rangle + \left(\frac{-nux}{xm}\right)\langle \sigma_{33}^2 \rangle \quad (a)$$

$$\langle e_{22}^2 \rangle = \left(\frac{1}{ym}\right)\langle \sigma_{22}^2 \rangle + \left(\frac{-nuy}{xm}\right)\langle \sigma_{33}^2 \rangle \quad (b) \quad (4\text{-}19)$$

$$0 = \left(\frac{-nuy}{xm}\right)\langle \sigma_{22}^2 \rangle + \left(\frac{1}{xm}\right)\langle \sigma_{33}^2 \rangle \quad (c)$$

From these systems of equations, elastic characteristic parameters of the upscaled cell can be calculated. This process is repeated for all coarse cells. In Appendix B, scripting file for two loading scenario (Figure 4-5) is shown for simple block example. In this example it has been tried to show how loads are applied to the block and illustrate averaged parameters which should be used in Equations 4-18 and 4-19.

EXAMPLE

Consider a synthetic reservoir surrounded by side, under and overburden (Figure 4-6). This geometry is used to test the proposed methodology with the goal of predicting the response of the central reservoir. Using sequential indicator simulation (SIS) a heterogeneous facies model is generated for the central zone of interest. The side, under and overburdens are included to minimize boundary effects and are assumed homogeneous (Table 4-1). Table 4-2 summarizes the number of cells used in each zone for the fine scale model.

The heterogeneous central zone is modeled with unconditional SIS (Figure 4-7) using GSLIB (Deutsch and Journel, 1998). A realistic shale proportion of 20% is assumed. Rock properties for each facies are listed in Table 4-1.

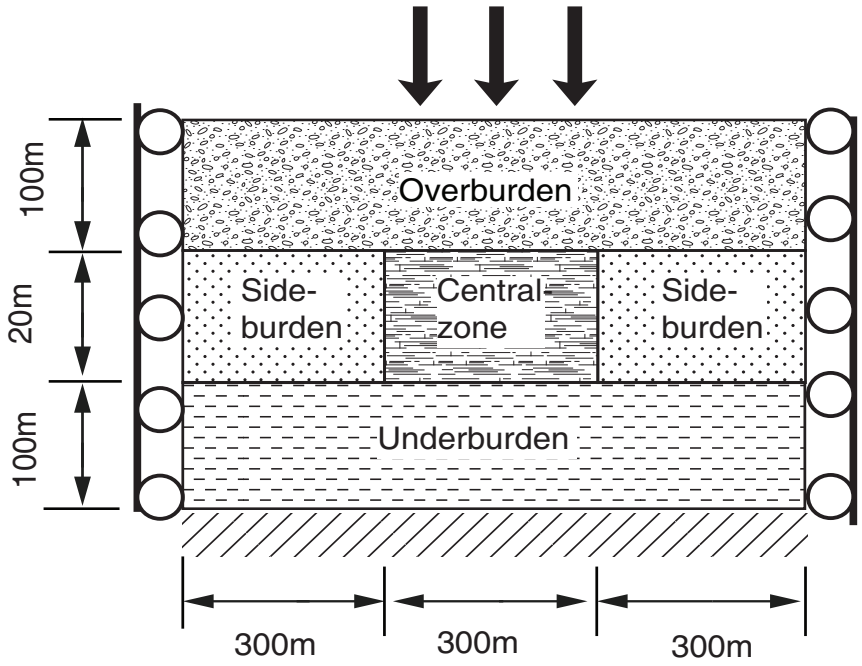

Figure 4-6 Geometry of the area of interest used.

Table 4-1 Material properties in each section of Figure 4-6.

Zone	Elastic deformation type	Young modulus (MPa)	Poisson ratio
Over burden	Isotropic	250	0.3
Side burden	Isotropic	480	0.3
Central	Transversely isotropic	Sand Facies: 600 Shale Facies: 300	0.3
Under burden	Isotropic	5000	0.3

Table 4-2 Number of grid cells.

Zone	Horizontal	Vertical
Over burden	360	10
Side burden	30	40
Central	300	40
Under burden	360	10

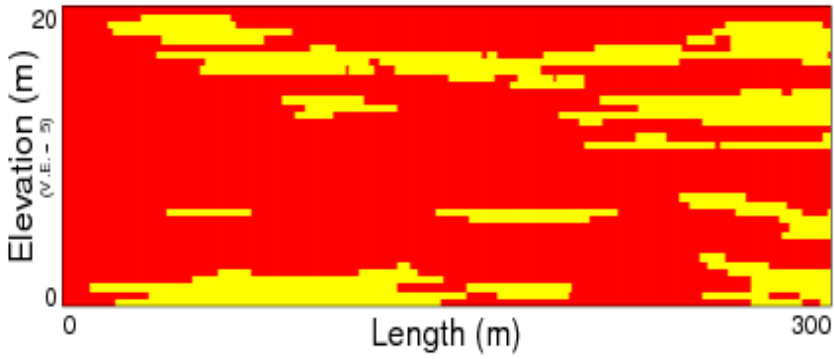

Figure 4-7 SIS facies realization considered with 20% shale. Red (dark) is sand; yellow (light) is shale. Variogram parameters: one spherical structure with a vertical range of 4m, horizontal range of 120m and no nugget effect.

RESULTS

Decreasing computational time while reproducing the fine scale model response with a coarser grid is the main objective of upscaling. Various upscaling ratios (number of fine scale cells in each upscaled block) with the previously described model are considered to assess the proposed upscaling methodology. In total, 15 upscaling ratios are considered; horizontal ratios of 1:1, 5:1, 15:1, 30:1, 60:1, 100:1 and vertical ratios of 1:1, 4:1 and 8:1. In the following section, upscaling maps of young modulus, error analysis results and computational time vs. number of cells are examined.

Young modulus response

In Figures 4-8 the results of upscaling of young modulus are shown. Blocks are scaled in the horizontal direction only as the vertical heterogeneity is typically very important in this type of reservoir. Similar results are obtained for other ratios. In Figure 4-9, by considering upscaling ratio of 4:1 in vertical direction the results of upscaling of young moduli in vertical direction are shown as well. In Figure 4-10, upscaled young moduli in two different directions, i.e. xm and ym, are shown for different horizontal upscaling ratios and for vertical upscaling ratio of 8:1.

Averaging in the vertical direction has a larger effect on upscaling because of the shorter vertical variogram range typical of the McMurray Formation. The effect of considering a 30:1 horizontal ratio is minimal as shale's are typically more continuous horizontally, but a 4:1 ratio vertically is significant.

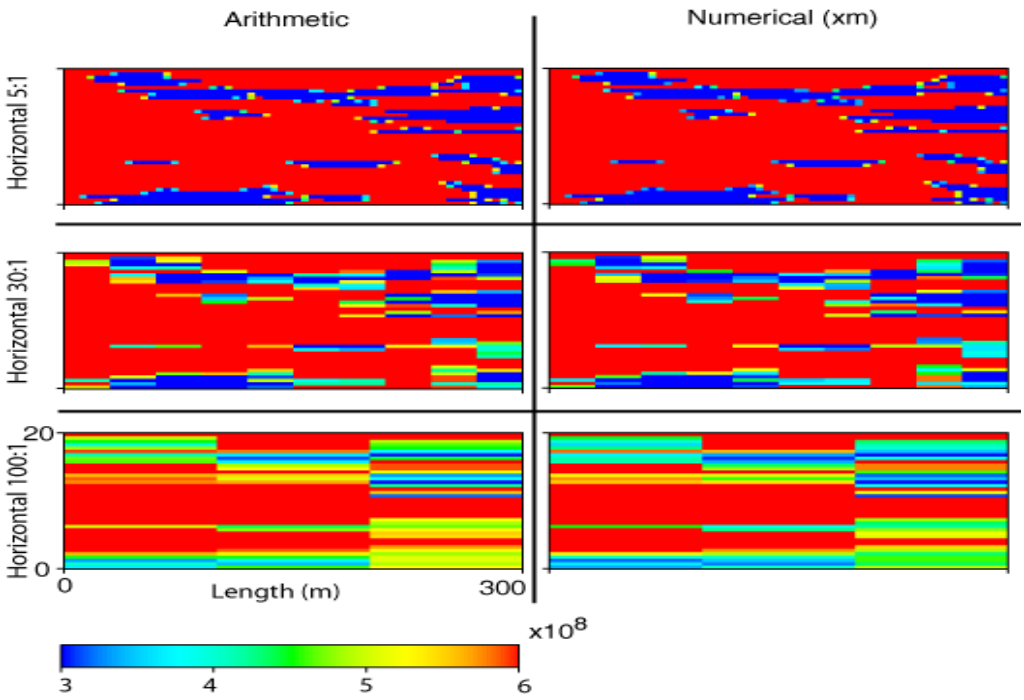

Figure 4-8 Young modulus for different horizontal upscaling ratios, vertical upscaling ratio is constant at 1:1.

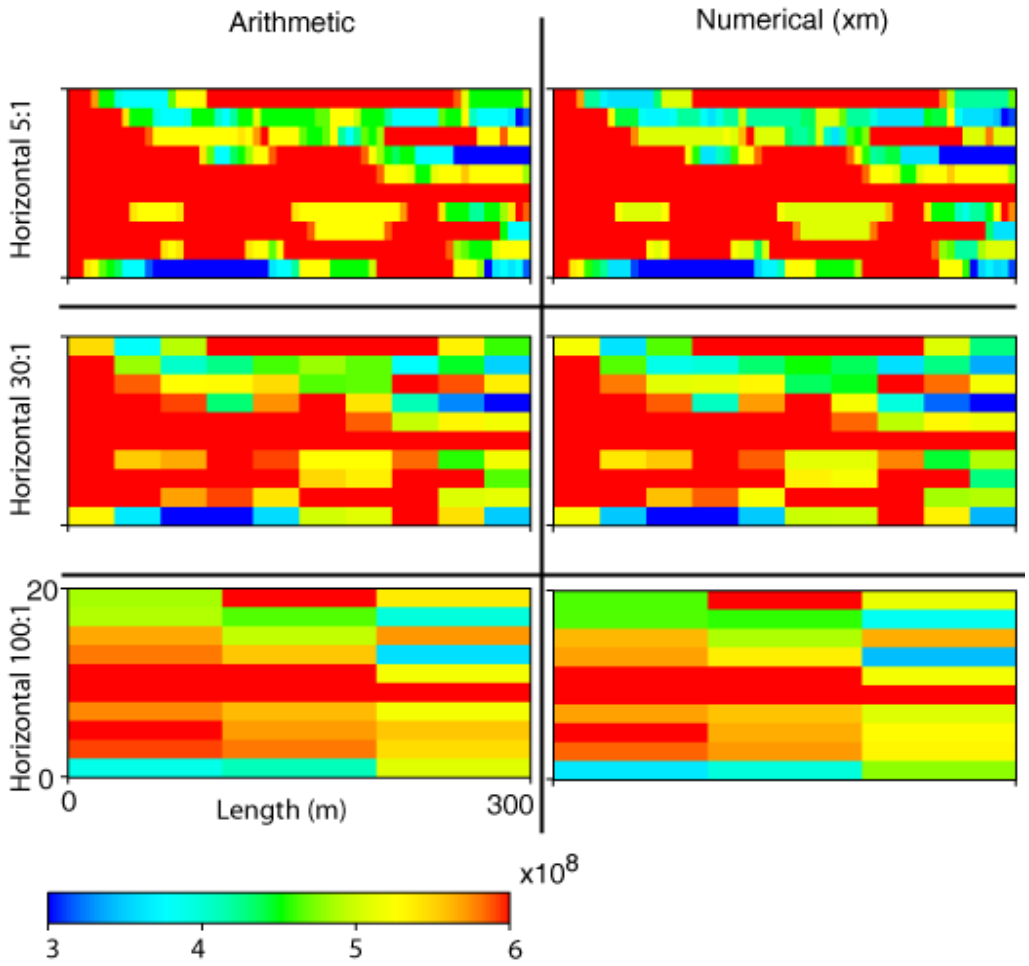

Figure 4-9 Young modulus for different horizontal upscaling ratios, vertical upscaling ratio is constant at 4:1.

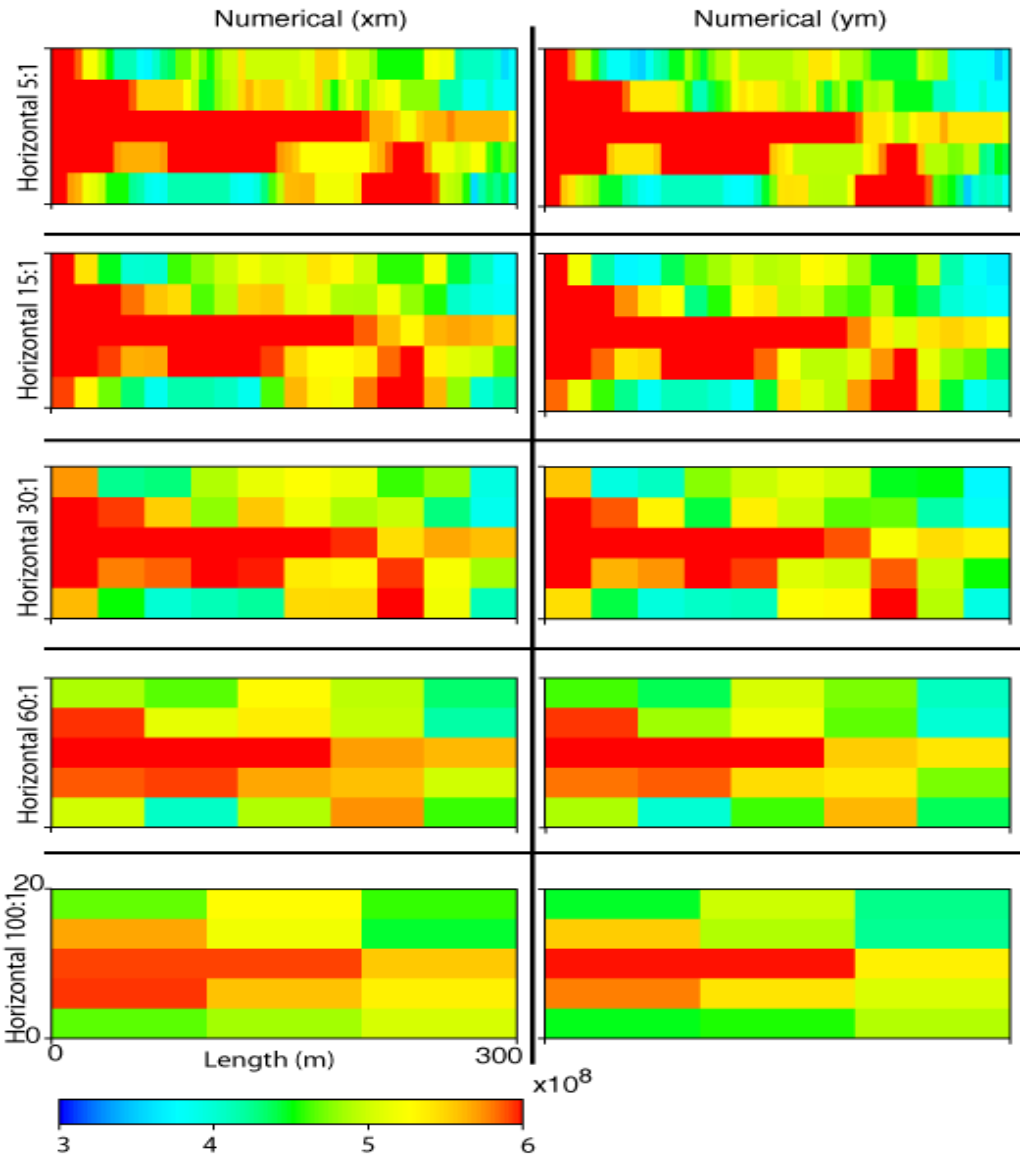

Figure 4-10 Young modulus for different horizontal upscaling ratios, vertical upscaling ratio is constant at 8:1.

The volumetric strain and shear strain behavior of the fine and coarse scale models are compared with an error function which is defined as:

$$[\%]e = \frac{\sum_r \left|1 - \frac{\overline{a_{v_r}}}{a_{v_r}}\right|}{n_r} * 100 \tag{4-20}$$

where,

$\overline{a_{v_r}}$: The average volumetric/shear strain of the fine scale cells in the r^{th} upscaled block, (Equation 4-21).

a_{v_r} : The volumetric/shear strain in the r^{th} upscaled block.

n_r: The number of blocks in the upscaled model.

$$\overline{a_{v_r}} = \frac{\sum_i a_{v_i}}{n_i} * 100 \tag{4-21}$$

where,

a_{v_i}: The volumetric/shear strain in the i^{th} fine scale cell within the upscaled block.

n_i: The number of fine scale cells in each upscaled block.

A volumetric/shear strain (Equation 4-21) map for the fine scale model at the same scale as the coarse scale model can be created. The geomechanical response of the fine and coarse scale models can be compared (Equation 4-20). Obviously, less error means more accurate upscaling process. The effect of different upscaling processes on volumetric strain and shear strain are shown in Figures 4-11 and 4-12. The proposed numerical averaging technique is superior for all vertical and horizontal upscaling dimensions considered. The error surface map of numerical upscaling for volumetric strain and shear strain are shown in Figure 4-13. Note that error increases significantly above a vertical upscaling of 4 blocks because the nominal thickness of the shale layers in this example is approximately 4 blocks.

One of the purposes of upscaling is to reduce simulation runtime. Considering fewer cells in the model has a significant effect on the CPU time (Figure 4-14). The idea would be to select a suitable compromise between error (Figures 4-11 through 4-13) and run time (Figure 4-14).

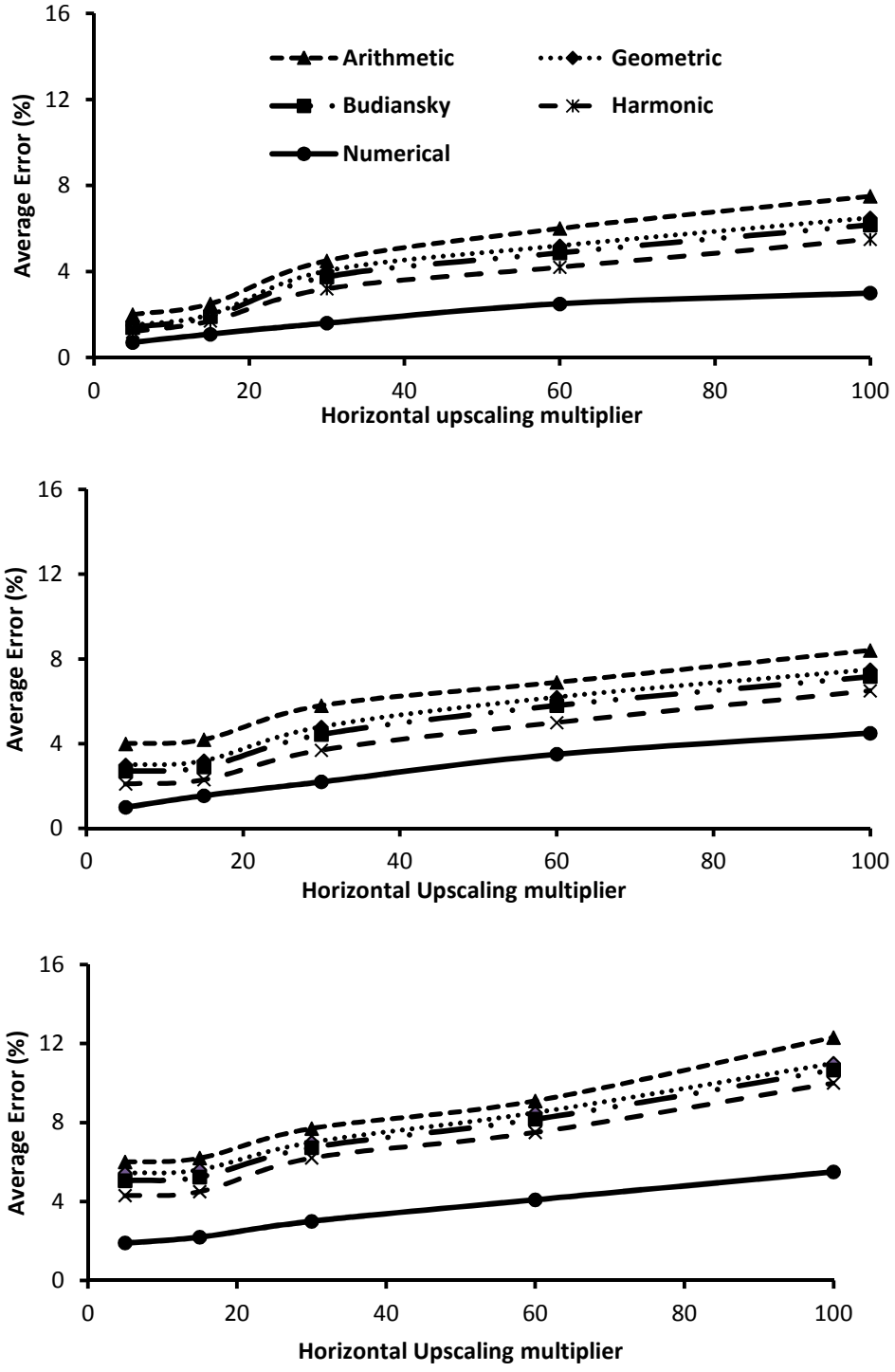

Figure 4-11 Average error for various horizontal upscaling multipliers; considering volumetric strain as geomechanical response. Vertical upscaling ratios are: 1:1 (above), 4:1 (middle) and 8:1 (below) (lines are trend lines only).

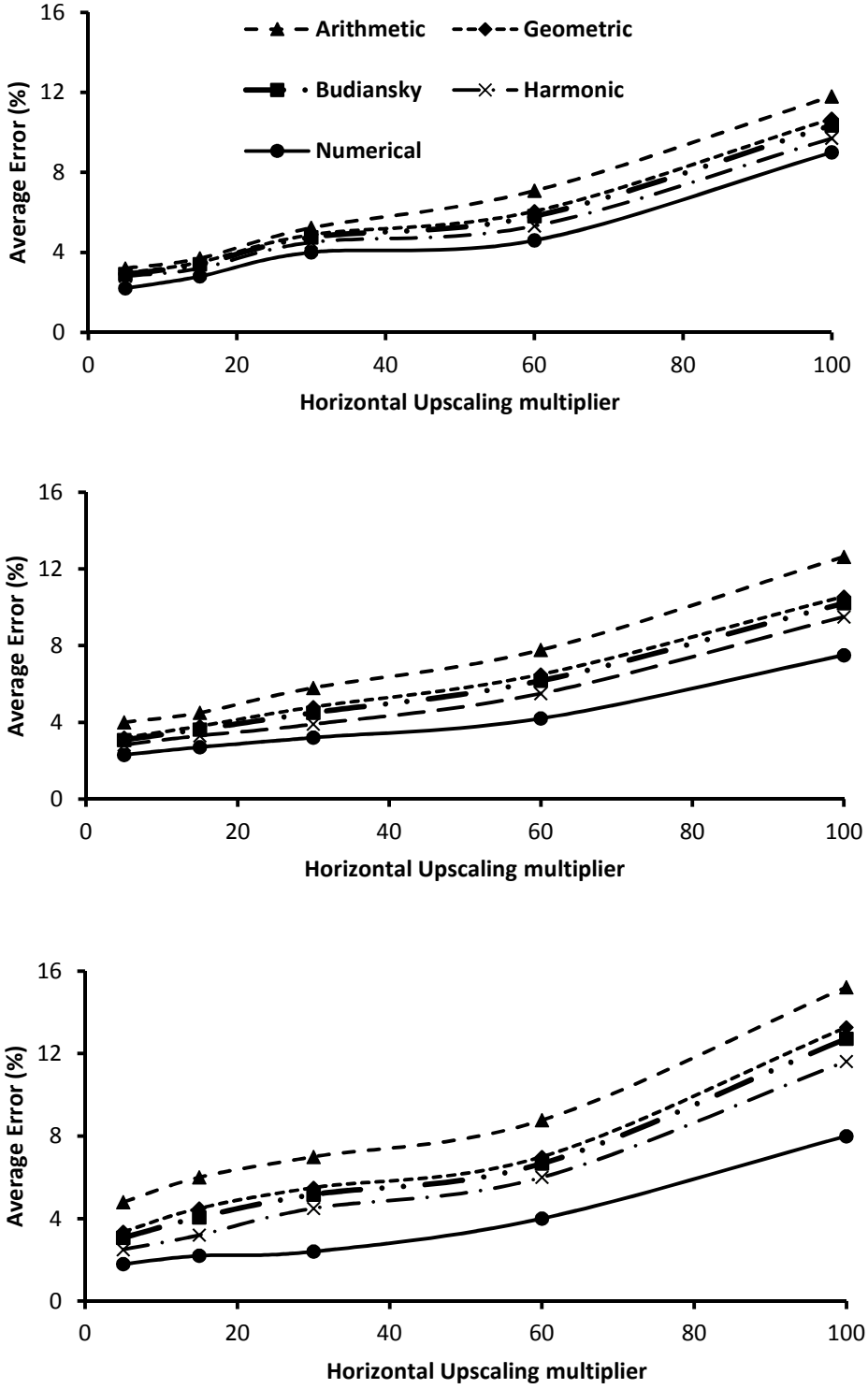

Figure 4-12 Average error for various horizontal upscaling multipliers; considering shear strain as geomechanical response. Vertical upscaling ratios are: 1:1 (above), 4:1 (middle) and 8:1 (below) (lines are trend lines only).

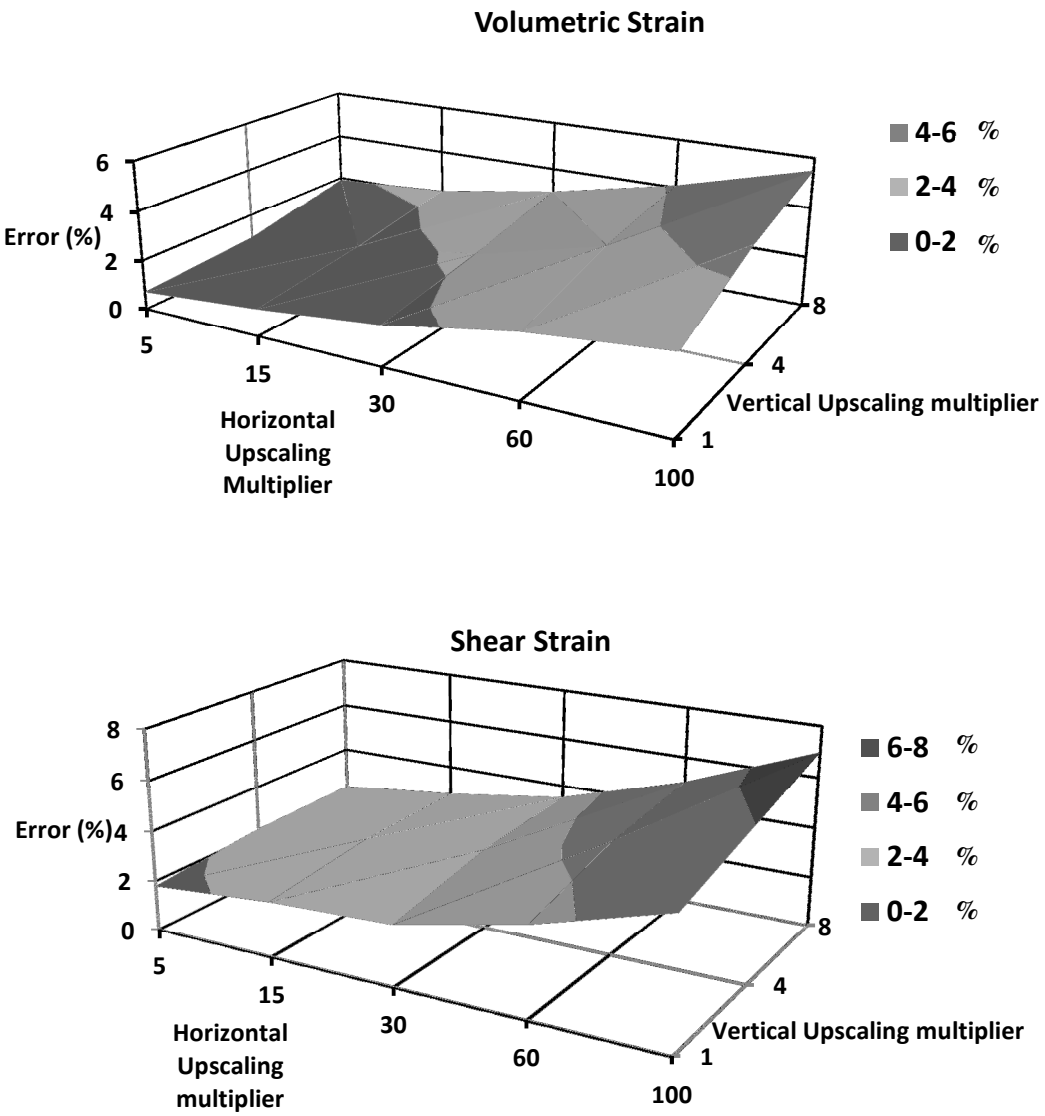

Figure 4-13 Error surface map of numerical upscaling for volumetric strain (above) and shear strain (below).

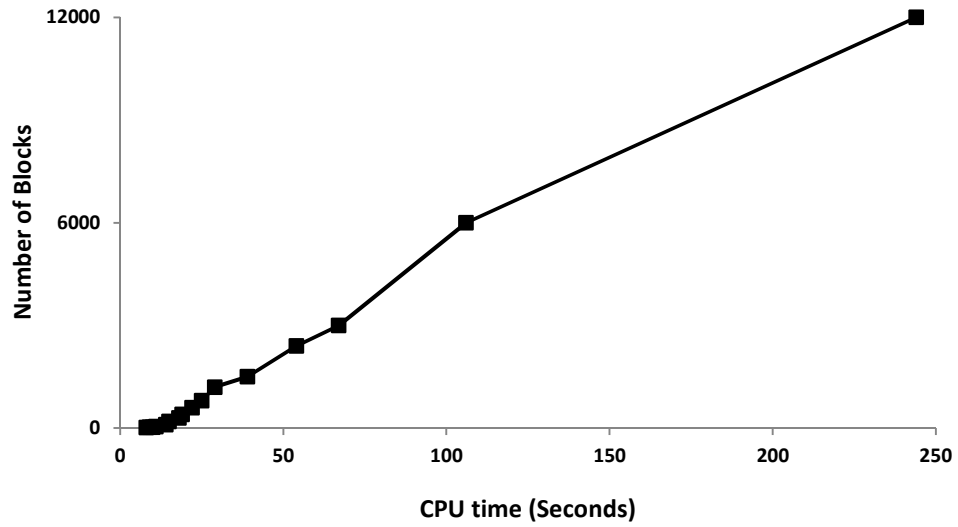

Figure 4-14 CPU time for geomechanical simulation of the model in Figure 4-7 (line is trend line only).

DISCUSSION AND CONCLUSION

A novel numerical local upscaling technique for elastic properties is proposed. Upscaling error was assessed by considering volumetric strain and shear strain as the geomechanical response. The difficulty with considering analytical upscaling is determining how restrictive the inherent assumptions are and they are often sensitive to parameter calibration. The proposed technique was able to better reproduce the fine scale response for the methods considered and is appropriate for domains that can be characterized by transverse isotropy. Additionally and in comparison to previously developed analytical averaging techniques there is no restriction on material distribution inside of the domain under study and it could be applied for all material configurations such as complex sand/shale facies configuration of the McMurray formation in Alberta-Canada.

It is important to consider the scale of the coarse blocks. As shown, error increases with increasing upscaling block sizes. In considered example in this chapter, variogram range in vertical direction was much lower than variogram range in horizontal direction. Accordingly, it is expectable to get more error by upscaling in vertical direction more than upscaling in horizontal direction. This error increase considerably upscaling ratios for which size of coarse block is more

than size variogram range. For a given problem, the acceptable error in the response should be quantified by the practitioner and an appropriate block size selected. Smaller block sizes are preferred but often the flow/geomechanical simulation time is the driving factor for block size selection. In geomechanical simulation, homogenous property models dominate the field and there are few upscaling options.

REFERENCES

Adhikary, D.P. 1991. Laboratory investigation of effects of stress changes of hydraulic conductivity of reconstituted oil sands. M.Eng Report, University of Alberta, Edmonton, Canada.

Backus, G. 1962. Long-wave elastic anisotropy produced by horizontal layering. Journal of Geophysical Research. 67(11): 4427-4440.

Budiansky, B. 1965. On the elastic moduli of some heterogeneous materials. Journal of the Mechanics and Physics of Solids. 13(4): 223-227.

Deutsch, C. V. and Journel, A. G. 1998. GSLIB: Geostatistical Software Library and User's Guide. Second edition, Oxford, New York.

Deutsch, C.V. 1989. Calculating Effective Absolute Permeability in Sandstone/Shale Sequences. SPE Formation Evaluation Journal. 4 (3): 343–3,348.

Durlofsky, L. J. 1991. Numerical calculation of equivalent grid block permeability tensors for heterogeneous porous media. Water Resources Research. 27(5): 669-708.

Durlofsky, L.J. 2005. Upscaling and gridding of fine scale geological models for flow simulation. Presented at 8th international forum of reservoir simulation, Stresa, Italy,

Elkateb, T. M. 2003. Quantification of Soil Heterogeneity. PhD dissertation, University of Alberta, Edmonton, Canada.

Fjaer, E., Holt, R.M., Horsrud, P., Raaen, A.M. and Risnes, R. 2008. Petroleum Related Rock Mechanics. Second edition, Elsevier.

Hashin, Z. and Shtrikman, S. 1962. On some variational principles in anisotropic and nonhomogeneous elasticity. Journal of the Mechanic and Physics of Solids. 10(4): 335-342.

Hashin, Z. and Shtrikman, S. 1963. A variational approach to the theory of the elastic behaviour of multiphase materials. Journal of the Mechanic and Physics of Solids. 11(2): 127-140.

Hill, R. 1963. Elastic properties of reinforced solids, some theoretical principles. Journal of the Mechanic and Physics of Solids. 11 (4): 281-287.

Kasap, E. and Lake, L. W. 1990. Calculating the effective permeability tensor of a gridblock. SPE Formation Evaluation. 5(2):192-200.

King, M. J. and Mansfield., M. 1999. Flow simulation of geologic models. SPE Reservoir Evaluation & Engineering. 2 (4): 351–367.

Lekhnitskii, S.G. 1981. Theory of Elasticity of an Anisotropic Body. Moscow: Mir Publishers.

Li, P. 2006. Numerical Simulation of the SAGD Process Coupled With Geomechanical Behaviour. PhD dissertation, University of Alberta, Edmonton, Canada.

Mackenzie, J. 1950. The elastic constants of a solid containing spherical holes. Proceedings of the Royal Society London. 63(1): 2-11.

Norris, R.J. and Lewis, J. M. 1991. The geological modelling of effective permeability in complex heterolithic facies. Proceeding of the 66th Annual Technical Conference and Exhibition, Dallas, USA, SPE No. 22692.

Oldakowski, K. 1994. Stress induced permeability changes of Athabasca oilsands. M.Sc. thesis, University of Alberta, Edmonton, Canada.

Pickup, G.E., Ringrose, P.S. Jensen, J.L. and Sorbie, K.S. 1994. Permeability tensors for sedimentary structures. Mathematical Geology. 26(2): 227-250.

Rijpsma, G., and Zijl, W. 1998. Upscaling of Hooke's Law for Imperfectly Layered Rocks. Journal of Mathematical Geology. 30(8): 943-969.

Salamon, M. 1968. Elastic moduli of a stratified rock mass. Journal of Rock Mechanics and Mining Sciences. 5(6):519-527.

Touhidi-Baghini, A. 1998. Absolute Permeability of McMurray Formation Oil Sands at Low Confining Stresses. PhD dissertation, University of Alberta, Edmonton, Canada.

Zoback, M.D. 2007. Reservoir Geomechanics. First edition, Cambridge university press.

CHAPTER 5: CASE STUDY

INTRODUCTION

Alberta's oil sands contain the largest crude bitumen resource in the world, having approximately 259 billion cubic meter of initial oil in place (AEUB, 2003). Surface mining can access approximately 10% of reserves located close to the surface; however the remaining 90% of reserves are only accessible through in-situ recovery technologies. Among all in-situ recovery techniques, Steam Assisted Gravity Drainage (SAGD), developed by Roger Butler (Butler, 1998) has been found to be the most effective.

A SAGD pad considers multiple horizontal well pairs drilled up to 1000 m long. The distance between upper injections well and lower production well is usually about 5m. After 3 to 6 months of steam injection through both wells to initiate inter-connectivity, steam continues to be injected through the upper injection well only. Oil is produced from the lower horizontal well. Cumulative oil production (COP) and Steam oil ratio (SOR) are two parameters which are usually used to evaluate the production performance of SAGD.

Although many parameters have an effect on SAGD performance, reservoir geology and heterogeneity distribution of facies and inherent properties are the most significant (Mclennan and Deutsch, 2004). Geostatistical techniques could be used to quantify uncertainty in geological model through construction of multiple equally probable realizations of reservoir properties and the difference between the performances of geological realizations is a measure of geological uncertainty (Deutsch et al., 2002). Each geological realization is a combination of a structural model, facies model and property models. In the case of conventional flow simulation, in which geomechanical effect is negligible, petrophysical properties are the only group of parameters which are required to be modeled

stochastically. These properties, i.e. porosity, permeability and water saturation, are used in fluid flow governing equations and the geological uncertainty is transferred to production uncertainty, i.e. uncertainty in production variable such as COP and SOR, by passing each realization through a flow simulator.

The oilsand in the McMurray Formation has an in-situ interlocked fabric (Dusseault and Morgenstern, 1978). Several experimental (e.g. Dusseault and Morgenstern, 1978, Chalaturnyk, 1996 and Touhidi-Baghini, 1998), and numerical studies,(e.g. Li, 2006, Chalaturnyk, 1996 and Azad, 2012), have been done and it has been shown that geomechanics has a significant effect on SAGD process and coupled geomechanical flow simulation should be considered to investigate the geomechanical effects on recovery for SAGD processes. Elastic and rock strength properties play the same role for rock mechanical governing equations as petrophysical properties play for fluid flow governing equations. These rock mechanical properties, i.e. elastic and rock strength properties have the same characteristics as petrophysical properties and could be modeled stochastically.

In Chapter 2 the effect of considering heterogeneous rock mechanical properties for coupled geomechanical flow simulation of SAGD on output variables of flow (COP and SOR) and geomechanics (vertical displacement profile (VDP)) was investigated by considering synthetic data. It was shown that, considering comprehensive geological models which include both flow and rock mechanical properties as heterogeneous maps instead of assuming homogeneous, layer cake, models for these properties, results in wider ranges of uncertainties and accordingly results in making more accurate decisions which should be made based on these types of analysis. If precise management of geological uncertainty is of interest coupled geomechanical flow simulation of SAGD should be used.

By considering real McMurray Formation data, providing a work flow for geological modeling of McMurray Formation, applying GR technique (developed in Chapter 3) to select one realization for further coupled geomechanical flow simulation of the SAGD process and comparing effect of upscaling of elastic

properties using harmonic averaging technique and proposed numerical technique (developed in Chapter 4) are the main purposes of this chapter. Set up of the study is summarized as follows:

a) Data preparation, stratigraphical transformation and upscaling
b) Gridding
c) Structural modeling
d) Statistical data analysis
e) Facies modeling
f) Property modeling and ranking of realizations
g) Upscaling and simulation results

Well log data used in this study are released from a current Athabasca oilsand SAGD project site. Due to confidentiality issues, the coordinates of wells are transformed to range of 0 to 10000 m in easting (X) direction and 0 to 5000 m in northing (Y) direction. 100 geological realizations are built through part (a) to part (f). P_{50} from the GR technique is selected for further simulation and upscaling steps. Using different upscaling ratios and considering harmonic and the upscaling technique described in Chapter 4 and considering volumetric strain as the metric for geomechanical response, the accuracy of the upscaling technique is compared against the harmonic averaging technique. The reason for selecting harmonic averaging technique among all other analytical techniques, considered in Chapter 4, is that this method of averaging/upscaling resulted in the least error in comparison to the other techniques but still considerable error with respect to developed numerical technique.

In the following sections, details of study (i.e. step (a) through (g)) are explained.

Step (a): Data preparation, stratigraphical transformation and upscaling

Conditioned data used for this study are digital well log data. Figure 5-1 illustrates the relative location of the wells in the project area. Grey square shown in the middle of this Figure is boundary of the region considered for further

geostatistical modeling. It should be noted that although stratigraphical and property modeling are performed in this section only, however variography is done based on all available data in big domain shown in Figure 5-1.

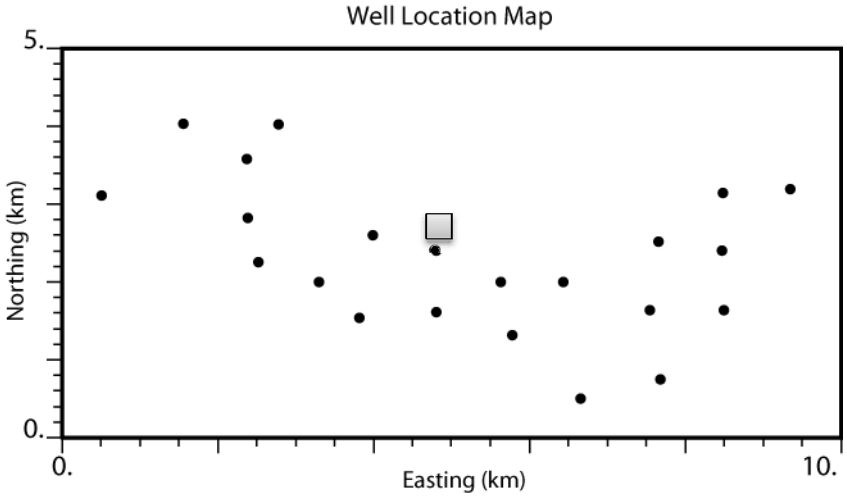

Figure 5-1 Location map of well data (black circles) and boundary of region considered for geostatistical modeling workflow (grey square).

Dipole sonic and bulk density logs (Δt_c, Δt_s and ρ_b) are the logs which are required for calculation of elastic properties. Equation 5-1 shows Young's modulus (E) formulations as a function of Δt_c, Δt_s and ρ_b respectively.

(5-1)

In which;

E_d: Dynamic Young modulus

Δt_s: Shear wave transformation time

Δt_c: Compression wave transformation time

ρ_b: Bulk Density

In Appendix C-1, by considering bulk density, compression and shear wave transformation time of one well, dynamic young modulus for that well is calculated by using Equation 5-1.

From the log analysis dynamic Young's modulus is obtained which is generally 2 to 5 times larger than static elastic properties. In reality and for simulation purposes, static elastic properties should be considered instead of dynamic ones. For calibrating dynamic young modulus and to move from dynamic to static, further information, e.g. experimental lab test results, is required. Due to lack of data, no calibration has been performed here.

In addition to these three logs, effective porosity information was also available. This information was available at intervals of 0.125 m. Structural markers for the top and bottom of the McMurray Formation are another group of data available for this study which are used to build top and bottom surface of McMurray Formation for the area under study.

No facies information was available. Two pseudo facies of sand and shale have been defined based on the cutoff on porosity values. For that purpose, data are initially transformed to a stratigraphical unit and then upscaled to 0.5 m interval. In Appendix C-2 the results of stratigraphical transformed and upscaled well log for one well is shown. To compare with 0.5 m interval, initial scale well log, i.e. 0.125 m interval, is shown with 0.5 m interval together.

In stratigraphical transformation, the vertical coordinate, which is measured depth (MD), is transformed to a stratigraphic coordinate, which is a depth relative to the top of McMurray Formation. In other words, after stratigraphical transformation, top of McMurray Formation is set to zero and all log readings below that get a negative value. The main objective of stratigraphical transformation is to construct a grid that preserves geological structure, e.g. variography, within each layer that is conform to the natural geological correlation (Deutsch, 2002).

After stratigraphical transformation, well log data are upscaled to thickness of grid which is going to be considered for further geostatistical modeling workflow, i.e. 0.5 m. Arithmetic averaging is used for upscaling of properties and all statistical analysis are performed on upscaled data. After stratigraphical transformation and upscaling process, appropriate cut offs, porosity in current work, should be defined for pseudo facies definition.

Facies with the value of porosity lower than 0.07 are considered as shale (Facies No. 0) and facies with the value of porosity more than 0.07 are considered as Sand (Facies No.1). In practical work flow, facies are defined based on expert knowledge and core analysis. Figure 5-2 shows histograms of porosity and facies after transformation of data to stratigraphical unit and upscaling to 0.5 m intervals. An average of 80% Sand facies and 20% of shale facies are obtained based on this facies definition.

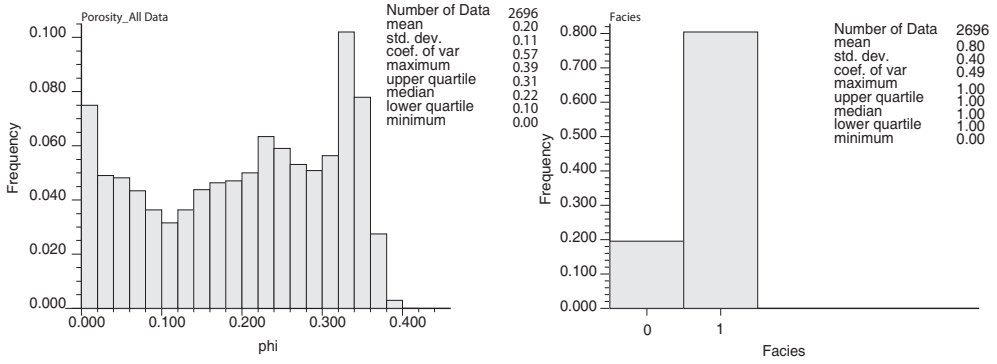

Figure 5-2 Histograms of porosity (left) and pseudo defined facies (right).

For experimental variogram calculation, which will be explained in the following step, data should be transformed to normal score unit first. Normal score transformation of stratigraphical transformed/upscaled data is performed at the end of this step.

Step (b): Gridding

Considering an appropriate gridding system is the primary step of each geological modeling process. The first consideration is that the model should be suitable for specific project goals. The second consideration is that important features, such as boundaries, fault, lithofacies and property changes, can be resolved with the final model and the third consideration is the resolution should be in such a manner to ensure a meaningful scale up from geological model to simulation model (Deutsch, 2002).

Based on the objective of this study (i.e. evaluation of upscaling technique developed in Chapter 4), a very fine gridding system has been considered. An aerial dimension of 100 m by 100 m from the center of zone shown in Figure 5-1

has been selected for structural modeling and a 1m by 1m grid size has been considered for this area. For facies and property modeling, a 2D slice from central part of this area has been considered. For vertical resolution, 0.5 m thickness has been selected.

Step (c): Structural Modeling

Understanding the geological framework prior to geostatistical modeling is essential. Reservoirs are made up of a number of reservoir layers and each layer corresponds to a particular time period. Each stratigraphic layer is modeled independently and the models subsequently merged to provide geological models of the whole reservoir. Generally McMurray Formation is subdivided in three units which are; lower, middle and upper units. Other subdivisions are also considered based on different purposes which are not as common as mentioned subdivision. In this study, the whole McMurray Formation is considered as single zone.

Before performing any geostatistical estimation/simulation, there is a need to quantify spatial correlation of data. Variogram calculation provides a positive-definite correlation between data for all distances and in any direction.

To find the spatial correlation of top and bottom surfaces, data are initially transformed to normal score units. Experimental and fitted theoretical 2D (areal) variograms used to generate top and bottom surfaces are shown in Figures 5-3 for top (Figure 5-3 top) and bottom (Figure 5-3 bottom) surfaces respectively.

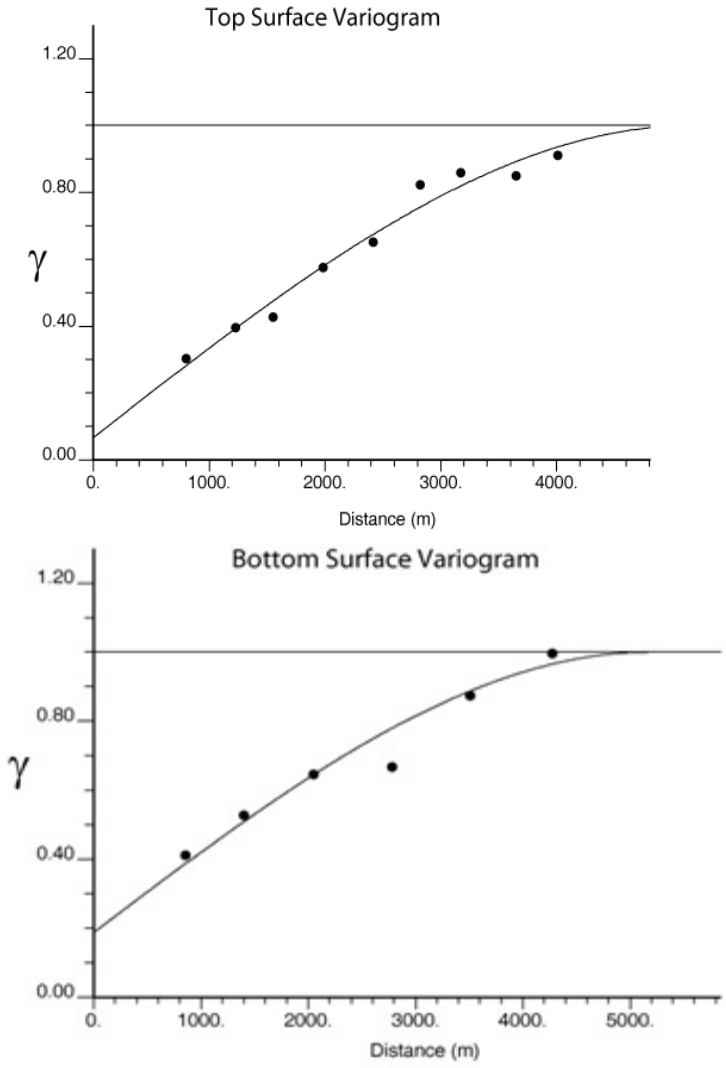

Figure 5-3 Experimental and fitted theoretical variogram of McMurray Formation top (top) and bottom (bottom) surfaces.

With the help of top and bottom markers, available within the data set provided for this study, and the variogram model, McMurray top surface, bottom surface and isochore thickness have been calculated and shown in Figure 5-4. Global kriging was used to generate structural surfaces. As could be seen, thickness of the considered section is between 67 to 72 m. Average thickness of 70 m is considered for facies and property modeling.

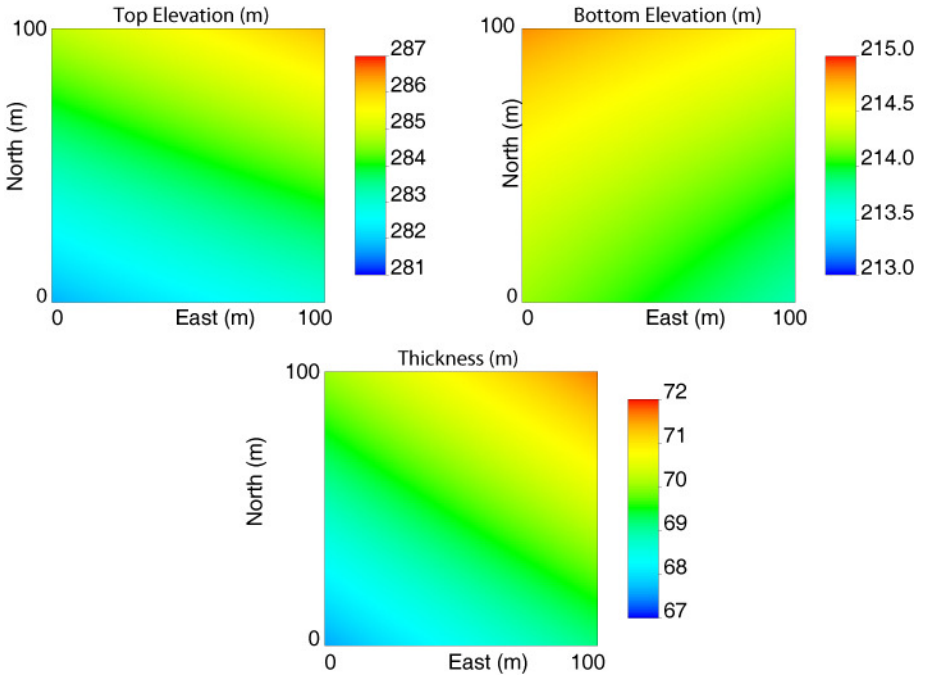

Figure 5-4 Top surface (1st row-left), bottom surface (1st row-right) and thickness (2nd row) map of area under study.

Step (d): Statistical data analysis

Prior understanding of statistical characteristics of data variable is required for geostatistical modeling. Figure 5-5 shows histograms of porosity and young modulus for sand and shale facies.

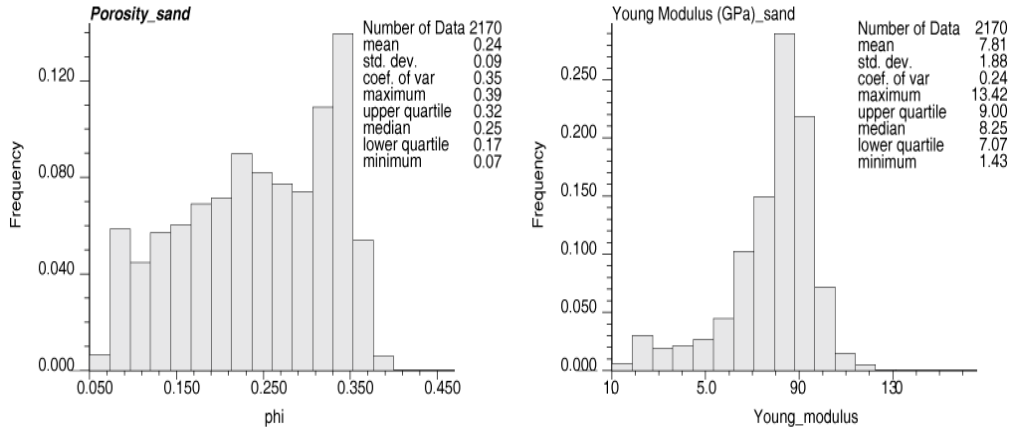

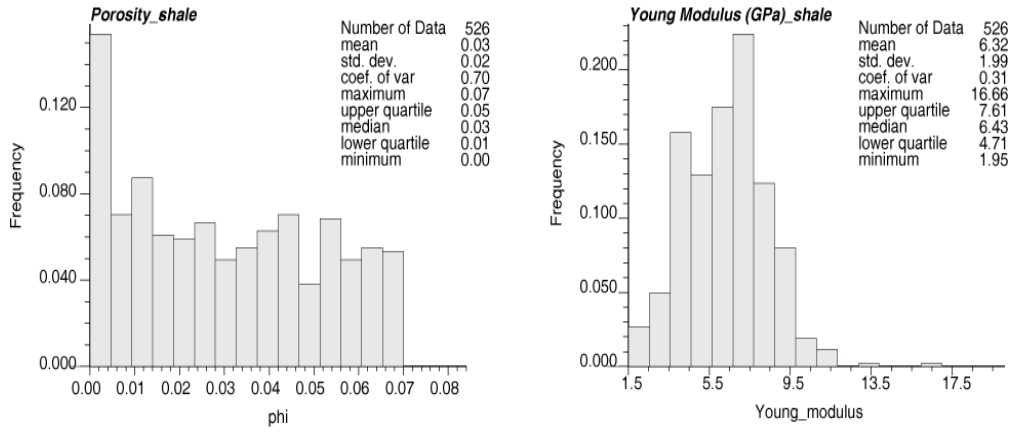

Figure 5-5 Porosity (left) and young modulus (right) histograms for pseudo defined sand (first row) and shale (second row) facies.

Step (e): Facies modeling

Facies modeling should be done for subsequent property modeling. In the McMurray Formation, there is considerable difference between petrophysical and rock mechanical properties of sand and shale facies. Sequential indicator simulation technique is used for modeling of pseudo defined shale/sand facies in this study. Assembling a 3D variogram prior to geostatistical simulation to see spatial correlation for each facies type is required. Figure 5-6 shows horizontal (top) and vertical (bottom) variograms used for subsequent facies simulation process. The indicator variogram sill is set based on global proportion of facies.

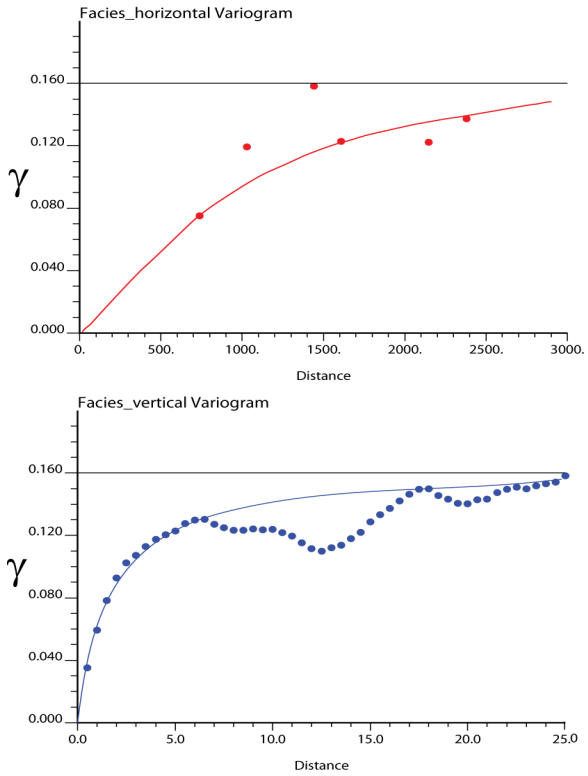

Figure 5-6 Experimental (bullet) and theoretical (solid line) variograms for sand and shale facies in vertical (top) and horizontal directions.

As expected, horizontal variography is more challenging in comparison to vertical due to the lack of data in the horizontal direction in comparison to vertical direction. Considering anisotropy ratio between vertical and horizontal variogram and/or using expert judgment are alternatives which are usually used for horizontal variography. Reasonable horizontal/vertical anisotropy ratios must be considered to get the horizontal variogram, for example, ratios of 50:1 to 250:1. These ratios are based on experimental data (Deutsch, 2002). A horizontal to vertical anisotropy ratio of 120:1 was applied to generate variogram models in horizontal direction. The 3D variogram was modeled based on the experimental variogram in the vertical direction.

Sequential indicator simulation (SISIM) from GSLIB package (Deutsch, 1998) is used for generating 100 realizations of shale/sand sequences. A 2D slice from central part of structural model, Figure 5-1, with length of 100 m and thickness of 70 m is considered as area of interest. grid resolution in X-Y-Z directions are 1m by 1m by 0.5m which results in 100 cells by 1 cell by 140 cells in X,Y and Z

directions respectively. Figure 5-7 shows 6 realizations in XZ direction. These 100 facies realizations will be used for the next following property modeling step.

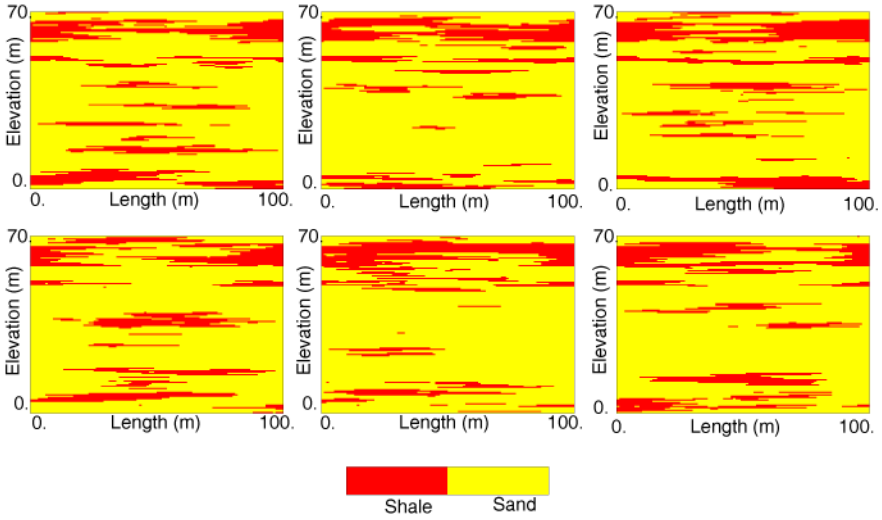

Figure 5-7 Six facies realizations in XZ directions.

Step (f): Property modeling and ranking of realizations

Petrophysical properties, i.e. porosity, permeability and saturations, and rock mechanical properties, i.e. elastic properties, are required for coupled geomechanical flow simulation of SAGD process. Sequential gaussian simulation (SGS) is considered for generating porosity and young modulus. SGSIM from GSLIB package (Deutsch, 1998) is used for this purpose. Property modeling is performed in by-facies manner which means that two different property models are built for sand and shale facies separately and then by considering the facies models generated in previous step (step 'e') they are combined.

Like facies modeling, variography should be performed before the simulation step. By assessing previously normal score transformed data, variography is performed for each facies and for each property separately in horizontal and vertical directions. In Figure 5-8 porosity (left) and young modulus (right) variograms in horizontal (top) and vertical (bottom) directions for sand facies are shown. The same process has been done for shale facies (Figure 5-9).

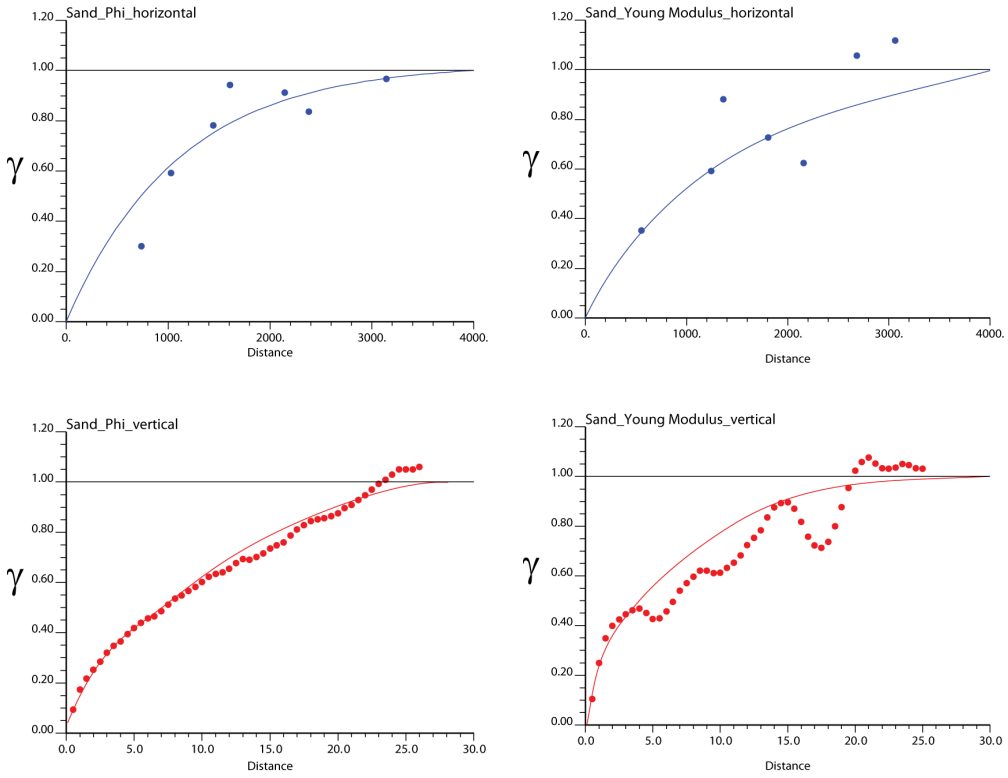

Figure 5-8 Experimental (bullet) and theoretical (solid line) variograms for porosity (left) and young modulus (right) in sand facies in horizontal (top) and vertical (bottom) directions.

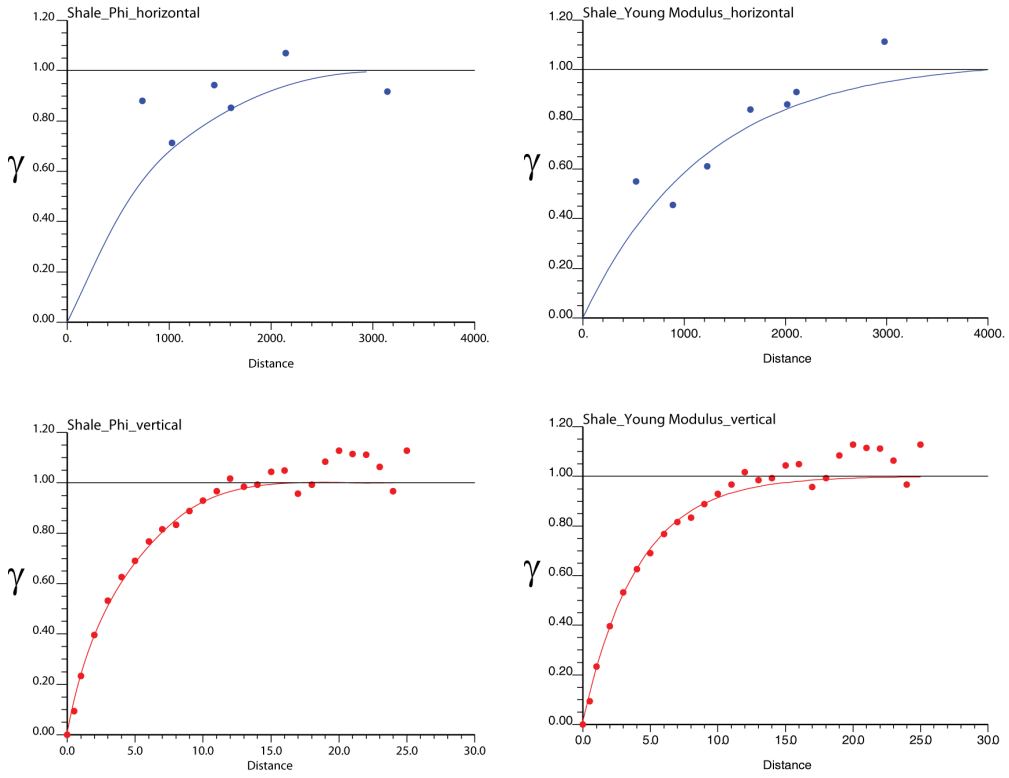

Figure 5-9 Experimental (bullet) and theoretical (solid line) variograms for porosity (left) and young modulus (right) in shale facies in horizontal (top) and vertical (bottom) directions.

As could be seen, horizontal variograms of porosity and Young's modulus are not as precise as vertical variograms of these properties and considering anisotropy ratio of 120:1 is applied to vertical variogram to generate horizontal variograms for both properties.

Permeability realizations are generated based on porosity realizations. For that purpose, permeability vs. porosity relationship is required. Deutsch (2010) proposed following relationship (Equation 5-2) for the McMurray Formation.

$$\log(K_h) = a_0 + a_1\Phi + a_2\left(1 - e^{\left(\frac{-3\Phi}{\Phi_c}\right)}\right) \tag{5-2}$$

Where,

K_h: horizontal permeability

Φ: porosity

Constants in Equation 5-2 are selected as: $a_0 = -2.0$, $a_1 = 3.67$, $a_2 = 4.15$ and $\Phi_c = 0.35$ (Deutsch, 2010). This equation is used to generate horizontal permeability. Constant vertical to horizontal permeability ratio of 0.5 is assumed to generate vertical permeability from horizontal permeability.

Oil saturation and poisson ratio are considered constant in this study; 0.8 and 0.3 respectively.

After building the geological realizations, coupled geomechanical flow simulation is the next step. Passing all realization through time consuming simulation process is not practical. Instead, geological realizations should be ranked and a number of them should be selected for the simulation process. GR technique, developed in Chapter 3, is considered for that purpose and P_{50} is selected for the simulation process. In Figure 5-10, P_{50} geological model is shown.

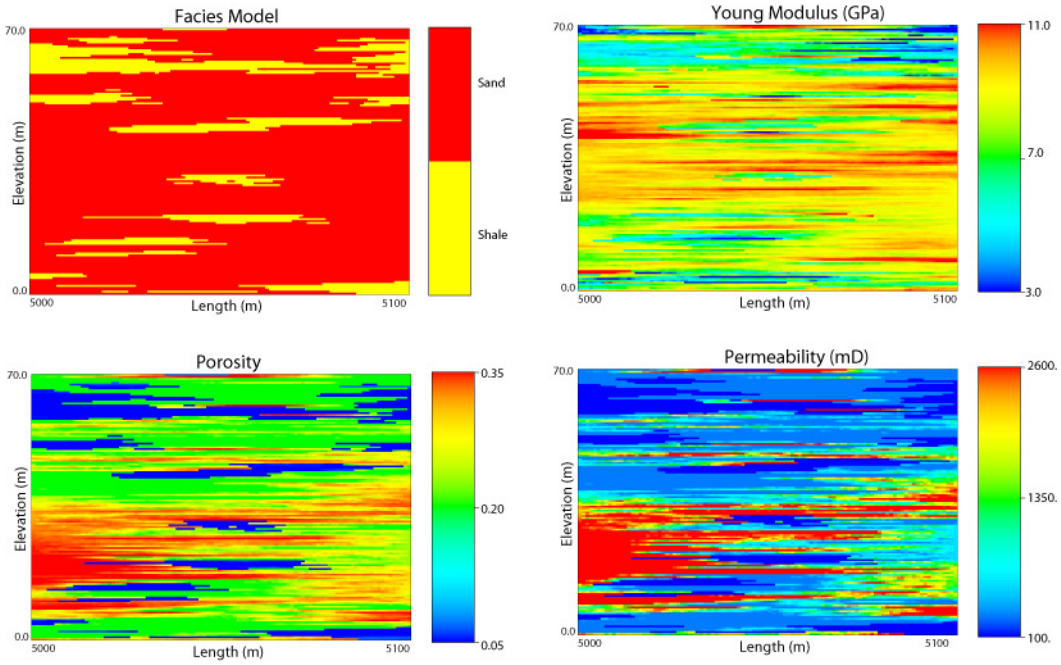

Figure 5-10 P_{50} realization used for simulation process.

Step (g): Upscaling and simulation results

An accurate and precise MEM is capable of characterizing reservoir accurately in terms of capturing small scale heterogeneities. However in terms of computer memory and storage; more detail means models of larger sizes. Although an accurate and well-characterized reservoir model is desired, the complexity, and

thus the size of the model can introduce significant computational problems when performing simulations (Durlofsky, 1991). Assessing to an appropriate upscaling methodology to reduces the CPU demand and run time while preserving the main features of geological heterogeneity is required. Upscaling process makes it possible to define elastic properties for coarse scale simulation models by using fine scale MEM's. In Chapter 4 numerical upscaling technique for upscaling of elastic properties was proposed. In this chapter developed upscaling technique on P_{50} realization (Figure 5-10) is considered for upscaling of young modulus. To check accuracy of developed numerical upscaling technique, geomechanical response, volumetric strain in this work, obtained from fine scale simulation is considered as truth response of geological model and compared with the volumetric strain maps obtained from harmonic averaging technique, which resulted in the least error among different analytical techniques considered in Chapter 4.

In addition to elastic properties, petrophysical properties, i.e. porosity and absolute permeability, are also required to be upscaled. However and since the focus is to check the accuracy of proposed numerical upscaling technique, consistent upscaling approaches for these properties are considered in all cases. Arithmetic averaging for porosity and numerical local upscaling, explained in Chapter 4, are the techniques used for upscaling of porosity and permeability respectively. Totally, 8 upscaling ratios are considered; horizontal ratios of 5:1, 10:1, 25:1, 50:1, and vertical ratios of 5:1 and 10:1.

Figure 5-11 shows geometry of the model considered for coupled geomechanical flow simulation.

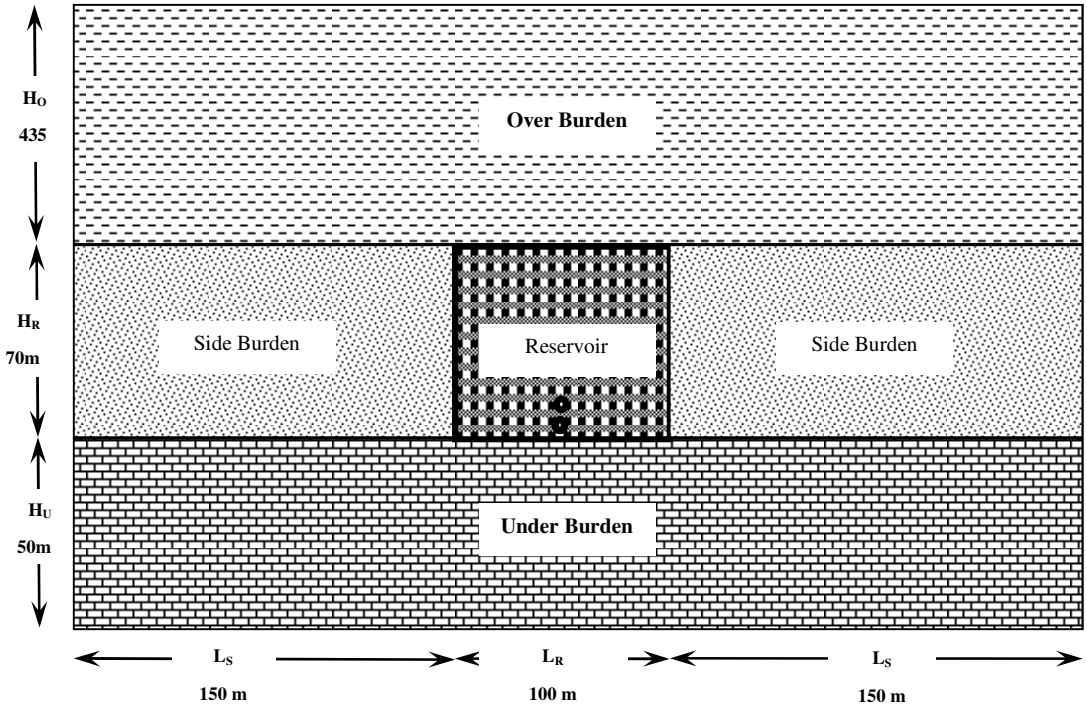

Figure 5-11 Model description and dimensions used for this study

Initial condition, boundary condition, in-situ stress condition, mechanism of deformation and elastic properties for side burden, underburden and over burden sections are the same as what was considered in Chapter 2 and Chapter 3. Transversely isotropic deformation is considered for reservoir section.

Figure 5-12 shows steam chamber propagation in reservoir section after five years of injection with 2500 kPa injection pressure.

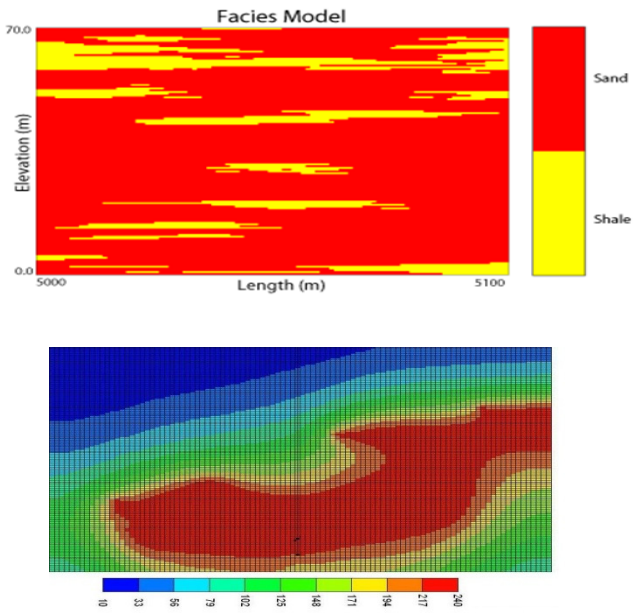

Figure 5-12 Facies (top) and steam chamber after 5 years (right) for P_{50} realization

As could be seen, spatial propagation of shale facies have significant effect on steam chamber growth and accordingly on deformation of reservoir.

Figure 5-13 and 5-14 shows upscaled maps of Young's modulus for two vertical upscaling ratios, 5:1 and 10:1 respectively, and for different horizontal upscaling ratios. The left column shows the result of upscaling by using harmonic averaging as upscaling technique and right column shows the same result but using the numerical upscaling technique developed in this research.

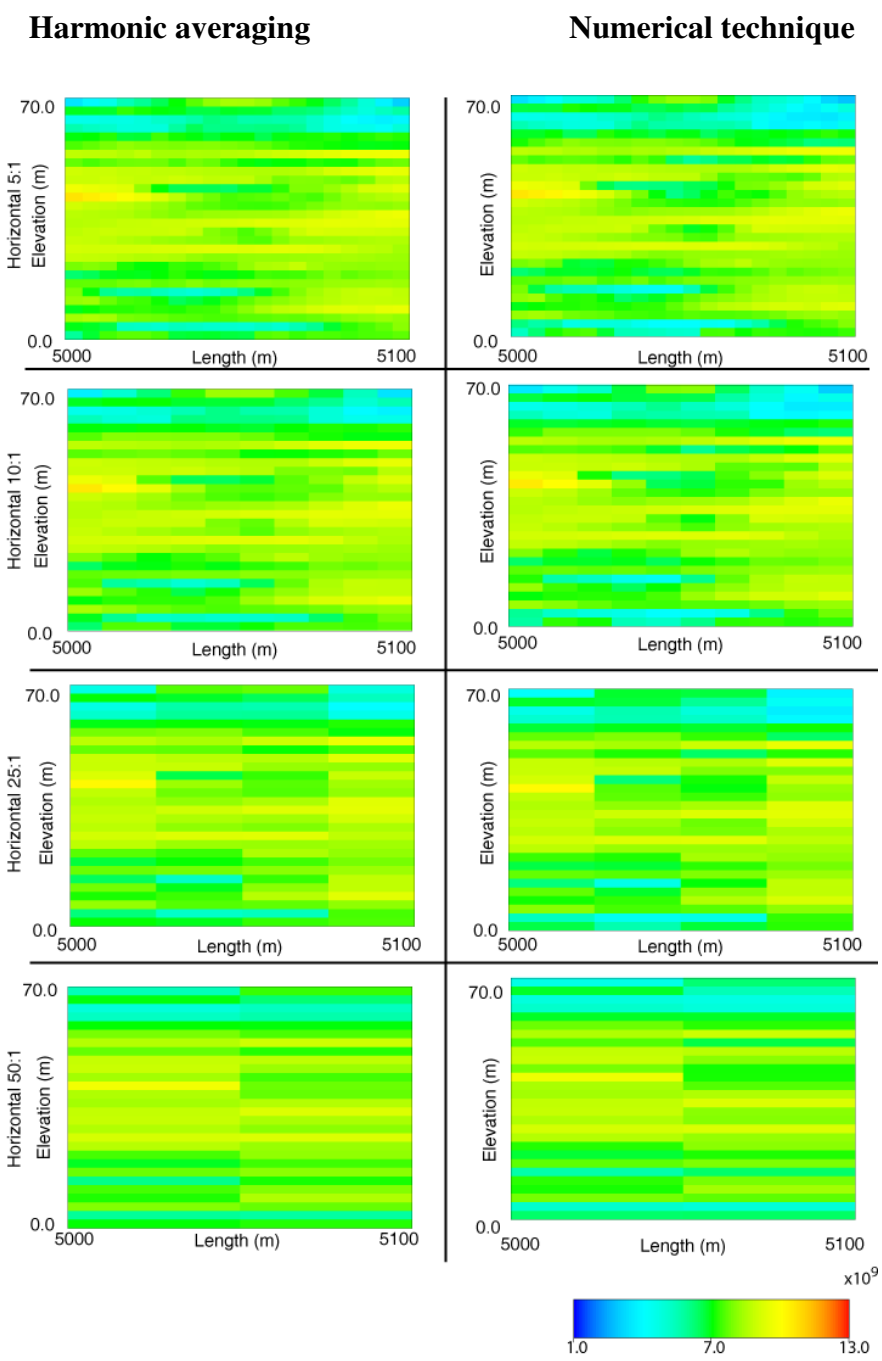

Figure 5-13 Young modulus for different horizontal upscaling ratios, vertical upscaling ratio is constant at 5:1.

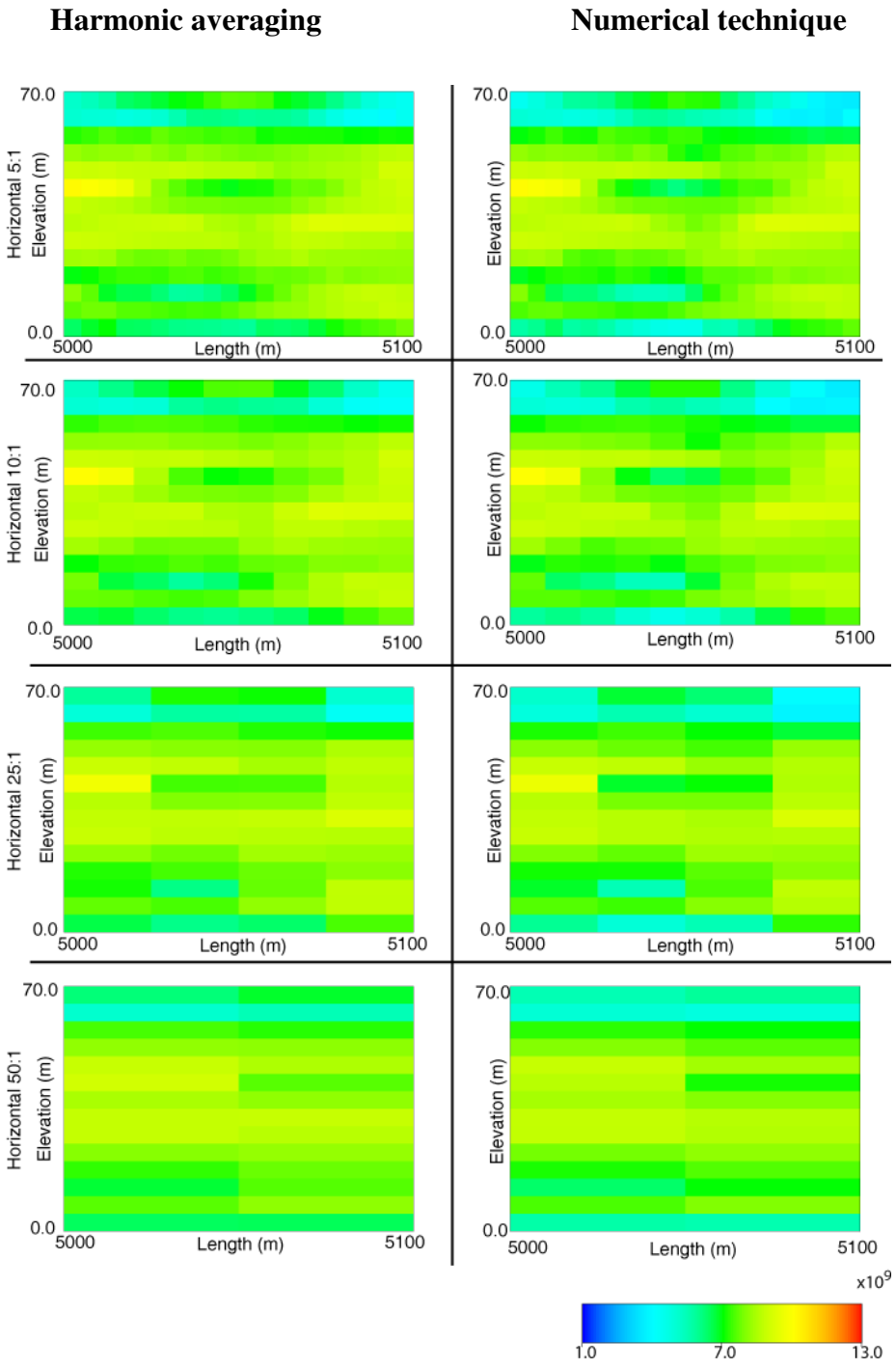

Figure 5-14 Young modulus for different horizontal upscaling ratios, vertical upscaling ratio is constant at 10:1.

These maps (Figure 5-13 and 5-14) and upscaled maps of porosity and permeability are considered in coupled geomechanical flow simulation process and volumetric strain results are compared with volumetric strain map of fine scale model. The same error analysis as what was considered in Chapter 4 is used in this chapter as well. Figure 5-15 shows effect of different upscaling processes on volumetric strain.

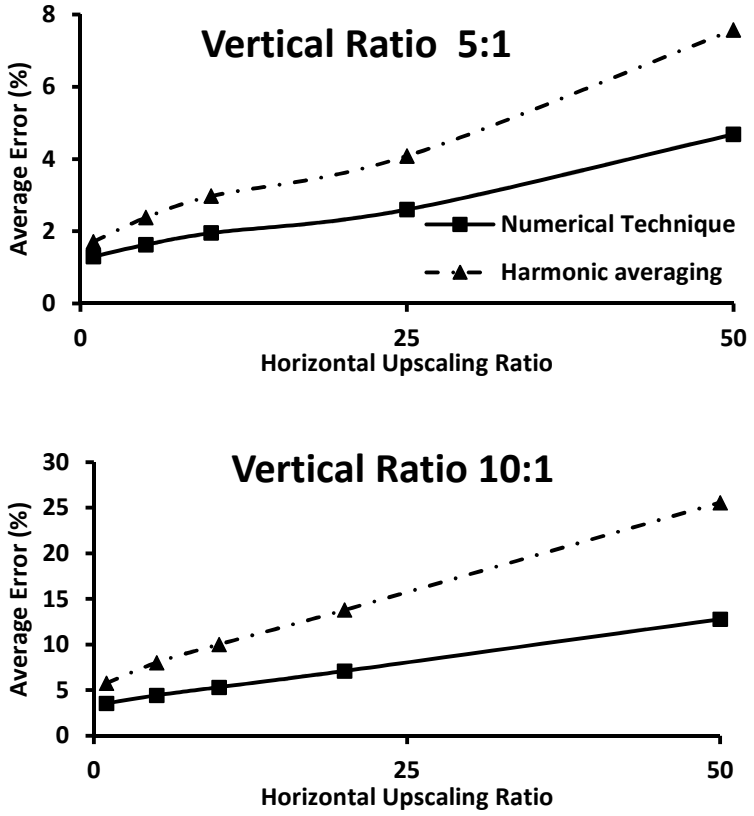

Figure 5-15 Average error for various horizontal upscaling ratios; vertical upscaling ratios are: 5:1 (above) and 10:1 (below).

It is clear that developed numerical averaging technique resulted in lower error in comparison to harmonic averaging technique.

Reducing simulation time is also a very important goal of the upscaling process. Reducing number of cells, as a result of upscaling, has a significant effect on the CPU time (Figure 5-16).

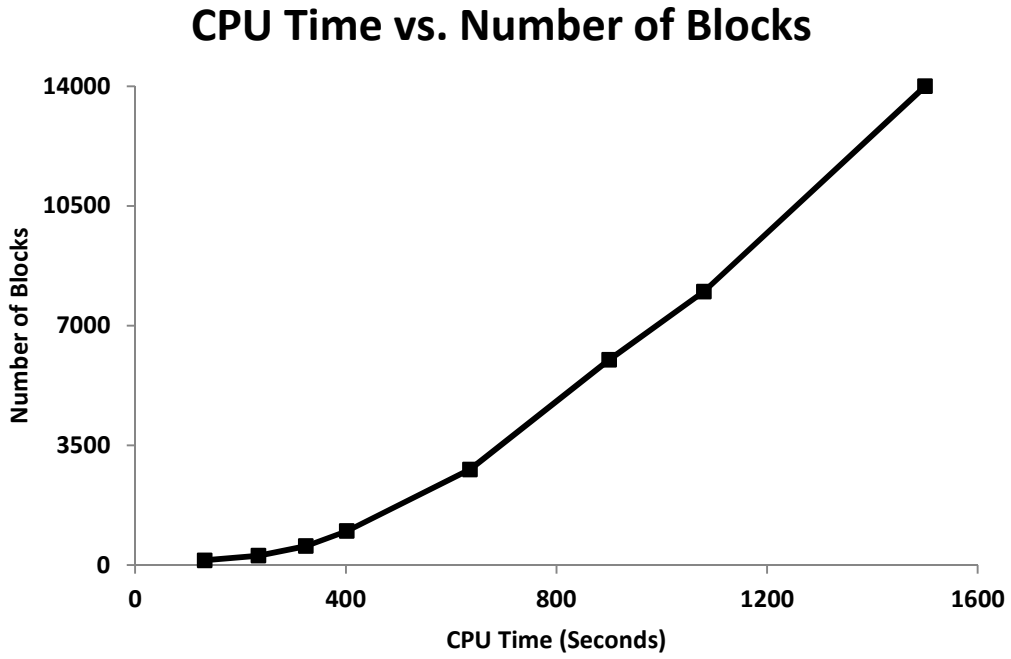

Figure 5-16 CPU time vs. number of blocks during coupled geomechanical flow simulation.

CONCLUSION

By considering a McMurray Formation data set, application of ranking methodology and upscaling technique, developed in Chapter 3 and Chapter 4 respectively, was assessed in this chapter. Using geostatistical techniques resulted in building 100 realizations. P_{50} realization was selected for coupled geomechanical flow simulation of SAGD process. Fine scale property models were moved to different upscaled maps. Harmonic averaging and previously developed numerical technique was used for coarsening of young modulus. Arithmetic averaging and numerical local upscaling were used for upscaling of porosity and permeability respectively. By using error function, defined in Chapter 4, and considering volumetric strain as geomechanical response, accuracy of numerical upscaling technique was compared with harmonic averaging technique and considerably lower error was obtained by using numerical upscaling technique. In addition, it was shown that coarsening of cells and

moving from fine scale/high resolution geological model to coarse scale/low resolution simulation model has significant effect on computational time.

REFERENCES

Alberta Energy and Utilities Board, (AEUB). 2003. Statistical Series 2003-98, Calgary, Canada.

Azad, A. 2012. Rapid SAGD Simulation Considering Geomechanics for Closed Loop Reservoir Optimization. PhD dissertation, University of Alberta, Edmonton, Canada.

Butler, R., M. 1998. SAGD comes of AGE. Journal of Canadian Petroleum Technology. 37(7): 9-12.

Chalaturnyk, R. 1996. Geomechanics of the Steam-Assisted Gravity Drainage Process in Heavy Oil Reservoirs. PhD dissertation, University of Alberta, Edmonton, Canada.

Deutsch, C. V. 2002. Geostatistical Reservoir Modeling. Oxford University Press. New York.

Deutsch, C. V. 2010. Estimation of vertical permeability in McMurray Formation. Journal of Canadian Petroleum Technology. 49(12): 10-18.

Deutsch, C. V. and Journel, A. G. 1998. GSLIB: Geostatistical Software Library and User's Guide. Second edition, Oxford, New York.

Deutsch, C., Dembicki, E. and Yeung, K. 2002. Geostatistical determination of production uncertainty: Application to Firebag project. Centre for Computational Geostatistics (CCG). University of Alberta, Edmonton, Canada.

Durlofsky, L. J. 1991. Numerical Calculation of Equivalent Grid Block Permeability Tensors for Heterogeneous Porous Media. Water Resources Research. 27(5): 699-708.

Dusseault, M. and Morgenstern, N.R. 1978. Shear strength of Athabasca oil sand. Canadian Geotechnical Journal 15: 216-238.

Li, P. 2006. Numerical simulation of the SAGD process coupled with geomechanical behavior. PhD dissertation, University of Alberta, Edmonton, Canada.

McLennan, J. and Deutsch, C. 2005. Ranking geostatistical realizations by measures of connectivity. Proceeding of SPE international thermal operations and heavy oil symposium, Calgary, Canada, SPE No. 98168.

Touhidi-Baghini, A. 1998. Absolute Permeability of McMurray Formation Oil Sands at Low Confining Stresses. PhD dissertation, University of Alberta, Edmonton, Canada.

CHAPTER 6: CONCLUSION AND RECOMMENDATIONS FOR FUTURE STUDIES

SUMMARY

The general objectives of this research study were to investigate heterogeneity effect of elastic properties on coupled geomechanical effect of SAGD process. Effect of heterogeneous mechanical properties on main output variables during numerical coupled geomechanical flow simulation of SAGD, proposing ranking criteria which is in good correlation with expected elastic deformation of reservoir during SAGD process and proposing numerical upscaling technique which capture both anisotropic elastic deformation and complex facies configuration were three main contributions of this work which were discussed in Chapters 2, 3 and 4 respectively.

To make more accurate decisions based on the results obtained from coupled geomechanical flow simulation of SAGD, it is of great significance to consider both petrophysical, required in flow simulation, and rock mechanical properties, required in geomechanical simulation, as heterogeneous models. Using comprehensive geological models, named as MEM, instead of traditional geological models, in which rock mechanical properties are considered as homogeneous, layer cake, models was contribution of Chapter 2.

Heterogeneous elastic properties results in more accurate simulation results. However, to capture uncertainty accompanied by inherent properties; it is required to build multiple equi probable geological realizations. In the other hand, it is not practical to pass all geological realizations through coupled geomechanical flow simulation. Developing geometric ranking criteria to rank geological realizations and select few of them out of many for further coupled geomechanical flow simulation was contribution of Chapter 3.

To capture small scale heterogeneities, geostatistically built geological models are usually built in fine scale manner which is not suitable for simulation process which is time consuming process. Upscaling, a bridge between fine scale geological models to coarse scale simulation model, is required to resolve this issue. Developing new numerical upscaling technique which can be applied for complex facies configuration, like sand/shale facies configuration of McMurray Formation, and also consider anisotropic elastic deformation was contribution of Chapter 4.

CONCLUSION

In Chapter 2, by considering COP, SOR and VDP as main output variables of coupled geomechanical flow simulation of SAGD range of uncertainties obtained from comprehensive geological realizations, in which both petrophysical and rock mechanical properties are considered as heterogeneous geological models, was compared with range of uncertainties obtained from geological models used in industry standard practice, in which heterogeneous petrophysical and homogeneous rock mechanical properties are considered. It has been concluded that Effect of heterogeneous rock mechanical properties when assessing SAGD performance should not be ignored and heterogeneous property models for both petrophysical and rock mechanical properties should be considered in order to properly assess the full range of uncertainty expected in SAGD performance.

In Chapter 3, efficiency of existing approaches to define homogenized EEM considered for coupled geomechanical flow SAGD simulation process was assessed. For that purpose different facies configurations with same shale/sand proportion were considered and EEM from three different approaches (sand properties, mixing rule and Budiansky technique) were compared for layer cake model, randomly distributed models (which could be considered as two extreme cases of sand/shale spatial distributions) and spatially correlated models. Geomechanical responses, VDP's along the top of the reservoir, obtained from homogenized models (in which EEM are calculated using standard approaches) are in poor agreement with fine scale response and the most precise VDP's was

obtained by considering EEM obtained through proposed numerical approach. Using sand properties as homogenized media is the most typical technique in current industrial SAGD projects dealing with coupled geomechanical flow simulation. In three facies configurations considered at beginning part, it was shown that using sand properties as homogenized media results in VDP's that depart the most from the fine scale model response. The Budiansky technique appeared to be applicable to cases where no spatial correlation was considered for facies modeling. It means that by using analytical techniques for determination of EEM spatial correlation in facies distribution has been ignored and random distribution of sand/shale facies is (perhaps unknowingly) assumed for many studies.

Sensitivity of change in VDP and accordingly EEM as a result of considering multiple realizations, 100 realizations in this study, has been investigated. It was concluded that ranges of EEM was determined for singular variogram parameters. Selecting few realizations out of many is a way that results in decreasing computational time required for running large number of realizations and analyzing uncertainties accompanied by heterogeneous geomechanical properties concurrently. Randomly selecting realizations is not logical and first they should rank based on appropriate ranking measure which is in high correlation with expected geomechanical response. Ranking criteria, named as GR technique was proposed in this chapter. Calibrated ranking measure is in considerably high correlation with geomechanical response obtained from coupled geomechanical flow simulation and it could be concluded that proposed ranking measure could be considered for similar application.

In Chapter 4, a novel numerical local upscaling technique for elastic properties was developed. Upscaling error was assessed by considering volumetric strain and shear strain as the geomechanical response and indicated that the proposed numerical technique has promise.

It is important to consider the scale of the coarse blocks. As shown, error increases with increasing upscaling ratios. For a given problem, the acceptable

error in the response should be quantified by the practitioner and an appropriate block size selected. This is standard practice in flow simulation where past experience can be relied upon to select an appropriate coarse scale; however, in geomechanical simulation, homogenous property models dominate and there is little guidance on upscaled block size selection.

The difficulty with considering analytical upscaling methods is determining their range of applicability as they are sensitive to parameter calibration. It may be inappropriate to apply analytical techniques to new geological situations beyond their intended. Conversely, the proposed numerical technique is appropriate for various domains that can be characterized by transverse isotropy.

RECOMMENDATIONS FOR FUTURE STUDIES

Elastic properties are the main focus of rock mechanical properties considered in this research. However, rock strength properties are other important parameters. It is highly recommended to consider this group of parameter as focus of future researches. Developing ranking criteria and developing upscaling technique based on considering rock strength properties as heterogeneous models could have significant effect on improvement of numerical simulation of coupled geomechanical flow simulation of SAGD process.

In developing numerical upscaling approach, local upscaling of permeability was considered as pattern. Extended local, global and local global upscaling techniques were developed after local upscaling of permeability. Developing same approaches for elastic and rock strength properties could result in more accurate upscaling of these properties and recommended to be considered.

At the moment SAGD is the most important recovery mechanism of heavy oil in McMurray Formation. However other recovery mechanisms, such as CSS are used as well. Application of developed ranking criteria is just limited to SAGD recovery mechanism. Developing more general ranking criteria based on geometric characteristics of geological realizations which have wider application

to developed one could be used in other thermal recovery mechanism as well and recommended to be investigated.

APPENDICES

Appendix A

A-1 STARS input data file

RESULTS SIMULATOR STARS 200900

***NOLIST*

****

*INUNIT *SI*

****

***CHECKONLY*

****

INTERRUPT STOP

****

WPRN GRID TIME

WPRN ITER TIME

OUTPRN WELL ALL

***PRES SWCRIT SW SO SG TEMP OBHLOSS VISO KRO KRG KRW MASDENO MASDENG MASDENW*

OUTPRN GRID NONE

***ALL **SMALL*

OUTPRN RES NONE

OUTPRN ITER BRIEF

****

WSRF GRID TIME

WSRF WELL TIME

WSRF SECTOR TIME

OUTSRF GRID PRES SG SO SW TEMP

```
**OUTSRF WELL COMPONENT ALL

OUTSRF WELL LAYER ALL

REWIND 0

**$  Distance units: m

RESULTS XOFFSET           0.0000

RESULTS YOFFSET           0.0000

RESULTS ROTATION           0.0000  **$  (DEGREES)

RESULTS AXES-DIRECTIONS 1.0 -1.0 1.0

WRST TIME

**$
********************************************************************
*********

**$ Definition of fundamental Cartesian grid

**$
********************************************************************
*********

GRID VARI 50 1 40

KDIR DOWN

DI IVAR

 50*2

DJ JVAR

 1

DK ALL

 2000*0.5

DTOP
```

*50*0*

NULL CON 1

PINCHOUTARRAY CON 1

***$ Property: Porosity Max: 0.3 Min: 0.3*

POR CON 0.30

**mod*

INCLUDE 'inc_files/poro_0.inc'

** porosity in each time step is updated. Keyword INCLUDE from STARS is used to omport heterogeneous map of porosity in each time step in current main STARS file.

***$ Property: Permeability I (md) Max: 4000 Min: 2000*

PERMI CON 3000

**mod*

INCLUDE 'inc_files/permi_0.inc'

** the same explanation as what was mentioned for porosity is applied for permeability as well.

***$ Property: Permeability J (md) Max: 2000 Min: 2000*

PERMJ CON 3000

**mod*

INCLUDE 'inc_files/permj_0.inc'

***$ Property: Permeability K (md) Max: 2000 Min: 2000*

PERMK CON 3000

**mod*

INCLUDE 'inc_files/permk_0.inc'

END-GRID

****

*****GRID OTHER PROPERTIES **********

ROCKTYPE 1

CPOR 1.2E-6

PRPOR 101.

CTPOR 3.84e-5

*ROCKCP 2.347E6 0. ** J/(m3 C) = 35 Btu/(ft3 F)*

****

*THCONR 600E3 ** J/(m d C)*

THCONW 55E3

THCONO 11E3

THCONG 2E3

THCONMIX SIMPLE

****

*HLOSSPROP OVERBUR 2.347E6 1.496E5 ** Vol. Heat Capacity / Thermal conductivity*

UNDERBUR 2.347E6 1.496E5

*********** Property: Thermal/rock Set Num Max: 1 Min: 1*

THTYPE CON 1

****

*** COMPONENT PROPERTIES**********

*MODEL 3 3 3 1 **Fluids of the model include water, dead oil and methane*

COMPNAME 'WATER' 'OIL' 'METHANE'

**----------

*CMM 0.018 0.523 0.016 ** kg/gmol = kg/mol (!)*

*PCRIT 0.0 0.0 4600 ** kPa. Default for water, not needed for dead oil*

*TCRIT 0.0 0.0 -82.55 ** oC. Default for water, not needed for dead oil*

*MOLDEN 55555 1931 20000 ** Molar density = Dens/MW.*

*** For water =1000/0.018= 55555*

*** For oil = 1010/0.523 = 1931*

*** For gas = 320/0.016 = 20000*

*CP 4.463E-7 6E-7 10E-7 ** 1/kPa.*

*CT1 0.0 10.04E-4 9.72E-4 ** 1/oC. Thermal expansion coefficients*

CT2 0.0 0.0 0.0

*CPG1 0.0 841. 35.2 ** Refer to both ARC and CMG decks*

CPL1 0.0 1000. 67.2

*HVAPR 0.0 1346. 1770. ** Heat of vaporization, J/(gmol oC)*

AVG 0.0 0.0 0.016

*BVG 0.0 0.0 0.0 ** Temperature-independent*

*** K-VALUE CORRELATIONS (From STARS' Table)*

*KV1 0.0 0.0 5.45E5 **kPa.*

*KV4 0.0 0.0 -879.84 **oC*

*KV5 0.0 0.0 -265.99 **oC*

*PRSR 500. **kPa. Ref. pressure of methane & others density = Initial gas cap res. pressure*

TEMR 10.

*PSURF 101.3 **=14.7 psia **Surface conditions*

*TSURF 15.6 **=60 oF*

VISCTABLE

**********Temp Water Bitumen Methane (liq)**********

2.0	*0*	*1461700*	*515.59*
10.0	*0*	*1241639*	*486.21*
12.2	*0*	*870699*	*427.72*
40.0	*0*	*22267.1*	*107.86*
60.0	*0*	*3183.8*	*49.21*
80.0	*0*	*694.3*	*25.58*
100.0	*0*	*209.2*	*14.74*
120.0	*0*	*81.1*	*9.23*
140.0	*0*	*38.2*	*6.17*
160.0	*0*	*21.1*	*4.37*
175.6	*0*	*14.5*	*3.44*
200.0	*0*	*9.1*	*2.48*
220.0	*0*	*6.8*	*1.97*
240.0	*0*	*5.4*	*1.6*
260.0	*0*	*4.5*	*1.34*
280.0	*0*	*4.0*	*1.13*
300.0	*0*	*3.6*	*0.98*

********** ROCK-FLUID DATA**********

ROCKFLUID

RPT 1

SWT

****

*** Additional points were added between (1-Sor) and 1**********

** Sw Krw Krow**

0.15 0.0000 1.0000

0.20 0.0001 0.8603

0.25 0.0009 0.7305

0.30 0.0028 0.6106

0.35 0.0066 0.5009

0.40 0.0125 0.4014

0.45 0.0212 0.3123

0.50 0.0332 0.2337

0.55 0.0489 0.1659

0.60 0.0688 0.1091

0.65 0.0935 0.0635

0.70 0.1232 0.0296

0.75 0.1586 0.0080

0.80 0.2000 0.0000

0.85 0.2960 0.0000

0.90 0.4540 0.0000

0.95 0.6780 0.0000

1.00 1.0000 0.0000

SLT

****

****Additional points were added between Swc and (Swc+Sor)**********

**Sliq	Krg	Krog	Krw**
0.1500	*1.0000*	*0.0000*	*0.0000*
0.1925	*0.8330*	*0.0000*	*0.0000*
0.2775	*0.6000*	*0.0000*	*0.0000*
0.3625	*0.4500*	*0.0000*	*0.0000*
0.4050	*0.3851*	*0.0081*	*0.0000*
0.4475	*0.3256*	*0.0277*	*0.0000*
0.4900	*0.2712*	*0.0570*	*0.0000*
0.5325	*0.2220*	*0.0951*	*0.0000*
0.5750	*0.1779*	*0.1415*	*0.0000*
0.6175	*0.1389*	*0.1957*	*0.0000*
0.6600	*0.1050*	*0.2575*	*0.0000*
0.7025	*0.0759*	*0.3266*	*0.0000*
0.7450	*0.0518*	*0.4028*	*0.0000*
0.7875	*0.0324*	*0.4859*	*0.0000*
0.8300	*0.0177*	*0.5758*	*0.0000*
0.8725	*0.0076*	*0.6722*	*0.0000*
0.9150	*0.0018*	*0.7751*	*0.0000*
0.9575	*0.0000*	*0.8844*	*0.0000*
1.0000	*0.0000*	*1.0000*	*0.0000*

*SGR 0.05 **Critical gas saturation*

*KRGCW 0.60 **Rel. perm. to gas at residual liquid saturation (Swc+Sor)*

********** Sand

KRTEMTAB SORW SORG KRWIRO

10 0.15 0.15 0.20

250 0.10 0.05 0.40

****

*****RELATIVE PERMEABILITY TYPE DESIGNATION**********

********** Property: Rel Perm Set Number Max: 1 Min: 1

KRTYPE CON 1

********** Property: Critical Water Saturation Max: 0.15 Min: 0.15

BSWCRIT CON 0.15

****

********** INTITIALIZATION **********

INITIAL

VERTICAL DEPTH_AVE

INITREGION 1

REFPRES 650

REFDEPTH 10

***$ Property: Temperature (C) Max: 10 Min: 10*

TEMP CON 10

***$ Property: Water Saturation Max: 0.15 Min: 0.15*

SW CON 0.15

**mod*

INCLUDE 'ini_prop/sw.inc'

***$ Property: Oil Saturation Max: 0.85 Min: 0.85*

SO CON 0.85

**mod*

INCLUDE 'ini_prop/so.inc'

** oil and water saturation are considered as heterogeneous maps and imported to this main input file via INCLUDE keyword.

***$ Property: Gas Saturation Max: 0 Min: 0*

SG CON 0

*** Initial "OIL" mol fraction in the oil liquid phase*

***$ Property: Oil Mole Fraction(OIL) Max: 0.999 Min: 0.999*

MFRAC_OIL 'OIL' CON 0.999

*** Initial "METHANE" mol fraction in the oil liquid phase*

***$ Property: Oil Mole Fraction(METHANE) Max: 0.001 Min: 0.001*

MFRAC_OIL 'METHANE' CON 0.001

****

********** NUMERICAL CONTROL**********

NUMERICAL

DTMAX 30.

MAXSTEPS 9999999

NORM TEMP 10

UPSTREAM KLEVEL

CONVERGE TOTRES LOOSE

ITERMAX 300

NORTH 100

****

********** WELL AND RECURRENT DATA**********

NCUTS 20

RUN

```
DATE 1901 1  1.00000
DTWELL 5
**$
WELL  'Injector'  FRAC  1.
INJECTOR MOBWEIGHT IMPLICIT 'Injector'
INCOMP  WATER  1.  0.  0.
TINJW  250.
QUAL  0.95
OPERATE  MAX  BHP  3000.  CONT
OPERATE  MAX  STW  800.  CONT
**$         rad  geofac  wfrac  skin
GEOMETRY  K  0.086  0.249  1.  0.
PERF  GEOA  'Injector'
**$ UBA     ff  Status  Connection
   25 1 34  1.  OPEN    FLOW-FROM  'SURFACE'
SHUTIN 'Injector'
**$
WELL  'Producer'  FRAC  1.
PRODUCER 'Producer'
OPERATE  MIN  BHP  500.  CONT
OPERATE  MAX  STL  800.  CONT
OPERATE  MIN  STEAMTRAP  10.  CONT REPEAT
**$         rad  geofac  wfrac  skin
GEOMETRY  K  0.086  0.249  1.  0.
```

PERF GEOA 'Producer'

***$ UBA ff Status Connection*

25 1 40 1. OPEN FLOW-TO 'SURFACE'

SHUTIN 'Producer'

***$ Property: Heat Transfer Rate (J/day) Max: 0 Min: 0*

HEATR CON 0

**MOD*

25:25 1:1 34:34 = 1e11

25:25 1:1 40:40 = 1e11

***$ Property: Temp. Setpoint for Controller (C) Max: 10 Min: 10*

TMPSET CON 10

**MOD*

25:25 1:1 34:34 = 240

25:25 1:1 40:40 = 240

***$ Property: Prop. Heat Transfer Coeff. (J/(day*C)) Max: 0 Min: 0*

UHTR CON 0

**MOD*

25:25 1:1 34:34 = 1e+10

25:25 1:1 40:40 = 1e+10

AUTOHEATER ON 25:25 1:1 34:34

AUTOHEATER ON 25:25 1:1 40:40

****

********** DATES**********

DATE 1901 1 5

INCLUDE 'date_files/date_NNNN.inc'

** dates are imported in this section via scripting workflow considered to automatically couple FLAC and STARS.

STOP

A-2 FLAC input data file

; Initialization File

; SAGD Modeling

config ats thermal ex 15

grid 70,55

; ---------- Settings ----------

set grav = 9.81

; ---------- Call Fish Functions ----------

call fish\functions.fis

; ---------- Define Grid ----------

; depth = 0 to 140 --- overburden (140 m)

gen 0,70 0,210 150,210 150,70 ratio 0.8,1.5 i=1,11 j=46,56

gen 150,70 150,210 250,210 250,70 ratio 1.0,1.5 i=11,61 j=46,56

gen 250,70 250,210 400,210 400,70 ratio 1.25,1.5 i=61,71 j=46,56

; depth = 140 to 160 --- reservoir (20 m)

gen 0,50 0,70 150,70 150,50 ratio 0.8,1 i=1,11 j=6,46

gen 150,50 150,70 250,70 250,50 i=11,61 j=6,46

gen 250,50 250,70 400,70 400,50 ratio 1.25,1 i=61,71 j=6,46

; depth = 160 to 210 --- bottom of grid (50 m)

gen 0,0 0,50 150,50 150,0 ratio 0.8,0.65 i=1,11 j=1,6

gen 150,0 150,50 250,50 250,0 ratio 1,0.65 i=11,61 j=1,6

gen 250,0 250,50 400,50 400,0 ratio 1.25,0.65 i=61,71 j=1,6

; ---------- Define Elastic Properties -------

group 'over' j= 46,55

model elastic th_i group 'over'

prop d=2200 b=208e6   s=96.2e6   group 'over'

prop cond=1 spec=1 thexp=2.00E-05 group 'over'

group 'side1' i=61,70 j= 6,45

model elastic th_i group 'side1'

prop d=2200 b=620e6   s=286e6   group 'side1'

prop cond=1 spec=1 thexp=2.00E-05 group 'side1'

group 'reservoir' i=11,60 j= 6,45

model elastic th_i group 'reservoir'

prop d=2200 group 'reservoir'

prop cond=1 spec=1 thexp=2.00E-05 group 'reservoir'

call ini_prop\elastic.inc

group 'side2' i=1,10 j= 6,45

model elastic th_i group 'side2'

prop d=2200 b=620e6   s=286e6   group 'side2'

prop cond=1 spec=1 thexp=2.00E-05 group 'side2'

group 'under' j= 1,5

model elastic th_i group 'under'

prop d=2200 b=4.167e9   s=1.923e9   group 'under'

prop cond=1 spec=1 thexp=2.00E-05 group 'under'

; ---------- Fluid Properties ----------

water den 1000 bulk 2e9

; ---------- Define Initial Stresses ----------

; Stress along x,y,z

ini szz -4620000 var 0,4620000   j=1,56

ini syy -4620000 var 0,4620000   j=1,56

ini sxx -9240000 var 0,9240000   j=1,56

; --------- Pore Pressure

ini pp 0   j=56

ini pp 1300e3 var 0,-1300e3 j=1,55

ini pp 650e3   j=6,46

; --------- Shear Stress

ini sxy 0

; --------- Temprature

ini temp 10

; ---------- Define Boundary Condition ----------

fix x y   j=1

fix x   i=1

fix x   i=71

; ---------- solve and initialize ----------

set mech on thermal off flow off   ; Mechanical only calculation

water bulk=0   ; Prevent mechanical generation of pore pressure

solve

ini xdis 0

ini ydis 0

ini xvel 0

ini yvel 0

; ---------- Save For the Next Step ----------

save run_0.sav

quit

; FLAC FILE For each time step (except initialization which explained above)

; SAGD Modeling

restore run_MMMM.sav

set echo off

; ---- Define Plastic Properties for the reservoir ONLY -------

model m th_i group 'side1'

prop cond=1 spec=1 thexp=2.00E-05 group 'side1'

prop dil=20 fric=60 group 'side1'

prop d=2200 b=620e6   s=286e6   group 'side1'

model m th_i group 'reservoir'

prop cond=1 spec=1 thexp=2.00E-05 group 'reservoir'

prop d=2200 group 'reservoir'

call ini_prop\elastic.inc

call ini_prop\plastic.inc

model m th_i group 'side2'

prop cond=1 spec=1 thexp=2.00E-05 group 'side2'

prop dil=20 fric=60 group 'side2'

prop d=2200 b=620e6   s=286e6   group 'side2'

; --------- Update Temprature and Pressure and material properties

set echo off

call tp_flac_in\temp_NNNN.flc

call tp_flac_in\pres_NNNN.flc

; ---------- Run Fish Functions ----------

```
set mech on thermal off flow off     ; Mechanical only calculation
solve
; -------------------- FISH Functions RUN ------------------------
SET _fil_name  'vol_strain_flac_out\ev_NNNN.out'
SET _fil_name_  'plast_out\pl_NNNN.out'
ev_out
pl_out
; -------------------- Save For the Next Step --------------------
save run_NNNN.sav
quit
;FISH FUNCTION CONSIDERED IN MAIN FLAC FILE IS
; ---------------- Volumetric Strain Output --------------
def ev_out
        num=1
        float ev_for_k
        array ev_for_k(2000)
                loop j (6,45)
                    loop i (11,60)
                            ev_for_k(num)=string(vsi(i,j))
                            num=num+1
                     endloop
                endloop
                status=open(_fil_name,1,1)
        status=write(ev_for_k,2000)
```

```
        status=close
end
; ---------------- Plastic Codes Output --------------
def pl_out
        num=1
        float pl_for_k
        array pl_for_k(2000)
                loop j (6,45)
                    loop i (11,60)
                        pl_for_k(num)=string(state(i,j))
                        num=num+1
                     endloop
                endloop
        status=open(_fil_name_,1,1)
        status=write(pl_for_k,2000)
        status=close
end
; ---------------------------------------------------------
return
```

Appendix B

B-1 Example of upscaling work flow described in Chapter 4

This testing approach applies a constant stress to the boundary of the model. The stress model is run to equilibrium and the average displacements on the boundaries are used to calculate strains.

For testing in the x-direction the x=0 axis is fixed and the stress is applied to the x=max_x boundary (Figure 4-5 a). For testing in the y-direction the y=0 axis is fixed and the stress is applied to the y=max_y boundary (Figure 4-5 b). In the following figure simple example is considered. There are 4 fine scale cells with different elastic properties and we are looking for calculating coarse scale elastic properties for this cell using same scenario as explained in Chapter 4 and shown in Figures 4-4 and 4-5.

It should be noted that FLAC is used for stress strain calculation. The following section shows FLAC main file and script which is written using FISH language for calculating averaged strain shown in Equations 4-18 and 4-19.

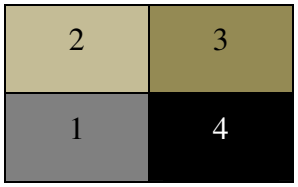

The main FLAC input file representative of above configuration is:

config extra 20

grid 2,2

gen 0 0 0 1 1 1 1 0 i=1,2 j=1,2

group 1 i=1,2 j=1,2

model=ani group 1

prop a=0 d=2250 group 1

prop nuy=0.3 nuz=0.3 group 1

prop s=2.308846E+08 xm=6.003E+08 ym=6.003E+08 group 1

ini ex_1 = 1 group 1

gen 1 0 1 1 2 1 2 0 i=2,3 j=1,2

group 2 i=2,3 j=1,2

model=ani group 2

prop a=0 d=2250 group 2

prop nuy=0.3 nuz=0.3 group 2

prop s=1.155E+08 xm=3.003E+08 ym=3.003E+08 group 2

ini ex_1 = 1 group 2

gen 0 1 0 2 1 2 1 1 i=1,2 j=2,3

group 5 i=1,2 j=2,3

model=ani group 5

prop a=0 d=2250 group 5

prop nuy=0.3 nuz=0.3 group 5

prop s=1.155E+08 xm=3.003E+08 ym=3.003E+08 group 5

ini ex_1 = 1 group 5

gen 1 1 1 2 2 2 2 1 i=2,3 j=2,3

group 6 i=2,3 j=2,3

model=ani group 6

prop a=0 d=2250 group 6

prop nuy=0.3 nuz=0.3 group 6

prop s=2.308846E+08 xm=6.003E+08 ym=6.003E+08 group 6

ini ex_1 = 1 group 6

SET Grav = 0

call test.fis

; the file test.fis is written in FISH language and shown in the following section.

SET _reg=1

run_test

SAVE upscale_1.sav

; this section is related to fish function (shown by test.fis in the above section)

def run_test

array e_i(4)

array output(2)

_apply_stress = -700000

; Since deformation is elastic, apply_stress magnitude is arbitrary.

; definition of boundaries in flac model

_fi1 = 1

_fi2 = 1

_fi3 = igp

_fi4 = igp

_fj1 = 1

_fj2 = jgp

_fj3 = jgp

_fj4 = 1

; open model for writing

fname = +string(_reg)+'.out'

status1 = open(fname,1,1)

; begin testing

; test 1 apply x stress in x direction (This is representative of calculation in Figure 4-5 a)

_s_11 = _apply_stress

_s_12 = 0

_s_21 = 0

_s_22 = 0

Command

ini sxx = 0 syy = 0 sxy=0

ini xdis = 0

ini ydis = 0

ini xvel = 0

ini yvel = 0

fix x y i=1

apply sxx _s_11 from _fi4,_fj4 to _fi3,_fj3

solve srat 1e-5

endcommand

; call output and calculation functions

_output_stress_strain_x

; test 2 apply y stress in y direction (This is representative of calculation in Figure 4-5 b)

_s_11 = 0

_s_12 = 0

_s_21 = 0

_s_22 = _apply_stress

command

ini sxx = 0 syy = 0 sxy=0

ini xdis = 0

ini ydis = 0

ini xvel = 0

ini yvel = 0

fix x y j=1

apply syy _s_22 from _fi2,_fj2 to _fi3,_fj3

solve srat 1e-5

endcommand

; call output and calculation functions

_output_stress_strain_y

status5 = close

end

; the following section is related to averaging of stress and strain (mentioned in Equation 4-18 and 4-19)

def _output_stress_strain_x

; call output and calculation functions

; displacement along i=1

_du1=0.

sum_du1=0.

_i = 1.

_jgp=jgp

loop _j(1,_jgp)

```
  sum_du1 = sum_du1 + xdisp(_i,_j)
endloop
_du1_lhs = abs((sum_du1)/_jgp)
 ; lhs is left hand side
; displacement along i=igp
 _du1=0.
 sum_du1=0.
 _i = igp
 _jgp=jgp
loop _j(1,_jgp)
  sum_du1 = sum_du1 + xdisp(_i,_j)
endloop
_du1_rhs = abs((sum_du1)/_jgp)  ; rhs is right hand side
; displacement along j=1
 _du2=0.
 sum_du2=0.
 _j = 1
 _igp = igp
loop _i(1,_igp)
  sum_du2 = sum_du2 + ydisp(_i,_j)
endloop
_du2_low = abs((sum_du2)/_igp)   ; lower is bottom of model
; displacement along j=jgp
_j = jgp
```

```
_igp = igp
_du2=0.
sum_du2=0.
loop _i(1,_igp)
  sum_du2 = sum_du2 + ydisp(_i,_j)
endloop
_du2_upp = abs((sum_du2)/_igp)   ; upp is top of model
; original length of model
_dx1 = x(igp,1) - x(1,1)
_dx2 = y(1,jgp) - y(1,1)
; calculate the strain
e_11_1 = (_du1_lhs/_dx1)
e_22_1 = (_du2_upp/_dx2)
e_11_2 = (_du1_rhs/_dx1)
e_22_2 = (_du2_low/_dx2)
e_11 = (e_11_1 + e_11_2) *(-1)
e_22 = (e_22_1 + e_22_2)
output(1)=+string(e_11)
output(2)=+string(e_22)
status2 = write(output,2)
end
def _output_stress_strain_y
; call output and calculation functions
; displacement along i=1
```

```
 _du1=0.
 sum_du1=0.
 _i = 1.
 _jgp=jgp
loop _j(1,_jgp)
  sum_du1 = sum_du1 + xdisp(_i,_j)
endloop
_du1_lhs = abs((sum_du1)/_jgp)  ; lhs is left hand side
; displacement along i=igp
 _du1=0.
 sum_du1=0.
 _i = igp
 _jgp=jgp
loop _j(1,_jgp)
  sum_du1 = sum_du1 + xdisp(_i,_j)
endloop
_du1_rhs = abs((sum_du1)/_jgp)  ; rhs is right hand side
; displacement along j=1
 _du2=0.
 sum_du2=0.
 _j = 1
 _igp = igp
loop _i(1,_igp)
  sum_du2 = sum_du2 + ydisp(_i,_j)
```

```
endloop
_du2_low = abs((sum_du2)/_igp)   ; lower is bottom of model
; displacement along j=jgp
_j = jgp
_igp = igp
_du2=0.
sum_du2=0.
loop _i(1,_igp)
  sum_du2 = sum_du2 + ydisp(_i,_j)
endloop
_du2_upp = abs((sum_du2)/_igp)   ; upp is top of model
; original length of model
_dx1 = x(igp,1) - x(1,1)
_dx2 = y(1,jgp) - y(1,1)
; calculate the strain
e_11_1 = (_du1_lhs/_dx1)
e_22_1 = (_du2_upp/_dx2)
e_11_2 = (_du1_rhs/_dx1)
e_22_2 = (_du2_low/_dx2)
e_11 = (e_11_1 + e_11_2)
e_22 = (e_22_1 + e_22_2) *(-1)
output(1)=+string(e_11)
output(2)=+string(e_22)
status2 = write(output,2)
```

end

return

After calculating averaged strain values using above work flow (Equations 4-18 and 4-19), finding coarse scale elastic properties is the next step which is done by solving Equations 4-18 and 4-19 one more time again but in this step, the unknowns are elastic properties instead of strains.

Appendix C

C-1 Example of calculation of young modulus based on available bulk density, compression wave and shear wave transition time logs for one well considered in case study chapter (Chapter 5)

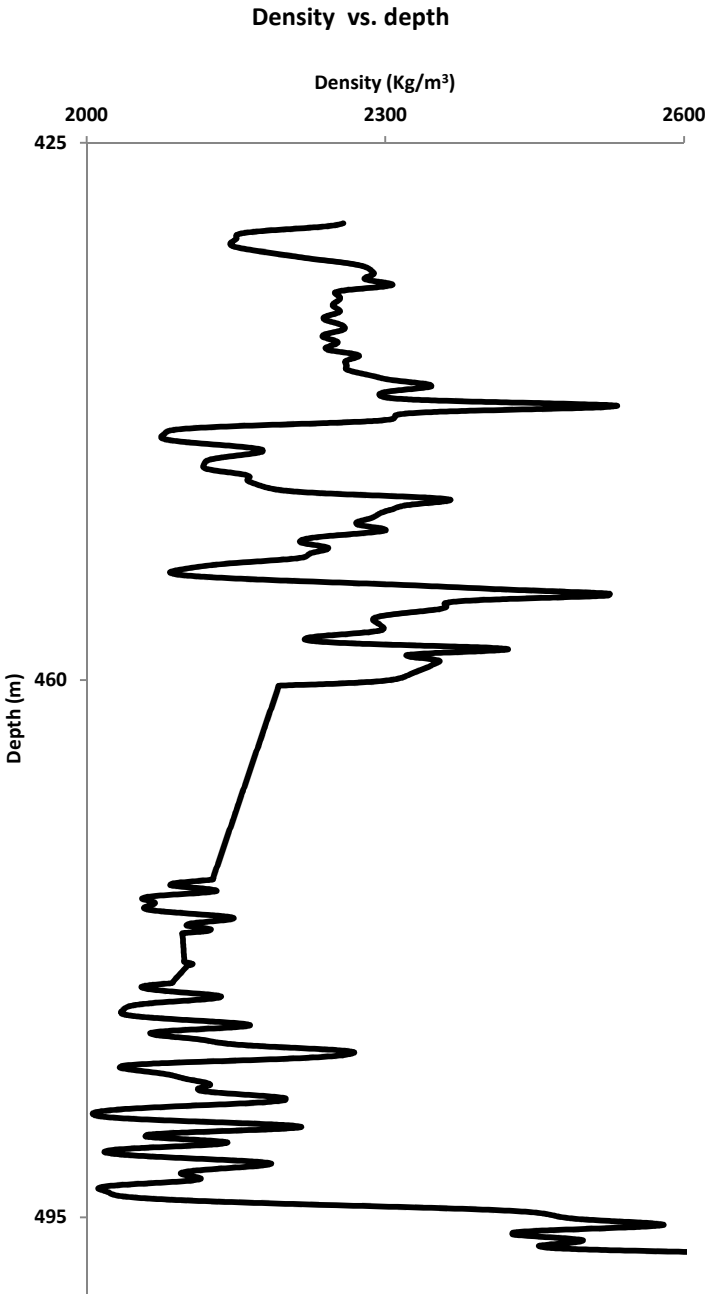

Figure C-1 Density vs. Depth for one well considered in case study chapter (Chapter 5).

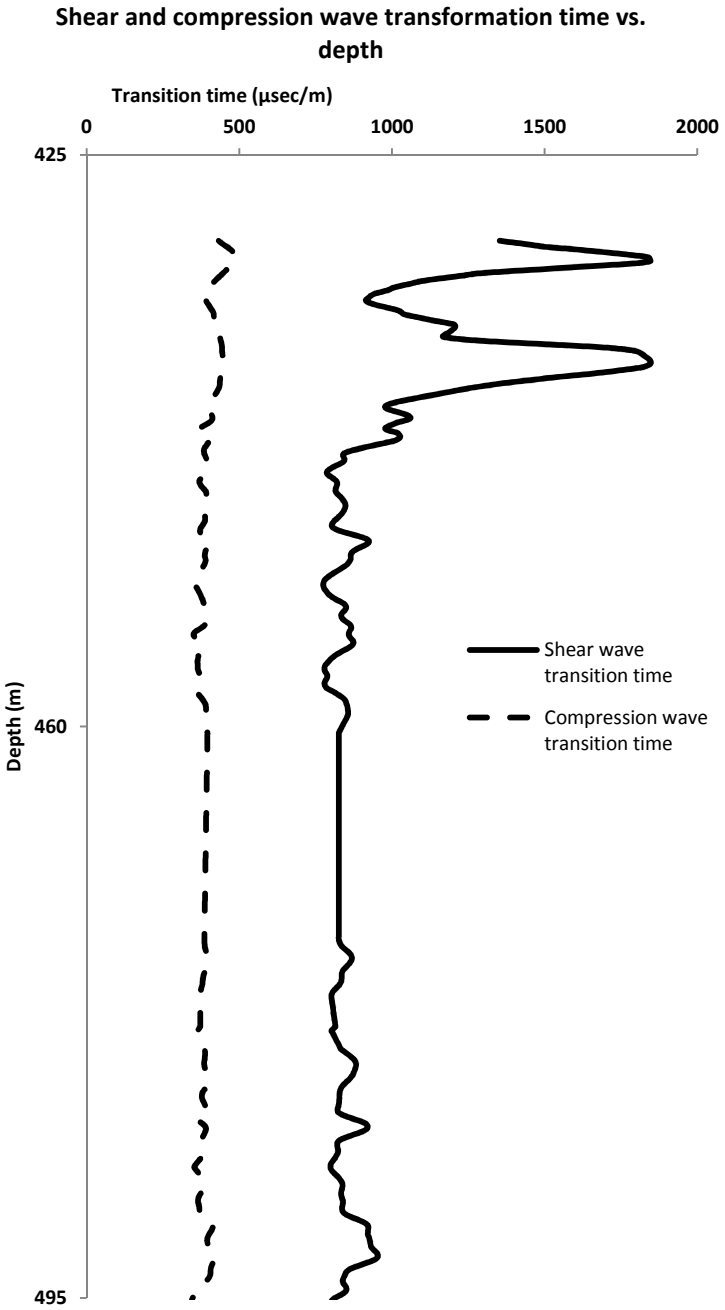

Figure C-2 Shear and compression transformation time vs. Depth for one well considered in case study chapter (Chapter 5).

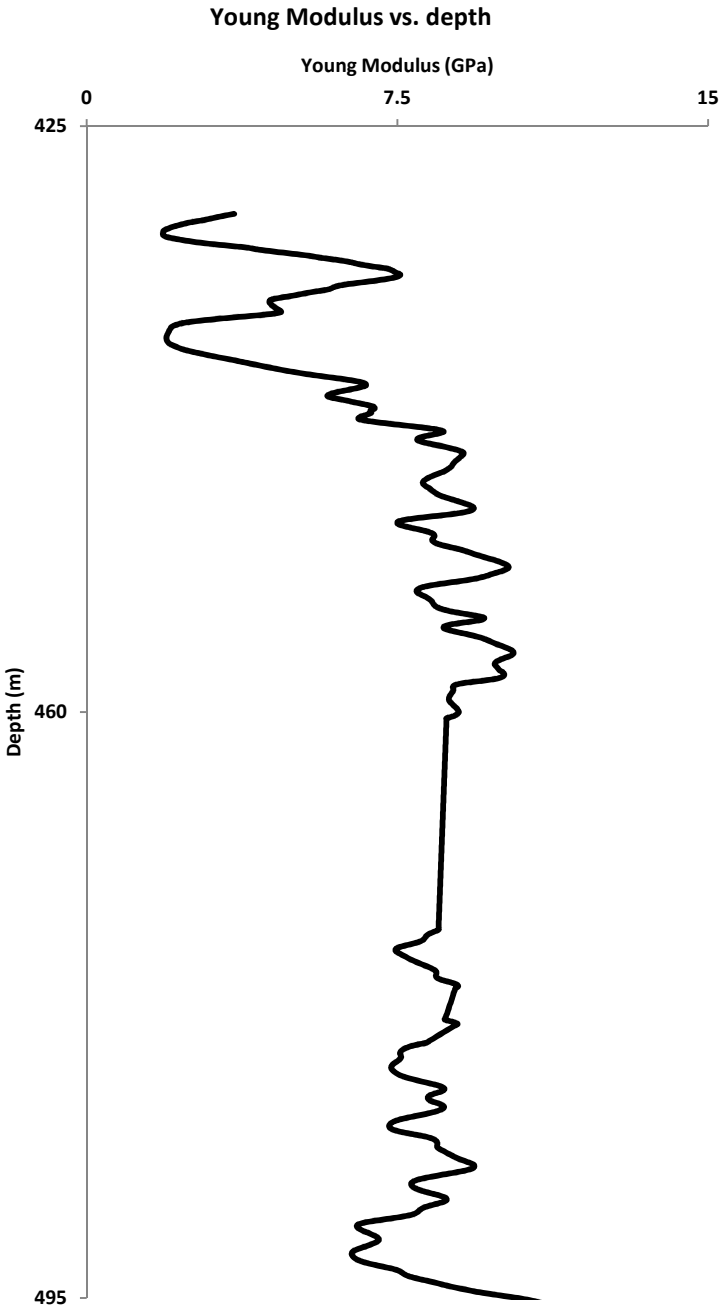

Figure C-3 Calculated young modulus vs. Depth for one well considered in case study chapter (Chapter 5).

C-2 Stratigraphical transformation and upscaled data for one well considered in case study chapter (Chapter 5)

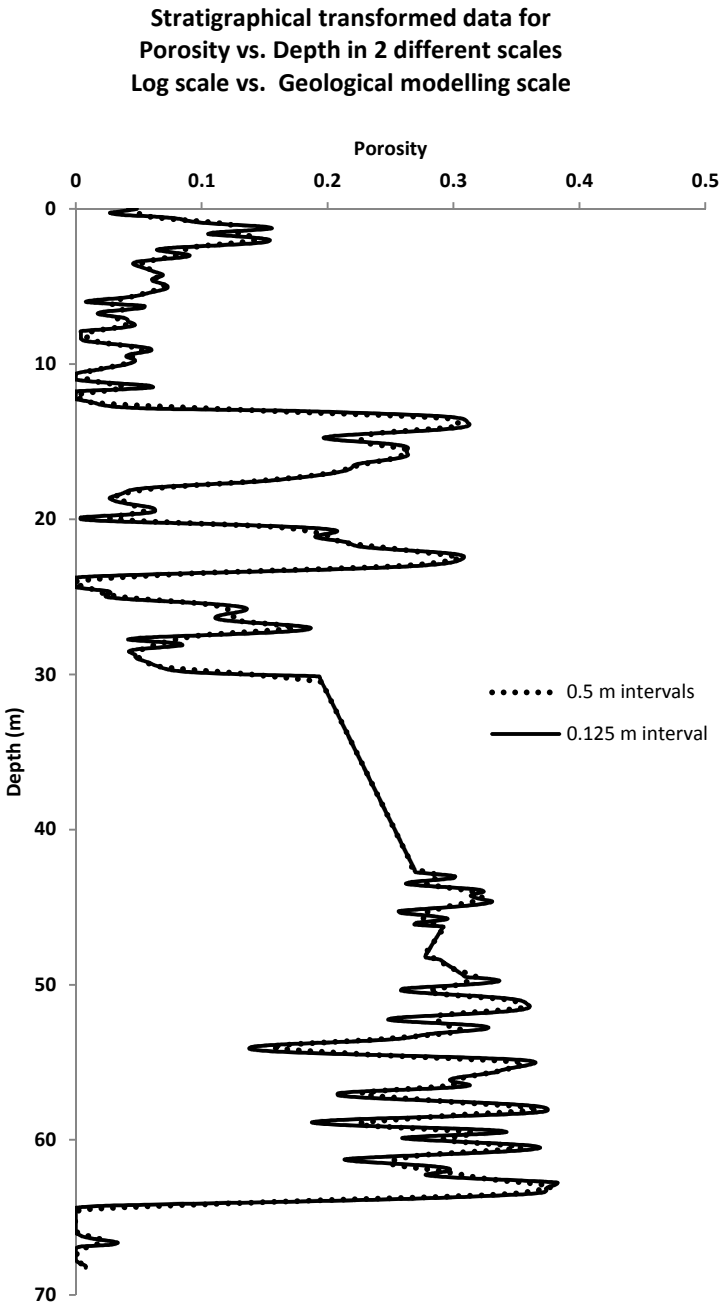

Figure C-4 Stratigraphical transformed porosity log for one well considered in case study chapter; solid line: 0.125 m interval and dashed line: 0.5 interval.